

平成二十六年年度 修士論文

Flux quench in the  $S = 1/2$  XXZ chain  
( $S = 1/2$  XXZ 鎖模型における磁束クエンチ)

東京大学大学院理学系研究科物理学専攻

中川裕也

(指導教員: 押川正毅)

March 10, 2015

# Abstract

In recent years, nonequilibrium quantum systems have become a major subject of study in condensed matter. Quantum quenches, abrupt changes of Hamiltonian of a system, offer simple protocols to tackle problems in nonequilibrium situations.

In this thesis, we study a *flux quench* problem in the spin-1/2 XXZ chain. The flux quench is a quantum quench where the flux  $\phi$  piercing the XXZ chain is turned off at  $t = 0$  suddenly. If we formulate the XXZ chain as a spinless fermion model, the flux  $\phi$  corresponds to a vector potential on each bond and this flux quench can be viewed as imposing a pulse (delta function) of electric field. Therefore the flux quench generates some particle (or spin) current at time  $t = 0$ . We focus on the time-evolution of the spin current after the quench, and calculate it numerically by the infinite time-evolving block decimation (iTEBD) method.

We find that the long-time limit ( $t \rightarrow \infty$ ) and the dynamics of the spin current depend strongly on the anisotropy parameter  $\Delta$  of the XXZ chain and the amount of flux initially inserted. The long-time limit of the current matches with predictions of linear response theory as the initial flux decreases. However, the deviation from linear response theory is largely affected by the sign of the anisotropy of the XXZ chain. Regarding the dynamics, the current decays in time after the quench, and its relaxation time is dependent on the anisotropy and the initial flux. Furthermore, for large initial flux and anti-ferromagnetic anisotropy, the current oscillates in long time scale. We numerically find that the frequency of the oscillation is proportional to  $|\Delta|$ . Remarkably, the dynamics of momentum distribution of spinless fermions reveals that this oscillation of current is governed by excitations deep inside the Fermi sea. This mechanism of oscillations cannot be captured by the effective Luttinger model corresponding to the microscopic XXZ chain, which is in contrast with the previous studies on different types of quench in the same model as ours.

# Contents

<b>1</b>	<b>Introduction</b>	<b>4</b>
1.1	Nonequilibrium physics . . . . .	4
1.1.1	Quantum quench . . . . .	5
1.2	One-dimensional quantum systems . . . . .	7
1.3	Purpose of this study . . . . .	8
1.4	Outline of the thesis . . . . .	8
<b>2</b>	<b>Definition of the problem: Flux quench in the <math>S = 1/2</math> XXZ chain</b>	<b>9</b>
2.1	$S = 1/2$ XXZ chain model . . . . .	9
2.1.1	XXZ chain with flux . . . . .	11
2.2	Flux quench in the $S = 1/2$ XXZ chain . . . . .	13
2.2.1	Analysis by linear response theory and the Drude weight . . . . .	15
2.3	Previous studies . . . . .	15
2.3.1	Previous studies on the long-time limit of the current . . . . .	16
2.3.2	Bosonic flux quench . . . . .	17
<b>3</b>	<b>Numerical Methods</b>	<b>18</b>
3.1	Introduction . . . . .	18
3.2	Tensor networks . . . . .	19
3.2.1	Basics of tensor networks . . . . .	19
3.2.2	Entanglement entropy and area law . . . . .	21
3.2.3	Ground states are well expressed by tensor networks . . . . .	22
3.3	Matrix product states (MPS) . . . . .	23
3.3.1	Schmidt decomposition . . . . .	24
3.3.2	Construction of MPS for arbitrary states in a system . . . . .	26
3.3.3	Canonical condition for MPS . . . . .	29
3.3.4	Calculation of physical quantity using MPS . . . . .	31
3.3.5	Example of MPS . . . . .	32
3.4	Time-Evolving Block Decimation method . . . . .	34
3.4.1	Suzuki-Trotter decomposition for time-evolution operator . . . . .	34
3.4.2	Updating canonical MPS after the action of local operator . . . . .	35
3.4.3	TEBD algorithm . . . . .	36
3.5	iTEBD . . . . .	38
3.5.1	infinite MPS . . . . .	38
3.5.2	Algorithm . . . . .	39

<b>4</b>	<b>Results and Discussions</b>	<b>41</b>
4.1	Numerical data of the dynamics . . . . .	41
4.2	Long-time limit of the current . . . . .	45
4.3	Frequency of oscillation . . . . .	46
4.3.1	Equation of motion of spin current . . . . .	47
4.3.2	Dynamics of momentum distribution $n_q$ . . . . .	47
4.4	Relaxation time . . . . .	50
<b>5</b>	<b>Conclusion, Future Work</b>	<b>52</b>
<b>A</b>	<b>Technical details on numerical calculations</b>	<b>53</b>
A.1	Details on numerical calculations, error estimate . . . . .	53
A.2	iTEBD algorithm exploiting a symmetry . . . . .	55

# Chapter 1

## Introduction

It is of great importance to study nonequilibrium physics, from the viewpoint of pure-theoretical interest as well as practical realizations of quantum devices such as quantum computers. In this chapter, we review background of our study. Nonequilibrium physics is overviewed and quantum quench problems are introduced in the first section. In the second section, we sketch the physics in one dimension. Emphasis is put on a drastic effect of interactions in one-dimensional quantum systems and a wide variety of methods to study them. An aim of our study and outline of this thesis are presented in the last part of this chapter.

### 1.1 Nonequilibrium physics

Equilibrium states are defined as states that have become stationary after long time-evolution in closed systems. They are designated by only a few parameters, such as temperature, pressure and volume. In the language of quantum statistical mechanics, equilibrium states are mixed states (Gibbs states) written as

$$\hat{\rho}_{\text{Gibbs}}^{\beta} = \frac{e^{-\beta\hat{H}}}{\text{Tr}(e^{-\beta\hat{H}})}, \quad (1.1)$$

where  $\hat{H}$  is Hamiltonian of a system and  $\beta$  is inverse temperature. In order to reveal properties of the equilibrium states, many theoretical methods are proposed: mean-field approximation, renormalization group, Landau-Ginzburg theory, and so on. These methods can capture essential points of experimental data on complicated real materials. So far, we have much established understanding of the equilibrium states.

On the other hand, less are known for nonequilibrium states. It is partly because most theoretical methods for equilibrium states cannot be applied to nonequilibrium situations directly and we do not have enough tools to tackle them especially beyond linear response regime. Recently, substantial experimental developments in nonequilibrium quantum systems have allowed one to compare theories with experiments at high accuracy and controllability. For example, optical lattices in cold atom systems [1] can simulate theoretical models, such as Hubbard model, with broad tunability of parameters and good time-resolutions of the dynamics. As a consequence, nonequilibrium quantum systems have become a major subject of study in condensed matter physics [2].

The field of nonequilibrium physics is really vast. There are various ways to drive systems into nonequilibrium: coupling them to thermal baths, adding interactions with noisy environments, applying external fields, etc. Among these protocols, in this study we choose one called quantum quench.

### 1.1.1 Quantum quench

Quantum quench, a hot topic in recent studies, is a sudden change of parameter(s) in a quantum system. It is one of the simplest protocols to make systems nonequilibrium and study the nature of such situations. In typical setup, initial state is prepared as the ground state of pre-quench Hamiltonian, and then a parameter of the system is changed in time. The change of parameter induces non-trivial dynamics of the system, and one studies the dynamics itself and/or its long-time limit.

For example, consider quantum quench of magnetic field in a quantum spin system. Initial state is taken to be the ground state of Hamiltonian  $\hat{H}(h)$  in the presence of magnetic field  $h$ . We assume that the initial state has magnetic order  $m$ . Then the magnetic field is quenched to zero at time  $t = 0$  abruptly. Because the ground state of pre-quench Hamiltonian  $\hat{H}(h)$  is not an eigenstate of post-quench Hamiltonian  $\hat{H}(h = 0)$ , non-trivial time-evolution<sup>1</sup> is evoked:

$$\hat{H}(h) |\psi(h)\rangle = E_0(h) |\psi(h)\rangle, e^{-i\hat{H}(h)t} |\psi(h)\rangle = e^{-iE_0(h)t} |\psi(h)\rangle, \quad (1.2)$$

$$\hat{H}(0) |\psi(h)\rangle \not\propto |\psi(h)\rangle, e^{-i\hat{H}(0)t} |\psi(h)\rangle \neq e^{-iE_0(h)t} |\psi(h)\rangle. \quad (1.3)$$

When the ground state and any thermal state of post-quench Hamiltonian  $\hat{H}(h = 0)$  do not exhibit magnetic order, the order parameter  $m(t)$  of the state  $|\psi(t)\rangle = e^{-i\hat{H}(0)t} |\psi(h)\rangle$  is expected to decay to zero if we assume thermalization. In studies of quantum quench, this kind of equilibration and resulting thermalization are investigated as well as the dynamics after the quench.

By quantum quench, we can study various kinds of phenomena. One example is universal dynamical scaling across a quantum critical point [3]. Universal scaling laws are found to hold when systems are quenched across quantum critical points, as in the Kibble-Zurek mechanism for classical systems. Some quantities (density of defects, adiabatic fidelity, etc.) show scaling laws whose critical exponents are universal and independent of microscopic details of a system. Another example of phenomena studied by quantum quench is equilibration and thermalization in closed quantum systems. In addition, the dynamics towards (thermal) equilibrium is investigated by employing quantum quench. Below we review these two in detail.

### Equilibration and thermalization in closed quantum systems

Equilibration in closed quantum systems is a phenomenon that quantum states become stationary in the long-time limit,  $t \rightarrow \infty$ . If such equilibrated states in the long-time limit look thermal, we call that phenomenon as thermalization. Specifically, thermalization is

<sup>1</sup> In this thesis, we set  $\hbar = 1$ .

## Chapter 1. Introduction

a phenomenon that equilibrated states have the same expectation values for any physical observable as those of certain Gibbs states  $\rho_{\text{Gibbs}}^\beta$  :

$$\exists \rho_{\text{Gibbs}}^\beta, \quad \lim_{t \rightarrow \infty} \langle \psi(t) | \hat{A} | \psi(t) \rangle = \text{Tr} \left( \rho_{\text{Gibbs}}^\beta \hat{A} \right) \quad \text{for all } \hat{A}. \quad (1.4)$$

We note that the detail of initial state  $|\psi(0)\rangle$  is lost in the right hand side and the equilibrated state is specified by only one parameter, inverse temperature  $\beta$ . The initial state *forgets* the information about itself during time-evolution and becomes featureless.

Thermalization is rigorously confirmed to happen in some special cases and expected to occur in generic systems [2,4]. However, for the so-called integrable systems, it is widely believed that there is no thermalization. Integrable systems are quantum systems that are exactly solved by Bethe ansatz, and there exist infinitely many conserved quantities in the system. Naively, the reason for the absence of thermalization in integrable systems is that the infinitely many conserved quantities prevent states from *forgetting* information about themselves. Nevertheless, for integrable systems we can construct another statistical ensemble to describe equilibrated states after quantum quench: Generalized Gibbs ensemble (GGE) [5]. GGE is an ensemble that contains additional conserved quantities other than Hamiltonian,

$$\hat{\rho}_{\text{GGE}}^{\beta, \{\lambda\}} = \frac{1}{Z_{\text{GGE}}} \exp \left( -\beta \hat{H} - \sum_{i=1} \lambda_i \hat{Q}_i \right), \quad (1.5)$$

where  $\hat{Q}_i$  are conserved quantities in a system,  $\lambda_i$  are Lagrange multipliers and  $Z_{\text{GGE}}$  is a normalization constant. The point of GGE is that while the total number of states (the dimension of Hilbert space) is exponentially large in system size  $L$ , the number of parameters to designate GGE,  $\beta$  and  $\{\lambda\}$ , is linearly large in  $L$ . In this sense, information of initial states is lost and thermalization-like behavior appears even in integrable systems.

For some integrable models essentially equivalent to free particles (e.g. transverse Ising model), it was shown [5] that GGE can represent equilibrated states after quantum quench. GGE was expected to be valid also in general integrable systems [2]. However, quite recently [6] it was proved that GGE having only local conserved quantities cannot represent states after quench in a certain model (the  $S = 1/2$  XXZ chain, the same model as our study). We will review this study (Ref. [6]) in section 2.3 as the previous studies related to our problem. A general proof (or denial) for GGE is still outstanding, and many problems remain to be solved in the field.

## Dynamics after quantum quench

Equilibration and thermalization phenomena say about only the long-time limit of states. Transient dynamics towards stationary states after quantum quench is also investigated by many authors [7,8], although the dynamical behaviors after quantum quench are quite diverse and it is not easy to conclude universal features of them. In section 2.1, we will review examples of studies that focused on the dynamics after quantum quench in the  $S = 1/2$  XXZ chain (the model we consider in this thesis).

## 1.2 One-dimensional quantum systems

In this thesis, we study a nonequilibrium problem in one dimension. Here we review the physics of one-dimensional quantum systems.

One-dimensional quantum systems have been studied for more than 50 years [9]. They have attracted theorists because of their remarkable features: a strong effect of interactions on systems and wide availability of theoretical methods and exact results, compared with higher-dimensional systems. One can regard them as a prototype of strongly-correlated systems; effects of interactions are quite strong but we can obtain exact (or very detailed) results. Furthermore, they are not only a subject of pure-theoretical studies but also realistic experimental systems: organic conductors, carbon nanotubes, quantum wires, optical lattices in cold atomic systems, and so on.

### Drastic effect of interactions in one dimension and Tomonaga-Luttinger liquid

Interactions play a crucial role in one dimension. The breakdown of Landau's Fermi liquid theory manifests the importance of interactions in one dimension. Fermi liquid is a universality class into which a wide variety of metallic systems of interacting fermions in higher dimensions ( $> 1$ ) flows under the renormalization group. Fermi liquid theory (as a textbook, we name Ref. [10]) is well established in dimensions higher than one. Its assumption is the existence of quasiparticle excitations that are adiabatically connected to excitations in a free system as interactions are turned off. In one dimension, however, interactions change properties of a system drastically and elementary excitations become collective and bosonic; they are not connected adiabatically to excitations in a free system. Consequently, Fermi liquid theory breakdowns in one dimension.

Metallic systems of interacting fermions in one dimension flow into another universality class under the renormalization group: Tomonaga-Luttinger Liquid (TLL). TLL is gapless and critical, and it has no symmetry-breaking orders. It is designated by only two universal parameters, the renormalized Fermi velocity  $v_F$  and the Luttinger parameter  $K$ . Low-energy physics of a system belonging to TLL universality class is fully determined by these two parameters. For example, the exponent of correlation function of fermions at long distance (low-energy) is written by  $K$ :  $G(r \gg 1) \sim 1/r^{1/2K+K/2}$ . Furthermore, one of the most important aspects of TLL is that not only fermionic but also bosonic and spin systems in one dimension mostly exhibit TLL behaviors. TLL is *ubiquitous* in one-dimensional quantum physics.

### Theoretical methods to study one-dimensional quantum systems

In spite of such strong (non-perturbative) effects of interactions, many analytical and numerical methods are available to study one-dimensional quantum systems compared to higher-dimensional systems. We briefly review some of the methods; Bethe ansatz [11] gives exact solutions for one-dimensional Heisenberg model and Hubbard model. The solvability of these models becomes a branch of mathematical physics under the name of *integrable systems*. Bosonization [9] is one of the most powerful theoretical methods to analyze one-dimensional quantum systems. Peculiarity of one dimension that particles cannot overtake each other allows us to map fermionic systems into bosonic systems

and vice versa, which results in making the method applicable to wide classes of models. Conformal field theory [12] predicts behaviors of a system at and nearby a critical point. For one-dimensional systems (1+1 dimension in space-time) conformal invariance emerging from criticality strongly dictates various physical quantities and we can obtain exact formulae for such quantities. As for numerical methods, we can employ exact diagonalization (ED) and quantum Monte Carlo for one-dimensional systems [13] in the same manner for higher-dimensional systems. Moreover, as peculiar methods in one dimension, density matrix renormalization group (DMRG) [14] and time-evolving block decimation (TEBD) [15] enable us to deal with very large systems (several hundreds of sites) that cannot be handled by ED or quantum Monte Carlo. We employ infinite-TEBD (iTEBD) method in this study and it is reviewed in chapter 3.

### 1.3 Purpose of this study

When we combine two concepts introduced in this chapter, we conceive of a stimulating field: nonequilibrium physics in one-dimensional quantum systems. Although nonequilibrium phenomena in strongly-correlated systems are formidably difficult to tackle, the wide availability of analytical and numerical methods in one dimension allows us to study them at depth. The study of nonequilibrium physics in one dimension can be regarded as a prototype to understand nonequilibrium phenomena in strongly-correlated systems.

As one of the simplest problems in nonequilibrium and strongly-correlated systems, in this thesis we study a quantum quench problem named *flux quench* in the  $S = 1/2$  XXZ chain by exploiting the iTEBD method (numerical method peculiar in one dimension). The flux quench is a quantum quench of flux piercing a ring of the XXZ chain and it induces spin current in the system. We study the long-time limit and dynamics of the induced spin current after the quench.

### 1.4 Outline of the thesis

This thesis is organized as follows. In chapter 2, the  $S = 1/2$  XXZ chain model is reviewed and the flux quench problem is defined. Besides, we introduce the previous studies related to our problem. In chapter 3, numerical methods employed in this study are reviewed. It is almost independent of other contents in this thesis, so those who are not interested in details of numerical calculations can skip it. It also can be read as an independent review of the TEBD method. In chapter 4, the results of numerical calculations are shown. Discussions on the numerical data are also presented. In chapter 5, we state a conclusion of this study and future works are discussed. Technical details of numerical calculations are described in appendix A.

## Chapter 2

# Definition of the problem: Flux quench in the $S = 1/2$ XXZ chain

In this chapter, we review properties of the  $S = 1/2$  XXZ chain model and define a problem of our study, *flux quench*.

### 2.1 $S = 1/2$ XXZ chain model

The  $S = 1/2$  XXZ chain model is a generalization of Heisenberg model which describes quantum magnets in one dimension. Hamiltonian of this model is defined as

$$H_{\text{XXZ}} = - \sum_{i=0}^{N-1} (S_i^x S_{i+1}^x + S_i^y S_{i+1}^y + \Delta S_i^z S_{i+1}^z) = - \sum_{i=0}^{N-1} \left( \frac{1}{2} (S_i^+ S_{i+1}^- + S_i^- S_{i+1}^+) + \Delta S_i^z S_{i+1}^z \right) \quad (2.1)$$

where

$$S_i^x = \frac{1}{2} \begin{pmatrix} 0 & 1 \\ 1 & 0 \end{pmatrix}, \quad S_i^y = \frac{1}{2} \begin{pmatrix} 0 & -i \\ i & 0 \end{pmatrix}, \quad S_i^z = \frac{1}{2} \begin{pmatrix} 1 & 0 \\ 0 & -1 \end{pmatrix}, \quad S_i^\pm = S_i^x \pm i S_i^y \quad (2.2)$$

are spin-1/2 operators acting on site  $i$ . We impose periodic boundary condition  $S_N^{x,y,z} = S_0^{x,y,z}$ .  $\Delta$  is called the anisotropy of the chain.  $\Delta > 0$  ( $\Delta < 0$ ) means ferromagnetic (anti-ferromagnetic) interactions between neighboring sites. When  $\Delta$  is  $\pm\infty$ , the model is equivalent to the Ising model.

This Hamiltonian can be mapped to a spinless fermion system by Jordan-Wigner transformation:

$$S_i^+ = \prod_{0 \leq j < i} (1 - 2c_j^\dagger c_j) c_i^\dagger, \quad S_i^- = \prod_{0 \leq j < i} (1 - 2c_j^\dagger c_j) c_i, \quad S_i^z = c_i^\dagger c_i - \frac{1}{2}, \quad (2.3)$$

$$H_{\text{fermion}} = - \sum_{i=0}^{N-1} \left( \frac{1}{2} (c_i^\dagger c_{i+1} + c_{i+1}^\dagger c_i) + \Delta \left( c_i^\dagger c_i - \frac{1}{2} \right) \left( c_{i+1}^\dagger c_{i+1} - \frac{1}{2} \right) \right). \quad (2.4)$$

Boundary condition for spinless fermions is determined by that for the XXZ chain, although the relationship between them is slightly complicated [16]. Here we ignore it

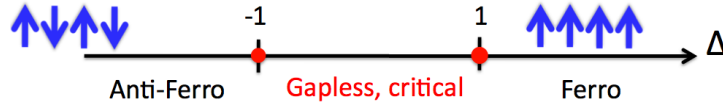
Chapter 2. Definition of the problem: Flux quench in the  $S = 1/2$  XXZ chain

Figure 2.1: Phase diagram of the ground state of the XXZ chain. For all anisotropies  $\Delta$ , Hamiltonian is integrable and the exact ground state energy is known.

because in numerical calculations we treat the thermodynamic limit of the system, where the boundary condition does not matter. In the spinless fermion formulation,  $\Delta$  is the strength of nearest density-density interactions.

At  $\Delta = 0$ ,  $H_{\text{fermion}}$  becomes tight-binding Hamiltonian and can be solved by Fourier transformation:

$$H_{\text{fermion,free}} = -\frac{1}{2} \sum_{i=0}^{N-1} \left( c_i^\dagger c_{i+1} + c_{i+1}^\dagger c_i \right) = - \sum_k \cos(k) \tilde{c}_k^\dagger \tilde{c}_k, \quad (2.5)$$

$$\tilde{c}_k := \frac{1}{\sqrt{N}} \sum_{r=0}^{N-1} c_r e^{-ikr}. \quad (2.6)$$

The ground state is thus the Fermi sea of spinless fermions,  $\prod_{k \leq k_F} \tilde{c}_k^\dagger \tilde{c}_k |\text{vacuum}\rangle$  ( $k_F$  is the Fermi momentum). Furthermore, it is known [11] that the XXZ Hamiltonian is exactly solvable by Bethe ansatz for arbitrary anisotropies  $\Delta$ . According to the exact solutions, Hamiltonian is gapless for  $-1 \leq \Delta \leq 1$ , gapped for  $\Delta < -1$  (anti-ferromagnetic phase) and  $1 < \Delta$  (ferromagnetic phase). Phase diagram of the ground state is shown in Fig. 2.1. In gapless phase, there is no magnetization  $\sum_i \langle S_i^z \rangle$  and correlation functions  $\langle S_0^x S_r^x \rangle$  and  $\langle S_0^z S_r^z \rangle$  show power-law decay. In addition, the model exhibits TLL universality [9]. The renormalized Fermi velocity  $v_F$  and the Luttinger parameter  $K$  are exactly known,

$$v_F = \frac{\pi \sqrt{1 - \Delta^2}}{2 \arccos(\Delta)}, \quad K = \frac{\pi}{2 \arccos(\Delta)}. \quad (2.7)$$

In gapped anti-ferromagnetic phase, non-zero staggered magnetization  $\sum_i (-1)^i \langle S_i^z \rangle$  appears and the magnetization is zero. All correlation functions decay exponentially in space. The ground state is similar to classical Néel state  $|\uparrow\downarrow\uparrow\downarrow \cdots\rangle$ . However, the true ground state energy is lower than that of the Néel state and neighboring correlation  $\langle S_i^+ S_{i+1}^- \rangle$  is finite. Only in the limit of  $\Delta \rightarrow -\infty$ , the ground state becomes the Néel state. In gapped ferromagnetic phase, the ground state is simply  $|\uparrow\uparrow \cdots\rangle$  or  $|\downarrow\downarrow \cdots\rangle$  for all  $\Delta > 1$ .

An important feature of the XXZ chain is integrability. The  $S = 1/2$  XXZ chain is integrable for any  $\Delta$  and its infinitely many conserved quantities  $\{Q_i\}_i$  can be calculated by algebraic Bethe ansatz [11]. It is one of the non-trivial integrable models in the sense that it is not equivalent to a model of free particles.

### Previous studies on quantum quench in XXZ chain

The XXZ chain is one of the simplest models in one-dimensional quantum systems that include interactions. For this reason, various types of quantum quench in the XXZ chain

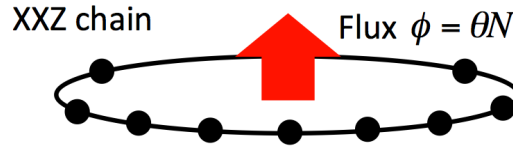


Figure 2.2: Hamiltonian  $H_\theta$  represents a ring of the XXZ chain pierced by magnetic flux  $\phi = \theta N$ .

have been studied. We review some of them here.

Barmettler *et al.* [17] studied quantum quench in the XXZ chain where initial state is prepared as the Néel state  $|\uparrow\downarrow\uparrow\downarrow\cdots\rangle$ . They numerically calculated the dynamics of staggered magnetization by the iTEBD method. They found oscillatory dynamics in gapless phase ( $|\Delta| < 1$ ) and nonoscillatory dynamics for large anti-ferromagnetic anisotropy ( $\Delta \ll -1$ ). Furthermore, they showed that at the critical point ( $\Delta = -1$ ) the relaxation time takes a minimum in contrary to the notion of critical slowing down, from which we expect a maximum. Fagotti *et al.* [18] investigated quantum quench in the XXZ chain by taking various initial states (Néel states, dimer states, etc.). They calculated the dynamic of some correlators such as  $\langle S_0^x S_1^x \rangle$  or  $\langle S_0^z S_2^z \rangle$  by time-dependent DMRG and iTEBD, and compared the long-time limit of the correlators with analytical predictions from GGE. They found the numerical data agree with the prediction from GGE well. The authors of Ref. [19] and Ref. [20] considered the so-called interaction quench in the XXZ chain. The interaction quench is a quantum quench of the anisotropy  $\Delta$  which is changed from zero (free fermion point) to some finite value. They focused on the  $Z$ -factor of momentum distribution of spinless fermions and kinetic energy of the system, and concluded that those quantities after the quench are well described by the effective TLL. Their results are in contrast with our present study, as we will see later. Finally, we comment that analytical methods based on the Bethe ansatz techniques to study quantum quench in the XXZ chain are proposed by Ref. [21, 22].

### 2.1.1 XXZ chain with flux

The XXZ Hamiltonian with flux is defined as

$$H_\theta = - \sum_i \left( \frac{1}{2} e^{i\theta} S_i^+ S_{i+1}^- + \frac{1}{2} e^{-i\theta} S_i^- S_{i+1}^+ + \Delta S_i^z S_{i+1}^z \right). \quad (2.8)$$

In the spinless fermion representation,

$$H_\theta = - \sum_i \left( \frac{1}{2} e^{i\theta} c_i^\dagger c_{i+1} + \frac{1}{2} e^{-i\theta} c_{i+1}^\dagger c_i + \Delta \left( c_i^\dagger c_i - \frac{1}{2} \right) \left( c_{i+1}^\dagger c_{i+1} - \frac{1}{2} \right) \right). \quad (2.9)$$

$\theta$  can be viewed as Aharonov-Bohm phase on hopping of particles, or vector potential. Hamiltonian  $H_\theta$  corresponds to a situation where a ring of the XXZ chain is pierced by magnetic flux  $\phi = \theta N$  (Fig. 2.2). This Hamiltonian has been studied in the context of the Drude weight (DC-conductivity) of the XXZ chain [23], spectral flow of the energy levels [24] and the Berry's phase induced by adiabatic insertion of the flux [25].

Chapter 2. Definition of the problem: Flux quench in the  $S = 1/2$  XXZ chain

For a finite size system, the presence of magnetic flux can be converted to twisted boundary condition by Lieb-Schultz-Mattis (LSM) operator [16]

$$U_\theta = \exp\left(-i\theta \sum_{r=0}^{N-1} r S_r^z\right). \quad (2.10)$$

We can show easily

$$U_\theta^\dagger H_\theta U_\theta = H_{0,\text{twisted}} = - \sum_{i=0}^{N-1} \left( \frac{1}{2} S_i^+ S_{i+1}^- + \frac{1}{2} S_i^- S_{i+1}^+ + \Delta S_i^z S_{i+1}^z \right), \quad S_N^\pm = S_0^\pm e^{\mp i\theta N}. \quad (2.11)$$

This is zero-flux XXZ Hamiltonian with twisted boundary condition. An exact solution is known [26] for the twisted boundary condition case and the ground state energy in the thermodynamic limit is the same as that of the XXZ chain without twist.

If  $\theta N \equiv 0 \pmod{2\pi}$ , there is no effects of twist even after the unitary transformation by LSM operator. In this case  $U_\theta^\dagger H_\theta U_\theta = H_0$  holds, and therefore the ground state of  $H_\theta$  is given by that of  $H_0$ :

$$|\theta\rangle_{\text{GS}} = U_\theta |\theta = 0\rangle_{\text{GS}}. \quad (2.12)$$

Note that the ground state of  $H_\theta$  and  $H_0$  is different from each other although the energy spectrum of them are the same.

In the spinless fermion language, LSM operator is written as

$$U_\theta = \exp\left(-i\theta \sum_{r=0}^{N-1} r c_r^\dagger c_r\right). \quad (2.13)$$

Here we ignored an unimportant constant factor in  $U_\theta$ .  $U_\theta$  acts on fermion operators as a boost in momentum space,

$$U_\theta^\dagger \tilde{c}_k U_\theta = \tilde{c}_{k+\theta}, \quad U_\theta^\dagger \tilde{c}_k^\dagger U_\theta = \tilde{c}_{k+\theta}^\dagger. \quad (2.14)$$

We will use this property later.

In this thesis, we study a spin current of the  $S = 1/2$  XXZ chain. The definition of spin current  $\hat{J}$  is

$$\hat{J} := \frac{1}{N} \sum_i j_i, \quad j_i = \frac{1}{2i} (S_i^+ S_{i+1}^- - S_i^- S_{i+1}^+), \quad (2.15)$$

which is taken to satisfy<sup>1</sup> the continuity equation

$$\frac{d}{dt} S_i^z = [iH_0, S_i^z] \stackrel{!}{=} j_i - j_{i-1}. \quad (2.16)$$

We define  $\hat{J}$  as an intensive quantity because we consider the thermodynamic limit  $N \rightarrow \infty$  in numerical calculations. In spinless fermion notation,  $\hat{J}$  is expressed as

$$\hat{J} = \frac{1}{2iN} \sum_i (c_i^\dagger c_{i+1} - c_{i+1}^\dagger c_i) = \frac{1}{N} \sum_k \sin(k) \tilde{c}_k^\dagger \tilde{c}_k. \quad (2.17)$$

<sup>1</sup> This definition of the spin current is for Hamiltonian  $H_0$  (zero-flux case). In the presence of flux, the continuity equation changes and we have to slightly modify the definition of the spin current if we want to make it hold,  $j_i^\theta = (2i)^{-1} (e^{i\theta} S_i^+ S_{i+1}^- - e^{-i\theta} S_i^- S_{i+1}^+)$ .

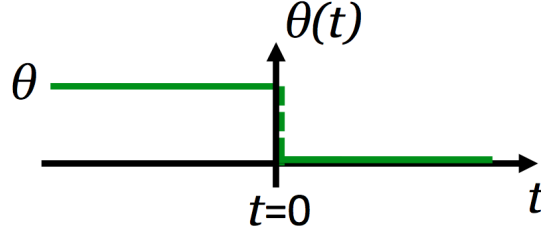


Figure 2.3: Quench protocol of the flux quench. In our study, we take  $\theta < 0$  so that initial spin currents become positive.

This is exactly the current of spinless particles. The spin current is not a constant of motion in the presence of interactions ( $\Delta \neq 0$ ):

$$[H_0, \hat{J}] = -\frac{\Delta}{2iN} \sum_i (S_i^+ S_{i+1}^- + S_i^- S_{i+1}^+) (S_{i-1}^z - S_{i+2}^z). \quad (2.18)$$

Non-conservation of the spin current is due to the Umklapp scattering by the term  $\Delta \sum_i S_i^z S_{i+1}^z$ .

## 2.2 Flux quench in the $S = 1/2$ XXZ chain

Let us define *flux quench* in the  $S = 1/2$  XXZ chain, a main problem of this study. The flux quench is a quantum quench of phase (or flux)  $\theta$  in the XXZ chain,

$$H(t) = -\sum_i \left( \frac{1}{2} e^{i\theta(t)} S_i^+ S_{i+1}^- + \frac{1}{2} e^{-i\theta(t)} S_i^- S_{i+1}^+ + \Delta S_i^z S_{i+1}^z \right), \quad \theta(t) = \begin{cases} \theta & (t < 0) \\ 0 & (t \geq 0) \end{cases}. \quad (2.19)$$

The protocol of quench is drawn in Fig. 2.3. At first ( $t < 0$ ), the system is taken to be the ground state. Suddenly the flux is turned off at  $t = 0$ , and then the system starts evolving in time. If we regard<sup>2</sup>  $-\theta$  as a vector potential for spinless fermions, changing the vector potential in time is equivalent to imposing electric field to fermions. In our quench protocol, the electric field is delta function,

$$E(t) = -\frac{d(-\theta(t))}{dt} = -\theta\delta(t). \quad (2.20)$$

Therefore, at  $t = 0$  the (spin) current is induced by the flux quench.

Equivalently, we can regard initial spin current at  $t = 0$  as a persistent current in the ground state of the XXZ chain with flux. This is manifested in the spinless fermion picture. As we discussed in the last section, when initial flux  $\phi = \theta N$  is zero in modulo  $2\pi$  the ground state of pre-quench Hamiltonian is written as  $U_\theta |\theta = 0\rangle_{\text{GS}}$ . Recalling that  $U_\theta$  acts on fermion operators as a boost in momentum space, we know that  $U_\theta |\theta = 0\rangle_{\text{GS}}$

<sup>2</sup> In a standard notation, a vector potential  $A$  is defined as  $H_A \approx H_{A=0} - Aj$  ( $j$  is current operator). In our case  $H_\theta = H_0 + \theta \sum_i j_i + O(\theta^2)$ , and therefore we define the vector potential as  $-\theta$ .

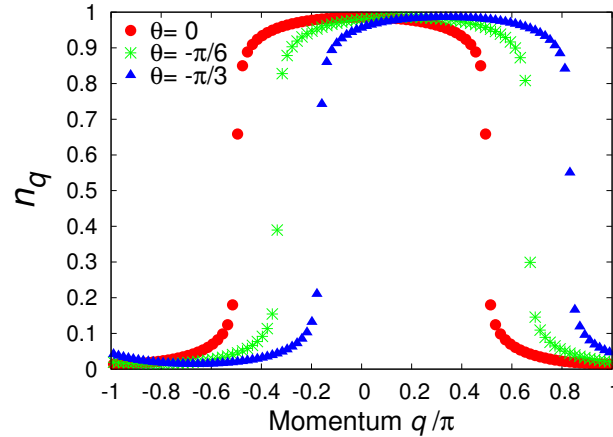


Figure 2.4: Initial momentum distribution  $n_q = \langle \tilde{c}_q^\dagger \tilde{c}_q \rangle$ .

is the *shifted* Fermi sea by momentum  $-\theta$  (initial momentum distribution  $n_q = \langle \tilde{c}_q^\dagger \tilde{c}_q \rangle$  is shown in Fig. 2.4). Since the (spin) current is given by  $\langle \hat{J} \rangle = N^{-1} \sum_q \sin(q) n_q$ , the shifted Fermi sea has non-zero persistent current, which is the origin of initial current of the flux quench.

In this study, we investigate the dynamics of spin current after the flux quench by numerical calculations. We focus on two points:

- (i) What is the fate of spin current in the long-time limit? As we will see below, from linear response theory in  $\theta$  the long-time limit of the current is given by the Drude weight of the XXZ chain. How dose nonlinearity appear for large  $\theta$ ?
- (ii) How is the dynamics after the quench? In gapless phase there is no *a priori* energy (or time) scales. What determines the time scale of the dynamics?

The main results of our study are presented in chapter 4. In the rest part of this section, we discuss possibilities of experimental realizations of the flux quench and the analysis by linear response theory on the flux quench.

### Experimental realizations of the flux quench

Before going to analyze the flux quench by linear response theory, we comment on possible experimental realizations of the flux quench. The flux quench can be viewed as a shift of momentum at  $t = 0$  in the spinless fermion picture. Therefore, it is equivalent to a situation where a moving lattice (its velocity gives an initial shift of momentum) stops suddenly at  $t = 0$ . This quench process was experimentally realized [27] in bosonic optical lattice. As for bosonic optical lattice, a quantum quench of artificial gauge field is also proposed [28]. This is a more direct realization of the flux quench (although it is a bosonic system). We expect that these kinds of quench will be performed for fermionic optical lattice in the near future. Furthermore, recently a optical lattice system which is equivalent to the Heisenberg chain ( $\Delta = 1$ ) was realized and an experiment

on nonequilibrium transports in the chain was done [29]. Considering these substantial experimental developments, we are optimistic about realizing our flux quench in optical lattice systems. We hope it provides us information that cannot be obtained by the numerical approach employed in this thesis.

### 2.2.1 Analysis by linear response theory and the Drude weight

When  $\theta$  is small, a term  $e^{i\theta}$  can be expanded as  $e^{i\theta} = 1 + i\theta + O(\theta^2)$ . Hamiltonian for the flux quench problem can be written as

$$H(t) \approx H_\theta - \theta JN\Theta(t), \quad (2.21)$$

where  $\Theta(t)$  is step function. We can employ linear response (LR) theory in  $\theta$  and obtain  $J(t) := \langle \hat{J}(t) \rangle$ ,

$$J(t) = \frac{1}{2\pi} \int_{-\infty}^{\infty} d\omega F(\omega) \sigma(\omega) e^{-i\omega t} + O(\theta^2), \quad (2.22)$$

where  $F(\omega) = -\theta$  is Fourier transformation of the imposed electric field  $E(t) = -\theta\delta(t)$  and  $\sigma(\omega)$  is spin conductivity<sup>3</sup>

$$\sigma(\omega) = \frac{N}{\omega} \int_0^{\infty} dt e^{i\omega t} \langle [\hat{J}(t), \hat{J}] \rangle_{\text{GS},0}. \quad (2.23)$$

Here  $\langle \dots \rangle_{\text{GS},0}$  means the expectation value for the ground state of  $H_0$ . The spin conductivity has anomalous zero-frequency component and it is called the Drude weight:

$$\sigma(\omega) = 2\pi D\delta(\omega) + \sigma_{\text{reg}}(\omega). \quad (2.24)$$

Thus the long-time limit of the current is given by  $D$  (we take  $\theta < 0$  in this study),

$$J(t = \infty) = -D\theta = D|\theta|. \quad (2.25)$$

The Drude weight  $D$  is related to change of the ground state energy as inserting small flux  $\Phi$  into the system, and was calculated exactly by the Bethe ansatz techniques [23],

$$D = \frac{\pi}{4} \frac{\sin \mu}{\mu(\pi - \mu)}, \quad \mu = \arccos(-\Delta). \quad (2.26)$$

$D$  is non-zero only for  $-1 \leq \Delta < 1$ . In gapped phase ( $|\Delta| > 1$ ) and  $\Delta = 1$ ,  $D$  is zero. Hence LR theory predicts that  $J(t = \infty)$  is non-zero only for  $-1 \leq \Delta < 1$ .

## 2.3 Previous studies

In this section, we review previous studies related to our flux quench, although motivations and setups of those studies are different from ours. We introduce two kinds of studies related to our problem; One is about the long-time limit of the current. The other is about a bosonic version of flux quench in the context of dynamical stability of superfluid.

<sup>3</sup> Non-perturbative Hamiltonian for LR theory in this case is  $H_\theta$ , not  $H_0$ . Therefore expectation values in LR formula should be taken for the ground state of  $H_\theta$ . However, in  $O(\theta)$  level we can obtain the same results if expectation values are taken for the ground state of  $H_0$ .

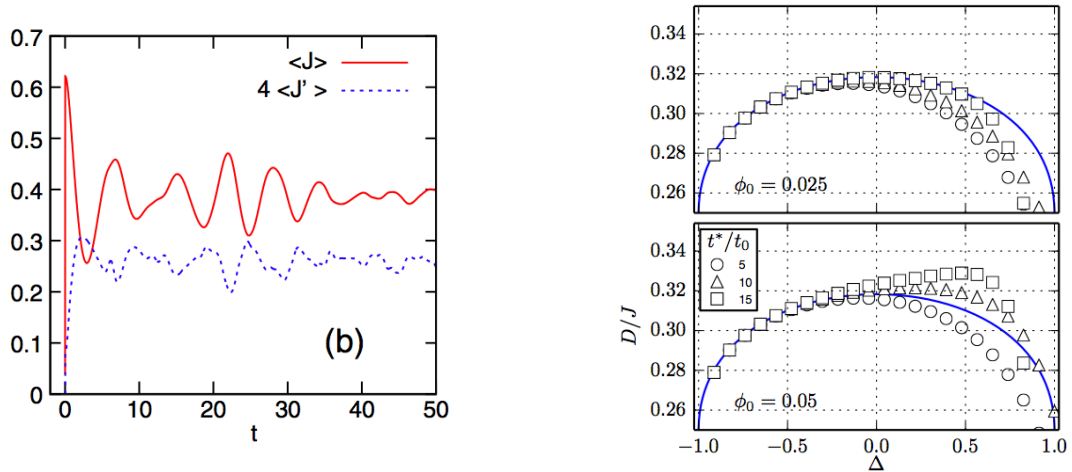


Figure 2.5: Left panel: The spin current after the flux quench for  $\theta = -\pi/2, \Delta = -0.5$  (red line). Note that in their notation the time scale and definition of the current is twice as ours. They used time-dependent Lanczos method for  $L = 26$  system [6]. Right panel: Estimation of the Drude weight by numerical data  $J(t)$  ( $t^*/t_0$  is the time at which estimation was done and  $\phi_0$  is initial flux). Blue line shows exact values of the Drude weight. Note that their definition of  $\Delta$  is different from ours by sign.  $\Delta > 0$  in the figure corresponds to  $\Delta < 0$  in our notation. They used time-dependent DMRG for  $L = 100$  system [28].

### 2.3.1 Previous studies on the long-time limit of the current

Mierzejewski *et al.* [6] studied the flux quench in spinless fermion formulation, exactly the same as our setup, to illustrate the breakdown of GGE. They showed that steady states after the flux quench cannot be described by GGE. This result is the first example that clearly denies GGE, and quite seminal for understanding the thermalization phenomena in integrable systems. Their argument was simple; conserved quantities  $Q_i$  contained in GGE ( $\rho_{\text{GGE}} \propto \exp(-\beta H - \sum_i \lambda_i Q_i)$ ) for the XXZ chain have even parity under the particle-hole transformation ( $c_i \rightarrow (-1)^i c_i^\dagger$ ). The spin current  $\hat{J}$  has odd parity under the same transformation. Therefore the expectation value of the spin current for any GGE must be zero,  $\text{Tr}(\rho_{\text{GGE}} \hat{J}) = 0$ . Nevertheless, as LR theory predicts and numerically verified by the authors, the long-time limit  $J(t = \infty)$  is obviously non-zero in some cases (left panel of Fig. 2.5). This is a clear illustration of the breakdown of GGE. The steady states after the flux quench cannot be expressed by GGE as well as Gibbs (thermal) states. From the viewpoint of our motivations for the flux quench, we comment that they did not study  $J(t = \infty)$  systematically varying  $\theta$  and  $\Delta$ .

Moreover, a recent publication [28] mainly studying the flux quench in the Bose-Hubbard model mentioned the long-time limit of the current in the XXZ chain. They dealt with the flux quench in the XXZ chain as a special limit of the Bose-Hubbard model. They plotted (right panel of Fig. 2.5) estimation of the Drude weight from numerical data  $J(t)$  at late times (we do not show the details here). If LR theory is exact, all points in the plot must be on the line. The deviation from the line (LR theory) is large for  $\Delta > 0$  (in our notation,  $\Delta < 0$ ). They argued that this tendency is due to a finite-size effect of

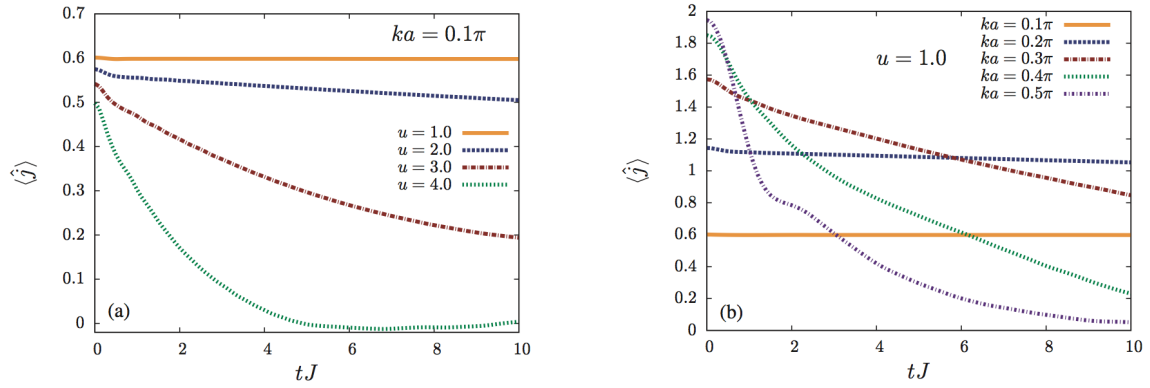


Figure 2.6: The spin current after the flux quench in one-dimensional Bose-Hubbard model [30]. They used iTEBD.

simulations and no further discussion was made. As we will see in section 4.2, we confirm this tendency but claim that the origin is not a finite-size effect; it is an intrinsic behavior of the system relating to superfluidity of the system.

### 2.3.2 Bosonic flux quench

Dynamics of the Bose-Hubbard model has been studied extensively because of its direct experimental realizations by optical lattices. In this context, the stability of currents in superfluid regime of the Bose-Hubbard model has been theoretically and experimentally investigated. The authors of Ref. [30] considered a problem of abrupt momentum boost (equivalent to quench of flux) for the ground state of one-dimensional Bose-Hubbard model,

$$H_{\text{BH}} = -J \sum_i (b_i^\dagger b_{i+1} + b_{i+1}^\dagger b_i) + \frac{U}{2} \sum_i n_i(n_i - 1). \quad (2.27)$$

$b_i$  is an annihilation operator of boson on site  $i$ ,  $n_i = b_i^\dagger b_i$  is the number of boson on site  $i$ . Definition of the current operator is the same as in our spinless fermion case,

$$j_i = \frac{J}{i} (b_{i+1}^\dagger b_i - b_i^\dagger b_{i+1}). \quad (2.28)$$

They took initial state as the boosted ground state of  $H_{\text{BH}}$  by momentum  $ka$ . The momentum  $ka$  corresponds to  $\theta$  in our flux quench problem. The dynamics they obtained is shown in Fig. 2.6. For small momentum  $ka$  and small interaction  $u = U/J$ , the current decays slowly and sometimes remains non-zero in the long-time limit. The behaviors of the current are similar to our results, although the model under investigation has different particle statistics (boson and spinless fermion). Besides, there are no oscillations in the dynamics of bosonic current, in contrast to our results. We will see other results of bosonic flux quench in section 4.4 to discuss the relaxation time of the current.

# Chapter 3

## Numerical Methods

We employ infinite Time-Evolving Block Decimation (iTEBD) method for numerical calculations in this study. In this chapter, we review numerical methods. The iTEBD is based on matrix product states (MPS), a kind of tensor networks. An overview of tensor networks is given in the first section. In the second section, background of tensor networks is reviewed. For a comprehensive and pedagogical review of tensor networks, see Ref. [31]. In the third section, the basics of matrix product states with some detailed proofs are presented. In the last two sections, Time-Evolving Block Decimation (TEBD) method and iTEBD method are explained. This chapter is almost independent of other contents in this thesis, so readers who are not interested in details of numerical methods can skip here.

### 3.1 Introduction

Quantum many-body systems are at the heart of studies in condensed matter physics. Interactions and correlations between a single degree of freedom (particles, spins, etc.) evoke interesting phenomena which cannot be attributed to the property of such a single constituent: for example, superconductivity, fractional quantum Hall effect, non-Fermi liquids and quantum spin liquids. In order to study these phenomena, a simple model is often proposed, such as Hubbard model for superconductivity or Heisenberg model for quantum magnets and spin liquids. However, it is far difficult to solve these models exactly, except for very limited examples. Therefore one often resorts to take numerical approaches to see the nature of these models. Nevertheless, numerical calculations have limitations, too. Exponential growth in a dimension of Hilbert space with a system size restricts available numerical calculations for large systems. For example, the dimension of Hilbert space of  $N$  site lattice model containing  $M$  spinless fermions is

$$\dim \mathcal{H} = \binom{N}{M} = \frac{N!}{M!(N-M)!}, \quad (3.1)$$

which is exponentially large in  $N$  for a fixed particle density  $M/N$ . There are many analytical and numerical methods to overcome this difficulty: mean-field theory, perturbative expansions and diagrammatic techniques, renormalization group, dynamical mean-field theory, quantum Monte Carlo, and so on. All of these methods have advantages and

disadvantages. For example, quantum Monte Carlo can deal with larger system size than exact diagonalization can, although the so-called negative sign problem [32] prevents us from applying the method to frustrated quantum magnets and fermionic systems.

Tensor network methods are one kind of approaches to tackle the problem of large dimension of Hilbert space. They do not have the negative sign problem and can be applied to bosonic, fermionic and spin systems in an almost same way<sup>1</sup>. One important concept in tensor networks is *entanglement*. If given quantum state has a small amount of entanglement, tensor networks can express it by a smaller amount of information compared with a usual expression using wave function. *Area law of entanglement entropy* assures that the ground states of Hamiltonian which we often deal with have smaller amounts of entanglement than the vast majority of states in Hilbert space. Tensor network methods have obvious criteria for their applicability, and the error in computation can be estimated in a clear way (especially for one-dimensional systems).

Famous examples of tensor network methods are density matrix renormalization group (DMRG) [14], time-evolving block decimation (TEBD) [15], projected entangled pair states (PEPS) [34] and multi-scale entanglement renormalization ansatz [35]. DMRG, proposed by S. White in 1992 [14], is one of the most successful numerical methods for one-dimensional quantum systems. Although DMRG was proposed independently from the notion of tensor networks, the close relationship between them was realized later (for a review, see Ref. [36]).

Finally, it should be stressed that tensor networks are not only numerical approaches but also conceptually new tools to understand quantum phases. Recently, quantum phases which cannot be classified in terms of Landau's symmetry breaking were noticed and named topological ordered phases [37, 38]. Symmetry protected topological phases, one variant of topological ordered phases, can be classified by MPS and PEPS (one-dimensional and two-dimensional version of tensor networks) [39–41].

## 3.2 Tensor networks

In tensor network methods, a wave function of quantum state is regarded as a large-rank (many legs) tensor and expressed as contracted sum of many small-rank tensors. One of the advantages of the tensor network methods is efficiency for expressing quantum states. In this section, we first introduce the notation and diagrammatic representation of tensor networks by taking a toy example of tensor network. Next, the area law of entanglement entropy, which is the most important fact behind tensor networks, is explained. Finally, the relationship between tensor network states and area-law states is discussed.

### 3.2.1 Basics of tensor networks

Consider rank-4 tensor  $A_{\alpha\beta\gamma\delta}$  as a simple toy example of tensor networks. Indices  $\alpha \dots \delta$  run from 1 to  $\chi$ .  $\chi$  is called the bond dimension<sup>2</sup> and can be different for each index of the

<sup>1</sup> Tensor networks for fermionic systems have a problem of sign originating from order of fermion creation operators. However it is not so serious as the negative-sign problem in quantum Monte Carlo [33].

<sup>2</sup> In DMRG literature, the bond dimension is written as  $m$  or  $D$ . In TEBD literature,  $\chi$  is usually used.

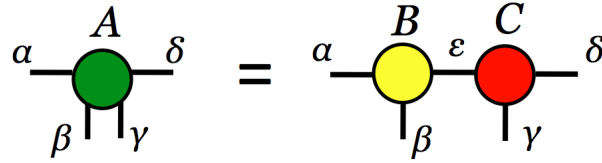


Figure 3.1: Diagrammatic representation of Eqn. (3.2).

tensor (for simplicity here we make  $\chi$  the same among indices). Assume that the tensor  $A$  is decomposed into two rank-3 tensors  $B$  and  $C$ ,

$$A_{\alpha\beta\gamma\delta} = \sum_{\epsilon=1}^{\tilde{\chi}} B_{\alpha\beta\epsilon} C_{\epsilon\gamma\delta}. \quad (3.2)$$

We introduce a diagrammatic representation for calculations in tensor networks, because it is helpful to understand complicated equations with many indices. Equation (3.2) is diagrammatically written as Fig. 3.1. Tensors are expressed in diagrams such as circles and the number of legs shows the rank of the tensor.

Let us consider this decomposition from the viewpoint of an amount of information.  $A_{\alpha\beta\gamma\delta}$  has  $\chi^4$  components, while  $B_{\alpha\beta\epsilon}$  and  $C_{\epsilon\gamma\delta}$  have  $\tilde{\chi}\chi^2$  components. If new bond dimension  $\tilde{\chi}$  is equal<sup>3</sup> to  $\chi$ , the number of components to describe the right hand side of Eqn. (3.2) is  $\chi^3 + \chi^3 = 2\chi^3$ . Hence when  $\chi$  is large, the expression in the right hand side of Eqn. (3.2) is more efficient than the left hand side (*raw* tensor) in terms of the amount of information required to store the tensors. This is an illustration of one of the advantages of tensor networks.

In tensor network methods, we decompose a wave function of a quantum state (it is a rank- $L$  tensor when system size is  $L$ ) into many small-rank tensors as in the previous toy example. That decomposition can greatly reduce the required memory storage and computational cost in numerical calculations. When attempting to use decompositions like the previous example for general wave functions in Hilbert space, one may pose these questions:

- (a) how to calculate decompositions for general wave functions and obtain tensor network descriptions of them?
- (b) in which conditions the bond dimension of small-rank tensors decomposing a wave function is small so as to make the tensor network description efficient?

For one-dimensional systems, we will answer both questions in section 3.3. For general dimensions we discuss only the latter question in the rest part of this section. The answer of the latter question is *entanglement* of a quantum state to be represented in tensor networks.

<sup>3</sup> In general,  $\tilde{\chi}$  becomes larger than  $\chi$ . As we will see later, the condition in which we can obtain small bond dimension  $\tilde{\chi}$  is related to entanglement of a tensor to be decomposed.

### 3.2.2 Entanglement entropy and area law

As we will see in section 3.3, the bond dimension  $\chi$  of tensor network methods can be estimated by entanglement entropy of a state to be expressed. Entanglement entropy is one of the most famous measures of entanglement in quantum systems. In this subsection, we show the definition of entanglement entropy and introduce the area law of entanglement entropy.

Consider a system whose Hilbert space  $\mathcal{H}$  can be written as a tensor product of Hilbert spaces of two subsystems  $A$  and  $\bar{A}$ ,  $\mathcal{H} = \mathcal{H}_A \otimes \mathcal{H}_{\bar{A}}$ . For lattice systems, it is always possible to do this decomposition. Entanglement entropy  $S_A$  of a pure state  $|\psi\rangle \in H$  is defined as

$$S_A := -\text{Tr}_A(\rho_A \ln \rho_A), \quad (3.3)$$

where  $\rho_A = \text{Tr}_{\bar{A}}(|\psi\rangle\langle\psi|)$  is the reduced density matrix of subsystem  $A$ . Entanglement entropy is von-Neumann entropy of the reduced density matrix  $\rho_A$ ; this means that the entanglement entropy  $S_A$  quantifies information contained in  $\rho_A$ . If two subsystems  $A$  and  $\bar{A}$  are entangled, tracing out the subsystem  $\bar{A}$  reduces the information in the subsystem  $A$  and then  $S_A$  becomes large. This is why entanglement entropy is a measure of entanglement.

Next we introduce the area law of entanglement entropy. This law assures that tensor networks can be useful to represent the ground states of Hamiltonians that we often encounter.

**Area law of entanglement entropy (review: [42])** *Consider a lattice system. Ground states of gapped, local Hamiltonians satisfy*

$$S_A \sim \text{const.} \cdot |\partial A| + o(|\partial A|), \quad (3.4)$$

where  $S_A$  is entanglement entropy for subsystem  $A$  and  $|\partial A|$  is the area of boundary of  $A$ ,  $\partial A$ . By local we mean that supports of each term in the Hamiltonian are finite, not scaling as system size  $L$ . Furthermore, in one-dimensional systems, the ground states of gapless and local Hamiltonians also exhibit area law with logarithmic corrections,

$$S_A \sim \text{const.} \cdot |\partial A| \ln(|A|) + O(|\partial A|). \quad (3.5)$$

A physical interpretation of the area law is following. The correlation length  $\xi$  of the ground state of gapped and local Hamiltonian is finite [43]. Then each site of the system cannot be entangled over the distance  $\xi$ , which means that entanglement between two subsystems  $A$  and  $\bar{A}$  is mostly carried by the interface of them (Fig. 3.2). Therefore,  $S_A$  is roughly estimated to be proportional to  $|\partial A|$ . There are rigorous proofs for the area law in one-dimensional quantum systems under some conditions [44]. For higher-dimensional systems, rigorous results are limited.

Since we mainly consider one-dimensional systems in this thesis, let us explain the area law in one dimension more concretely. Consider a  $L$  site lattice system (chain) in one dimension and a gapped and local Hamiltonian on it. The area law implies that entanglement entropy of the ground state for a half chain (one half of the system) does not scale as system size  $L$ ,

$$S_{\text{half chain}} \sim O(1), \quad (3.6)$$

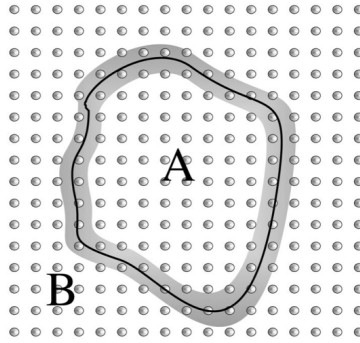


Figure 3.2: Division of a lattice system into two subsystems  $A$  and  $B = \bar{A}$ . If the correlation length  $\xi$  is finite, only the sites close to the boundary of  $A$  within the distance  $\xi$  (shaded area) can contribute to the entanglement between  $A$  and  $\bar{A}$ . Therefore the entanglement entropy  $S_A$  is roughly proportional to the size of boundary  $|\partial A|$ . Figure is taken from Ref. [45].

even though the size of the half chain scales as  $L/2$ . As we will see in section 3.3, this result greatly affects applicability of tensor networks in one dimension. For gapless Hamiltonian, the area law indicates  $S_{\text{half chain}} \sim \ln(L)$ . Moreover, we can exploit conformal field theory to calculate entanglement entropy for this case; the result is [46]

$$S_{\text{half chain}} \sim \frac{c}{6} \ln L, \quad (3.7)$$

where  $c$  is the central charge of conformal field theory describing the critical (gapless) ground state.

### 3.2.3 Ground states are well expressed by tensor networks

In addition to the area law, it is known [47] that if we randomly choose a state in Hilbert space the state has entanglement entropy which obeys *volume law*,  $S_A \sim |A|$ , with probability one. In other words, almost all of the states in Hilbert space obey the volume law of entanglement entropy. Therefore, the ground state of gapped and local Hamiltonian, which obeys the area law, sits on the very tiny corner of the Hilbert space (Fig. 3.3). Furthermore, it is proved [48] that the amount of quantum many-body states that can be generated by arbitrary time-dependent local Hamiltonians in a time that scales polynomially in the system size is exponentially small in Hilbert space. The vast majority of states in Hilbert space is not physical or reachable in this sense. Considering these two facts, we can say that the whole Hilbert space is *too large* to describe the physics around the ground state.

Tensor network states with constant (not scaling as system size) bond dimensions exhibit the area law (although we do not show a explanation [31] here). Hence they are good candidates to describe states around the ground states. Actually, it is proved [45, 49] that tensor network states with constant bond dimensions can express states around the ground states efficiently. This is an important conceptual point of tensor network methods.

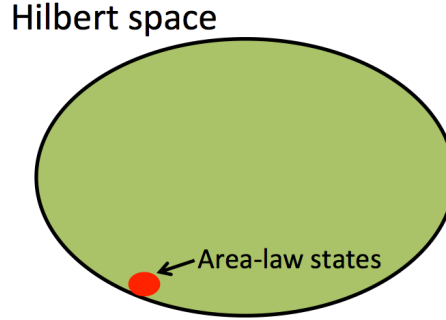


Figure 3.3: Almost all of the states in Hilbert space obey the volume law. States which exhibit area law (including the ground state) occupy a tiny amount of Hilbert space. Tensor network states can describe such area-law states efficiently.

### 3.3 Matrix product states (MPS)

MPS is a kind of tensor networks for one-dimensional quantum systems. MPS is a basis of two successful numerical methods for one-dimensional quantum systems, DMRG and (i)TEBD. In this section, we review MPS. First we define MPS and introduce Schmidt value decomposition, which is important to understand the structure of MPS. Next we show that any pure state in a finite lattice system can be expressed in a MPS form. Then canonical conditions of MPS are stated and calculations of physical quantities in MPS language are described. We show examples of MPS in the last part of this section.

Let us consider a lattice system of  $L$  site whose Hilbert space consists of  $L$  times tensor product of local Hilbert space,  $\mathcal{H} = \mathbb{C}^d \otimes \mathbb{C}^d \otimes \dots \otimes \mathbb{C}^d = (\mathbb{C}^d)^{\otimes L}$ . The basis of local Hilbert space is written as  $\{|i\rangle\}_{i=1}^d$  and  $d$  is called the local dimension. For spin- $S$  systems,  $\{|i\rangle\} = \{|s^z = -S\rangle, \dots, |s^z = S\rangle\}$  and  $d = 2S + 1$ . For spinless fermion systems,  $\{|i\rangle\} = \{|0\rangle, |1\rangle\}$  and  $d = 2$ . For bosonic systems,  $\{|i\rangle\} = \{|0\rangle, |1\rangle, \dots\}$  and  $d = \infty$  (we set the cut-off  $d_{\max}$  on  $d$  in actual numerical calculations). Given pure state  $|\psi\rangle$  in this system can be expressed by a wave function  $c_{i_1 i_2 \dots i_L}$ ,

$$|\psi\rangle = \sum_{i_1 i_2 \dots i_L=1}^d c_{i_1 i_2 \dots i_L} |i_1 i_2 \dots i_L\rangle. \quad (3.8)$$

Here,  $|i_1 i_2 \dots i_L\rangle$  is a tensor product of the basis of local Hilbert space and constitutes the complete orthonormal basis of  $\mathcal{H}$ . Matrix product state  $\{\Gamma, \lambda\}$  for  $|\psi\rangle$  is defined<sup>4</sup> as

$$|\psi\rangle = \sum_{i_1 i_2 \dots i_L}^d \sum_{\alpha_1 \dots \alpha_{L-1}=1}^{\chi_i} \Gamma_{\alpha_1}^{[1]i_1} \lambda_{\alpha_1}^{[1]} \Gamma_{\alpha_1 \alpha_2}^{[2]i_2} \lambda_{\alpha_2}^{[2]} \dots \Gamma_{\alpha_{L-2} \alpha_{L-1}}^{[L-1]i_{L-1}} \lambda_{\alpha_{L-1}}^{[L-1]} \Gamma_{\alpha_{L-1}}^{[L]i_L} |i_1 i_2 \dots i_L\rangle. \quad (3.9)$$

<sup>4</sup> There are two major notations of MPS. We used  $\Gamma\lambda$ -notation here. The other notation is  $A$ -notation

$$|\psi\rangle = \sum_{i_1 i_2 \dots i_L}^d \sum_{\alpha_1 \dots \alpha_{L-1}}^{D_i} A_{\alpha_1}^{[1]i_1} A_{\alpha_1 \alpha_2}^{[2]i_2} \dots A_{\alpha_{L-2} \alpha_{L-1}}^{[L-1]i_{L-1}} A_{\alpha_{L-1}}^{[L]i_L} |i_1 i_2 \dots i_L\rangle,$$

which is often used in the DMRG literature.

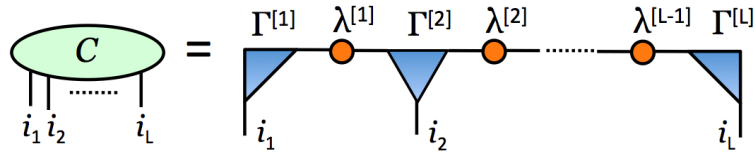


Figure 3.4: A diagrammatic representation of MPS.

This seems complicated at first sight, but a diagrammatic representation in Fig. 3.4 is helpful to understand the structure of tensors. Note that the bond dimension  $\chi_i$  depends on site  $i$ . If we regard tensors  $\Gamma_{\alpha_{l-1}\alpha_l}^{[l]i_l}$  as  $\chi_{l-1} \times \chi_l$  matrices and  $\lambda_{\alpha_l}^{[l]}$  as  $\chi_l \times \chi_l$  diagonal matrices for each  $i_l$  ( $\Gamma_{\alpha_1}^{[1]i_1}$  and  $\Gamma_{\alpha_{L-1}}^{[L]i_L}$  as  $1 \times \chi_{1(L-1)}$  vectors),  $|\psi\rangle$  can be written as the sum of products of matrices,

$$|\psi\rangle = \sum_{i_1 i_2 \dots i_L} \left( \vec{\Gamma}_{\alpha_1}^{[1]i_1} \right)^T \hat{\lambda}^{[1]} \hat{\Gamma}^{[2]i_2} \hat{\lambda}^{[2]} \dots \hat{\Gamma}^{[L-1]i_{L-1}} \hat{\lambda}^{[L-1]} \vec{\Gamma}_{\alpha_L}^{[L]i_L} |i_1 i_2 \dots i_L\rangle. \quad (3.10)$$

This is the origin of the name *Matrix Product States*.

One of the advantages of using MPS representations for quantum states is that MPS requires the smaller number of parameters than the usual wave function descriptions  $c_{i_1 i_2 \dots i_L}$  do. In order to retain the information of wave function  $c_{i_1 i_2 \dots i_L}$ ,  $d^L \sim \exp(L)$  parameters are needed. On the other hand, at most  $d\chi^2 L + L\chi$  parameters are needed to store the tensors  $\Gamma$  and  $\lambda$  of MPS ( $\chi := \max_i(\chi_i)$ ). The value  $\chi$  determines efficiency of MPS. As we will discuss later,  $\chi$  is roughly estimated by the entanglement entropy of  $|\psi\rangle$ . For general states in Hilbert space, or volume-law states,  $\chi$  scales as  $\exp(L)$  and two representations (wave functions and MPS) are equivalent in terms of the amount of information required to express the states. However, for the ground state of local Hamiltonian in one dimension, or area-law states,  $\chi$  does not scale as  $L$  (in gapped systems) or scales as polynomials of  $L$  (in gapless systems). In both cases, we can bound  $d\chi^2 L + L\chi \lesssim \text{poly}(L)$ . This is far smaller than  $\exp(L)$ , and therefore MPS is more efficient than the wave functions to express the ground state of local Hamiltonian.

### 3.3.1 Schmidt decomposition

Schmidt decomposition of a state in Hilbert space is essential to construct (canonical) MPS representations for general quantum states. In order to define Schmidt decomposition, we first introduce singular value decomposition for general matrices [50, §2.5].

**Singular Value Decomposition (SVD).** *Let  $M$  be a  $m_1 \times m_2$  matrix. Singular value decomposition of  $M$  is defined as*

$$M = USV, \quad (3.11)$$

where  $U$  and  $V$  are  $m_1 \times \min(m_1, m_2)$  and  $\min(m_1, m_2) \times m_2$  matrices which satisfy  $U^\dagger U = 1$  and  $VV^\dagger = 1$ ,  $S$  is  $\min(m_1, m_2) \times \min(m_1, m_2)$  diagonal matrix with non-negative diagonal elements  $S_\alpha \geq 0$ .  $S$  is unique up to permutation of the diagonal elements. When

$m_1 = m_2$ ,  $UU^\dagger = 1$  and  $V^\dagger V = 1$  also hold and  $U$  and  $V$  are unitary matrices.

Diagonal elements of  $S$  are called singular values of matrix  $M$ . We can define  $\{S_\alpha\}$  in descending order and omit zero(s)<sup>5</sup> from them,  $S_1 \geq S_2 \geq \dots \geq S_\chi > 0$ .  $\chi$  depends on matrix  $M$  and satisfies  $1 \leq \chi \leq \min(m_1, m_2)$ . Then we can write down SVD as

$$M_{ij} = \sum_{\alpha=1}^{\chi} U_{i\alpha} S_\alpha V_{\alpha j}, \quad S_\alpha > 0. \quad (3.12)$$

We will use this notation of SVD in the following.

By using SVD, we define Schmidt decomposition of a state  $|\psi\rangle$ . Let  $\{|i\rangle_A\}_{i=1}^{d_A}$  and  $\{|j\rangle_B\}_{j=1}^{d_B}$  be complete orthonormal bases of two subsystems  $A$  and  $B$ , where  $A \cup B$  is equal to a total system.  $|\psi\rangle$  can be expanded as

$$|\psi\rangle = \sum_{i,j=1}^{d_A, d_B} c_{ij} |i\rangle_A |j\rangle_B. \quad (3.13)$$

Coefficient matrix  $c_{ij}$  is decomposed by SVD as

$$c_{ij} = \sum_{\alpha=1}^{\chi} U_{i\alpha} \lambda_\alpha V_{\alpha j}, \quad \lambda_\alpha > 0. \quad (3.14)$$

Here we write the singular values as  $\lambda$ . Putting this decomposition into Eqn. (3.13), one obtains

$$|\psi\rangle = \sum_{i,j=1}^{d_A, d_B} \sum_{\alpha=1}^{\chi} U_{i\alpha} \lambda_\alpha V_{\alpha j} |i\rangle_A |j\rangle_B = \sum_{\alpha=1}^{\chi} \lambda_\alpha |\alpha\rangle_A |\alpha\rangle_B, \quad (3.15)$$

where

$$|\alpha\rangle_A := \sum_{i=1}^{d_A} U_{i\alpha} |i\rangle_A, \quad |\alpha\rangle_B := \sum_{j=1}^{d_B} V_{\alpha j} |j\rangle_B. \quad (3.16)$$

$|\psi\rangle = \sum_{\alpha=1}^{\chi} \lambda_\alpha |\alpha\rangle_A |\alpha\rangle_B$ ,  $\{|\alpha\rangle_{A,B}\}$  and  $\{\lambda_\alpha\}$  are called Schmidt decomposition, Schmidt vectors and Schmidt values, respectively. Because of the conditions  $U^\dagger U = 1$  and  $V V^\dagger = 1$ ,  $\{|\alpha\rangle_{A,B}\}_{\alpha=1}^{\chi}$  are orthonormal ( $\langle\alpha|\beta\rangle_{A,B} = \delta_{\alpha\beta}$ ). From this property,  $\sum_{\alpha} (\lambda_\alpha)^2 = \langle\psi|\psi\rangle = 1$  follows if the state  $|\psi\rangle$  is normalized. Besides, the reduced density matrix  $\rho_A$  is written down in a simple form,

$$\rho_A = \text{Tr}_B (|\psi\rangle \langle\psi|) = \text{Tr}_B \left( \sum_{\alpha,\beta} \lambda_\alpha \lambda_\beta^* |\alpha\rangle_A |\alpha\rangle_B \langle\beta|_A \langle\beta|_B \right) = \sum_{\alpha} (\lambda_\alpha)^2 |\alpha\rangle_A \langle\alpha|_A. \quad (3.17)$$

Entanglement entropy  $S_A$  is

$$S_A = -\text{Tr}_A (\rho_A \ln \rho_A) = -\sum_{\alpha} (\lambda_\alpha)^2 \ln (\lambda_\alpha)^2. \quad (3.18)$$

<sup>5</sup> Here we assume  $M \neq 0$ .

## Chapter 3. Numerical Methods

Note that Schmidt value decomposition depends on the way of dividing total Hilbert space.

The number of Schmidt values,  $\chi$ , reflects the quantum nature of  $|\psi\rangle$ . When  $\chi = 1$ ,  $|\psi\rangle$  is a direct product of two states in each subsystem and can be considered as classical.  $\chi > 1$  means that two subsystems  $A$  and  $B$  are entangled and that  $|\psi\rangle$  cannot be written as a classical direct product of two states. If two subsystems are maximally entangled,  $\chi = \min(d_A, d_B)$ ,  $\lambda_\alpha \equiv 1/\sqrt{\chi}$  and  $S_A = \ln(\chi)$ . Conversely, when we fix  $\chi$ , the states written in the form of Schmidt decomposition (3.15) can represent states that have entanglement entropy  $S_A = \ln \chi$  at most. This argument implies a rough relation<sup>6</sup> between  $\chi$  and  $S_A$ ,

$$\chi \sim e^{S_A}. \quad (3.19)$$

### 3.3.2 Construction of MPS for arbitrary states in a system

To prove that any quantum state can be expressed in a MPS form, we repeatedly apply SVD to a wave function of a state. Given quantum state  $|\psi\rangle$  can be expanded as

$$|\psi\rangle = \sum_{i_1 i_2 \cdots i_L} c_{i_1 i_2 \cdots i_L} |i_1 i_2 \cdots i_L\rangle. \quad (3.20)$$

As a first step, we regard  $i_2 \cdots i_L$  as one index and perform SVD for matrix  $c_{i_1, (i_2 \cdots i_L)}$ :

$$c_{i_1, (i_2 \cdots i_L)} \stackrel{\text{SVD}}{=} \sum_{\alpha_1=1}^{\chi_1} U_{i_1 \alpha_1}^{[1]} \lambda_{\alpha_1}^{[1]} V_{\alpha_1 (i_2 \cdots i_L)}^{[1]} =: \sum_{\alpha_1=1}^{\chi_1} \Gamma_{\alpha_1}^{[1] i_1} \lambda_{\alpha_1}^{[1]} V_{\alpha_1 (i_2 \cdots i_L)}^{[1]}. \quad (3.21)$$

This is actually Schmidt decomposition of  $|\psi\rangle$  for the subsystem of site 1 and the subsystem of site  $[2 \cdots L]$ ,

$$\begin{aligned} |\psi\rangle &= \sum_{i_1 i_2 \cdots i_L} c_{i_1 i_2 \cdots i_L} |i_1 i_2 \cdots i_L\rangle = \sum_{i_1 \cdots i_L \alpha_1} \Gamma_{\alpha_1}^{[1] i_1} \lambda_{\alpha_1}^{[1]} V_{\alpha_1 (i_2 \cdots i_L)}^{[1]} |i_1\rangle |i_2 \cdots i_L\rangle \\ &= \sum_{\alpha_1=1}^{\chi_1} \lambda_{\alpha_1}^{[1]} |\tau_{\alpha_1}^{[1]}\rangle |\tau_{\alpha_1}^{[2 \cdots L]}\rangle, \end{aligned} \quad (3.22)$$

where

$$|\tau_{\alpha_1}^{[1]}\rangle := \sum_{i_1} \Gamma_{\alpha_1}^{[1] i_1} |i_1\rangle, \quad |\tau_{\alpha_1}^{[2 \cdots L]}\rangle := \sum_{i_2 \cdots i_L} V_{\alpha_1 (i_2 \cdots i_L)}^{[1]} |i_2 \cdots i_L\rangle. \quad (3.23)$$

Schmidt vectors  $\{|\tau_{\alpha_1}^{[1]}\rangle\}_{\alpha_1}$  and  $\{|\tau_{\alpha_1}^{[2 \cdots L]}\rangle\}_{\alpha_1}$  are orthonormal vectors in Hilbert spaces  $\mathcal{H}_{[1]}$  and  $\mathcal{H}_{[2 \cdots L]}$ . Next we apply SVD to

$$\bar{V}_{\alpha_1 i_2 \cdots i_L}^{[1]} := \lambda_{\alpha_1}^{[1]} V_{\alpha_1 (i_2 \cdots i_L)}^{[1]} \quad (3.24)$$

by regarding  $\alpha_1 i_2$  as one index,  $\bar{V}_{(\alpha_1 i_2)(i_3 \cdots i_L)}^{[1]}$ . We obtain  $\Gamma^{[2]}$  and  $\lambda^{[2]}$  by

$$\bar{V}_{(\alpha_1 i_2)(i_3 \cdots i_L)}^{[1]} \stackrel{\text{SVD}}{=} \sum_{\alpha_2=1}^{\chi_2} U_{(\alpha_1 i_2) \alpha_2}^{[2]} \lambda_{\alpha_2}^{[2]} V_{\alpha_2 (i_3 \cdots i_L)}^{[2]} =: \sum_{\alpha_2=1}^{\chi_2} \lambda_{\alpha_1}^{[1]} \Gamma_{\alpha_1 \alpha_2}^{[2] i_2} \lambda_{\alpha_2}^{[2]} V_{\alpha_2 (i_3 \cdots i_L)}^{[2]}. \quad (3.25)$$

<sup>6</sup> This is a physical, not mathematically rigorous relation. What we can say rigorously is that the value of entanglement entropy sets restrictions on the distribution of the singular values  $\{\lambda_i\}_{i=1}^{\chi}$ , not on the value  $\chi$  itself. The detailed discussion is found in Ref. [44].

Note that we define  $\Gamma_{\alpha_1\alpha_2}^{[2]i_2}$  as  $U_{(\alpha_1 i_2)\alpha_2}^{[2]}/\lambda_{\alpha_1}^{[1]}$ , which is always possible because of the property of SVD,  $\lambda_{\alpha_1}^{[1]} > 0$ . Using  $\Gamma^{[2]}$ , we can define orthonormal vectors in Hilbert space  $\mathcal{H}_{[12]}$  and  $\mathcal{H}_{[3\cdots L]}$ ,

$$|\tau_{\alpha_2}^{[12]}\rangle := \sum_{i_2\alpha_1} \lambda_{\alpha_1}^{[1]} \Gamma_{\alpha_1\alpha_2}^{[2]i_2} |\tau_{\alpha_1}^{[1]}\rangle |i_2\rangle = \sum_{i_1 i_2\alpha_1} \Gamma_{\alpha_1}^{[1]i_1} \lambda_{\alpha_1}^{[1]} \Gamma_{\alpha_1\alpha_2}^{[2]i_2} |i_1 i_2\rangle, \quad (3.26)$$

$$|\tau_{\alpha_2}^{[3\cdots L]}\rangle := \sum_{i_3\cdots i_L} V_{\alpha_2(i_3\cdots i_L)}^{[2]} |i_3\cdots i_L\rangle. \quad (3.27)$$

Orthonormality of  $\{|\tau_{\alpha_2}^{[12]}\rangle\}_{\alpha_2}$  follows from that of  $\{|\tau_{\alpha_1}^{[1]}\rangle\}_{\alpha_1}$  and the property of matrix  $(U^{[2]})^\dagger U^{[2]} = 1$ . Again, this is Schmidt decomposition of  $|\psi\rangle$  for the subsystems  $[12]$  and  $[3\cdots L]$ ,

$$|\psi\rangle = \sum_{\alpha_2=1}^{\chi_2} \lambda_{\alpha_2}^{[2]} |\tau_{\alpha_2}^{[12]}\rangle |\tau_{\alpha_2}^{[3\cdots L]}\rangle. \quad (3.28)$$

One can prove this equation from the definitions of  $\Gamma^{[1]}$ ,  $\Gamma^{[2]}$ ,  $\lambda^{[1]}$  and  $\lambda^{[2]}$ .

We repeat this procedure of SVD until the end of system is reached ( $k = 2, \dots, L-2$ ).

$$\begin{aligned} \bar{V}_{(\alpha_k i_{k+1})(i_{k+2}\cdots i_L)}^{[k]} &:= \lambda_{\alpha_k}^{[k]} V_{(\alpha_k i_{k+1})(i_{k+2}\cdots i_L)}^{[k]} \\ &\stackrel{\text{SVD}}{=} \sum_{\alpha_{k+1}=1}^{\chi_{k+1}} U_{(\alpha_k i_{k+1})\alpha_{k+1}}^{[k+1]} \lambda_{\alpha_{k+1}}^{[k+1]} V_{\alpha_{k+1}(i_{k+2}\cdots i_L)}^{[k+1]} \\ &=: \sum_{\alpha_{k+1}} \lambda_{\alpha_k}^{[k]} \Gamma_{\alpha_k\alpha_{k+1}}^{[k+1]i_{k+1}} \lambda_{\alpha_{k+1}}^{[k+1]} V_{\alpha_{k+1}(i_{k+2}\cdots i_L)}^{[k+1]}, \end{aligned} \quad (3.29)$$

$$\begin{aligned} |\tau_{\alpha_{k+1}}^{[1\cdots k+1]}\rangle &:= \sum_{i_{k+1}\alpha_k} \lambda_{\alpha_k}^{[k]} \Gamma_{\alpha_k\alpha_{k+1}}^{[k+1]i_{k+1}} |\tau_{\alpha_k}^{[1\cdots k]}\rangle |i_{k+1}\rangle \\ &= \sum_{\substack{i_1\cdots i_{k+1} \\ \alpha_1\cdots\alpha_k}} \Gamma_{\alpha_1}^{[1]i_1} \lambda_{\alpha_1}^{[1]} \Gamma_{\alpha_1\alpha_2}^{[2]i_2} \cdots \Gamma_{\alpha_k\alpha_{k+1}}^{[k+1]i_{k+1}} |i_1\cdots i_{k+1}\rangle, \end{aligned} \quad (3.30)$$

$$|\tau_{\alpha_{k+1}}^{[k+2\cdots L]}\rangle := \sum_{i_{k+2}\cdots i_L} V_{\alpha_{k+1}(i_{k+2}\cdots i_L)}^{[k+1]} |i_{k+2}\cdots i_L\rangle. \quad (3.31)$$

Finally, we obtain a MPS representation of  $|\psi\rangle$

$$\begin{aligned} |\psi\rangle &= \sum_{i_1\cdots i_L} c_{i_1\cdots i_L} |i_1\cdots i_L\rangle \\ &= \sum_{\substack{i_1\cdots i_L \\ \alpha_1}} \Gamma_{\alpha_1}^{[1]i_1} \lambda_{\alpha_1}^{[1]} V_{\alpha_1 i_2\cdots i_L}^{[1]} |i_1\cdots i_L\rangle \\ &= \sum_{\substack{i_1\cdots i_L \\ \alpha_1\alpha_2}} \Gamma_{\alpha_1}^{[1]i_1} \lambda_{\alpha_1}^{[1]} \Gamma_{\alpha_1\alpha_2}^{[2]i_2} \lambda_{\alpha_2}^{[2]} V_{\alpha_2 i_3\cdots i_L}^{[2]} |i_1\cdots i_L\rangle \\ &= \sum_{\substack{i_1\cdots i_L \\ \alpha_1\cdots\alpha_{L-1}}} \Gamma_{\alpha_1}^{[1]i_1} \lambda_{\alpha_1}^{[1]} \Gamma_{\alpha_1\alpha_2}^{[2]i_2} \cdots \lambda_{\alpha_{L-1}}^{[L-1]} \Gamma_{\alpha_{L-1}}^{[L]i_L} |i_1\cdots i_L\rangle \end{aligned} \quad (3.32)$$

## Chapter 3. Numerical Methods

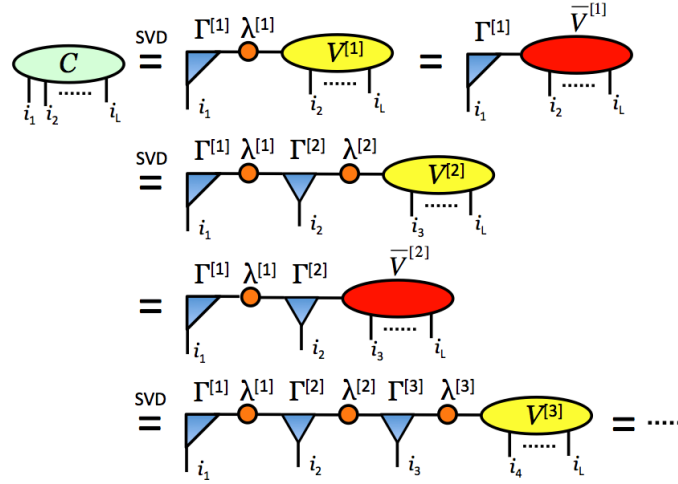


Figure 3.5: Diagrammatic representation of the construction of MPS for arbitrary states  $|\psi\rangle = \sum_{i_1 \dots i_L} c_{i_1 \dots i_L} |i_1 \dots i_L\rangle$ .

with Schmidt vectors for decomposing the system into  $\mathcal{H}_{[1 \dots k]} \otimes \mathcal{H}_{[k+1 \dots L]}$

$$|\psi\rangle = \sum_{\alpha_k=1}^{\chi_k} \lambda_{\alpha_k}^{[k]} |\mathcal{T}_{\alpha_k}^{[1 \dots k]}\rangle |\mathcal{T}_{\alpha_k}^{[k+1 \dots L]}\rangle \quad (3.33)$$

$$|\mathcal{T}_{\alpha_k}^{[1 \dots k]}\rangle = \sum_{\substack{i_1 \dots i_{k+1} \\ \alpha_1 \dots \alpha_{k-1}}} \Gamma_{\alpha_1}^{[1]i_1} \lambda_{\alpha_1}^{[1]} \dots \Gamma_{\alpha_{k-1}\alpha_k}^{[k]i_k} |i_1 \dots i_k\rangle, \quad (3.34)$$

$$|\mathcal{T}_{\alpha_k}^{[k+1 \dots L]}\rangle = \sum_{\substack{i_{k+1} \dots i_L \\ \alpha_{k+1} \dots \alpha_{L-1}}} \Gamma_{\alpha_k \alpha_{k+1}}^{[k+1]i_{k+1}} \lambda_{\alpha_{k+1}}^{[k+1]} \dots \Gamma_{\alpha_{L-1}}^{[L]i_L} |i_{k+1} \dots i_L\rangle. \quad (3.35)$$

A diagrammatic representation of this construction of MPS is shown in Fig. 3.5.

Let us discuss what determines the bond dimension of MPS,  $\chi := \max_k(\chi_k)$ .  $\chi_k$  is the number of Schmidt values for dividing the system into sites  $[1 \dots k]$  and sites  $[k+1 \dots L]$ . Therefore, from the property of SVD,  $\chi_k \leq \min(\dim \mathcal{H}_{[1 \dots k]}, \dim \mathcal{H}_{[k+1 \dots L]}) = \min(d^k, d^{L-k})$ . This yields a general bound

$$\chi = \max_k \chi_k = \max_k (\min(d^k, d^{L-k})) \leq d^{L/2}. \quad (3.36)$$

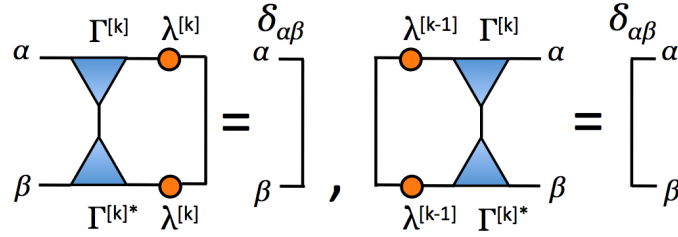
Furthermore, the decompositions that we used to construct MPS are Schmidt decompositions indeed, so  $\chi$  is related to the entanglement entropy of  $|\psi\rangle$ . Recalling the relation (3.19), we know

$$S_{[1 \dots k]} \sim \ln \chi_k \quad \Leftrightarrow \quad \chi_k \sim e^{S_{[1 \dots k]}}. \quad (3.37)$$

Hence a physical estimation of  $\chi$  is obtained:

$$\chi \sim e^{S_{\max}}. \quad (3.38)$$

Here  $S_{\max}$  is the maximum value of entanglement entropy of  $|\psi\rangle$  for all possible divisions of the system.

Figure 3.6: Canonical conditions of MPS for  $1 < k < L$ .

For a vast majority of states in Hilbert space, the volume law of entanglement entropy  $S_{\max} \sim L$  holds and therefore  $\chi$  scales as  $\exp(L)$ . As we already discussed, in that case MPS representations require the same number of parameters to describe states as the usual wave functions do, and MPS is not efficient to express states. However, for the ground state of local Hamiltonian, the area law ensures  $S_{\max} \sim O(1)$  in gapped case and  $S_{\max} \sim (c/6) \ln L$  in gapless case. This leads  $\chi \sim O(1)$  in gapped case and  $\chi \sim L^{c/6}$  in gapless case. In both cases, the descriptions by MPS are far efficient than that by wave functions. This is why MPS is suitable and efficient to describe the ground state of local Hamiltonian.

### 3.3.3 Canonical condition for MPS

We have constructed MPS for any state in the previous subsection. However, there are different sets of matrices that express the same state. In other words, there is a choice of freedom in MPS representations. Specifically, if MPS  $\{\Gamma^{[k]i_k}, \lambda^{[k]}\}_{k=1}^L$  represents  $|\psi\rangle$ , then

$$\tilde{\Gamma}^{[k]i_k} = (X^{[k-1]})^{-1} \Gamma^{[k]i_k} X^{[k]} \quad (3.39)$$

$$\tilde{\lambda}^{[k]} = (X^{[k]})^{-1} \lambda^{[k]} X^{[k+1]} \quad (3.40)$$

is also a MPS representation<sup>7</sup> of  $|\psi\rangle$  for arbitrary invertible  $\chi_k \times \chi_k$  matrices  $X^{[k]}$ .

Among many MPS representations for a given quantum state, we introduce canonical conditions for MPS, which greatly reduce computational cost of physical quantities. The canonical conditions of MPS are defined as<sup>8</sup>

$$\sum_{i_k, \alpha_k} \Gamma_{\alpha \alpha_k}^{[k]i_k} \lambda_{\alpha_k}^{[k]} \left( \Gamma_{\beta \alpha_k}^{[k]i_k} \lambda_{\alpha_k}^{[k]} \right)^* = \delta_{\alpha \beta}, \quad (3.41)$$

$$\sum_{i_k, \alpha_{k-1}} \lambda_{\alpha_{k-1}}^{[k-1]} \Gamma_{\alpha_{k-1} \alpha}^{[k]i_k} \left( \lambda_{\alpha_{k-1}}^{[k-1]} \Gamma_{\alpha_{k-1} \beta}^{[k]i_k} \right)^* = \delta_{\alpha \beta}. \quad (3.42)$$

These two equations are called as right canonical condition and left canonical condition (diagrammatic representations are shown in Fig. 3.6). As we will see later, retaining canonical conditions of MPS is crucial for efficient computation of physical quantities.

<sup>7</sup> For  $k = 1$  and  $L$ ,  $\tilde{\Gamma}^{[1]i_1} = \Gamma^{[1]i_1} X^{[1]}$ ,  $\tilde{\Gamma}^{[L]i_L} = (X^{[L-1]})^{-1} \Gamma^{[L]i_L}$ .

<sup>8</sup> For  $k = 1$  and  $L$ ,  $\sum_{i_1} \Gamma_{\alpha}^{[1]i_1} \left( \Gamma_{\beta}^{[1]i_1} \right)^* = \delta_{\alpha \beta}$ ,  $\sum_{i_L} \Gamma_{\alpha}^{[L]i_L} \left( \Gamma_{\beta}^{[L]i_L} \right)^* = \delta_{\alpha \beta}$ .

Chapter 3. Numerical Methods

---

It is proved that [51] MPS representations for given state that satisfy canonical conditions are unique up to permutation of the degenerate Schmidt values. The  $\Gamma$  and  $\lambda$  obtained in the last subsection satisfy the canonical conditions (this is shown by straightforward calculations). Therefore, it is always possible to represent any quantum state in a canonical MPS.

### 3.3.4 Calculation of physical quantity using MPS

We will show MPS expressions of expectation values for one-site and two-site operators. The canonical conditions of MPS are important to obtain simple formulae for the expectation values.

#### Expectation value for one-site operator

Let  $\hat{O}_1^{[l]}$  be a one-site operator acting nontrivially on site  $l$  and trivially on the other sites,  $\hat{O}_1^{[l]} = \hat{1} \otimes \cdots \otimes \hat{O}_1 \otimes \cdots \otimes \hat{1}$ . The expectation value  $\langle \psi | \hat{O}_1^{[l]} | \psi \rangle$  can be written as

$$\begin{aligned}
& \langle \psi | \hat{O}_1^{[l]} | \psi \rangle \\
&= \sum_{\substack{i_1 \cdots i_L, j_1 \cdots j_L \\ \{\alpha\}, \{\beta\}}} \left( \Gamma_{\beta_1}^{[1]j_1} \lambda_{\beta_1}^{[1]} \cdots \Gamma_{\beta_{L-1}}^{[L]j_L} \right)^* \left( \Gamma_{\alpha_1}^{[1]i_1} \lambda_{\alpha_1}^{[1]} \cdots \Gamma_{\alpha_{L-1}}^{[L]i_L} \right) \langle j_1 \cdots j_L | \hat{O}_1^{[l]} | i_1 \cdots i_L \rangle \\
&= \sum_{\substack{i_1 \cdots i_L, j_l \\ \{\alpha\}, \{\beta\}}} \left( \Gamma_{\alpha_1}^{[1]i_1} \left( \Gamma_{\beta_1}^{[1]i_1} \right)^* \right) \left( \lambda_{\alpha_1}^{[1]} \Gamma_{\alpha_1 \alpha_2}^{[2]i_2} \left( \lambda_{\beta_1}^{[1]} \Gamma_{\beta_1 \beta_2}^{[2]i_2} \right)^* \right) \cdots \left( \lambda_{\alpha_{l-1}}^{[l-1]} \Gamma_{\alpha_{l-1} \alpha_l}^{[l]i_l} \lambda_{\alpha_l}^{[l]} \langle j_l | \hat{O}_1 | i_l \rangle \left( \lambda_{\beta_{l-1}}^{[l-1]} \Gamma_{\beta_{l-1} \beta_l}^{[l]j_l} \lambda_{\beta_l}^{[l]} \right)^* \right) \\
&\quad \times \cdots \left( \Gamma_{\alpha_{L-2} \alpha_{L-1}}^{[L-1]i_{L-1}} \lambda_{\alpha_{L-1}}^{[L-1]} \left( \Gamma_{\beta_{L-2} \beta_{L-1}}^{[L-1]i_{L-1}} \lambda_{\beta_{L-1}}^{[L-1]} \right)^* \right) \left( \Gamma_{\alpha_{L-1}}^{[L]i_L} \left( \Gamma_{\beta_{L-1}}^{[L]i_L} \right)^* \right) \\
&= \sum_{\substack{i_2 \cdots i_{L-1}, j_l \\ \{\alpha\}, \{\beta\}}} \delta_{\alpha_1 \beta_1} \left( \lambda_{\alpha_1}^{[1]} \Gamma_{\alpha_1 \alpha_2}^{[2]i_2} \left( \lambda_{\beta_1}^{[1]} \Gamma_{\beta_1 \beta_2}^{[2]i_2} \right)^* \right) \cdots \left( \lambda_{\alpha_{l-1}}^{[l-1]} \Gamma_{\alpha_{l-1} \alpha_l}^{[l]i_l} \lambda_{\alpha_l}^{[l]} \langle j_l | \hat{O}_1 | i_l \rangle \left( \lambda_{\beta_{l-1}}^{[l-1]} \Gamma_{\beta_{l-1} \beta_l}^{[l]j_l} \lambda_{\beta_l}^{[l]} \right)^* \right) \\
&\quad \times \cdots \left( \Gamma_{\alpha_{L-2} \alpha_{L-1}}^{[L-1]i_{L-1}} \lambda_{\alpha_{L-1}}^{[L-1]} \left( \Gamma_{\beta_{L-2} \beta_{L-1}}^{[L-1]i_{L-1}} \lambda_{\beta_{L-1}}^{[L-1]} \right)^* \right) \delta_{\alpha_{L-1} \beta_{L-1}} \\
&= \sum_{\substack{i_3 \cdots i_{L-2}, j_l \\ \alpha_2 \cdots \alpha_{L-2} \\ \beta_2 \cdots \beta_{L-2}}} \delta_{\alpha_2 \beta_2} \cdots \left( \lambda_{\alpha_{l-1}}^{[l-1]} \Gamma_{\alpha_{l-1} \alpha_l}^{[l]i_l} \lambda_{\alpha_l}^{[l]} \langle j_l | \hat{O}_1 | i_l \rangle \left( \lambda_{\beta_{l-1}}^{[l-1]} \Gamma_{\beta_{l-1} \beta_l}^{[l]j_l} \lambda_{\beta_l}^{[l]} \right)^* \right) \cdots \delta_{\alpha_{L-2} \beta_{L-2}} \\
&= \cdots \\
&= \sum_{i_l, j_l, \alpha_{l-1}, \alpha_l} \lambda_{\alpha_{l-1}}^{[l-1]} \Gamma_{\alpha_{l-1} \alpha_l}^{[l]i_l} \lambda_{\alpha_l}^{[l]} \langle j_l | \hat{O}_1 | i_l \rangle \left( \lambda_{\alpha_{l-1}}^{[l-1]} \Gamma_{\alpha_{l-1} \alpha_l}^{[l]j_l} \lambda_{\alpha_l}^{[l]} \right)^*. \tag{3.43}
\end{aligned}$$

A diagrammatic representation of this computation is shown in Fig. 3.7.

Therefore, we can calculate expectation values of one-site operators by using *only* three tensors of MPS,  $\lambda^{[l-1]}$ ,  $\lambda^{[l]}$  and  $\Gamma^{[l]}$ . The canonical conditions of MPS play an important role in the derivation of this formula.

#### Expectation value for two-site operator

Let  $\hat{O}_2^{[l, l+1]}$  be a two-site operator acting nontrivially on site  $l$  and  $l+1$  and trivially on the other sites,  $\hat{O}_2^{[l, l+1]} = \hat{1} \otimes \cdots \otimes \hat{O}_2 \otimes \cdots \otimes \hat{1}$ . The expectation value  $\langle \psi | \hat{O}_2^{[l, l+1]} | \psi \rangle$  is

## Chapter 3. Numerical Methods

expressed in a simple equation by similar calculations as in the previous one:

$$\begin{aligned} & \langle \psi | \hat{O}_2^{[l,l+1]} | \psi \rangle \\ = & \sum_{\substack{i_l, i_{l+1}, j_l, j_{l+1} \\ \alpha_{l-1}, \alpha_l, \alpha_{l+1} \\ \beta_l}} \left( \lambda_{\alpha_{l-1}}^{[l-1]} \Gamma_{\alpha_{l-1} \alpha_l}^{[l] i_l} \lambda_{\alpha_l}^{[l]} \Gamma_{\alpha_l \alpha_{l+1}}^{[l+1] i_{l+1}} \lambda_{\alpha_{l+1}}^{[l+1]} \right) \langle j_l j_{l+1} | \hat{O}_2 | i_l i_{l+1} \rangle \left( \lambda_{\alpha_{l-1}}^{[l-1]} \Gamma_{\alpha_{l-1} \beta_l}^{[l] j_l} \lambda_{\beta_l}^{[l]} \Gamma_{\beta_l \alpha_{l+1}}^{[l+1] j_{l+1}} \lambda_{\alpha_{l+1}}^{[l+1]} \right)^* . \end{aligned} \quad (3.44)$$

A diagrammatic proof for this formula is shown in Fig. 3.8. Again, due to the canonical conditions of MPS, we can calculate the expectation value by using only several tensors of MPS. Expectation values for  $n$ -site operators can be expressed in the same way.

### 3.3.5 Example of MPS

We show some examples of MPS representation.

#### $S = 1/2$ Néel state

$S = 1/2$  Néel state is the ground state of anti-ferromagnetic Ising chain and written as  $|\text{Néel}\rangle = |\cdots \uparrow \downarrow \uparrow \downarrow \cdots\rangle$ . It is a product state, and therefore has a simple MPS representation with bond dimension  $\chi = 1$ :

$$\lambda^{[2n]} = \lambda^{[2n+1]} = 1, \quad (3.45)$$

$$\Gamma^{[2n]\uparrow} = 1, \quad \Gamma^{[2n]\downarrow} = 0, \quad (3.46)$$

$$\Gamma^{[2n+1]\uparrow} = 0, \quad \Gamma^{[2n+1]\downarrow} = 1. \quad (3.47)$$

The index  $\alpha_n$  is omitted because  $\chi_n = 1$  for all sites  $n$ .

#### $S=1/2$ dimer state

$S = 1/2$  dimer state is a chain of singlet pairs  $\frac{1}{\sqrt{2}}(|\uparrow\rangle|\downarrow\rangle - |\downarrow\rangle|\uparrow\rangle)$ ,

$$|\text{Dimer}\rangle = \frac{1}{\sqrt{2}} (|\uparrow\rangle_1 |\downarrow\rangle_2 - |\downarrow\rangle_1 |\uparrow\rangle_2) \otimes \frac{1}{\sqrt{2}} (|\uparrow\rangle_3 |\downarrow\rangle_4 - |\downarrow\rangle_3 |\uparrow\rangle_4) \otimes \cdots . \quad (3.48)$$

MPS for the dimer state has the bond dimension  $\chi_{2n+1} = 2$  and  $\chi_{2n} = 1$ :

$$\lambda^{[2n+1]} = \begin{pmatrix} \frac{1}{\sqrt{2}} & 0 \\ 0 & \frac{1}{\sqrt{2}} \end{pmatrix}, \quad \Gamma^{[2n+1]\uparrow} = \begin{pmatrix} 1 & 0 \\ 0 & 0 \end{pmatrix}, \quad \Gamma^{[2n+1]\downarrow} = \begin{pmatrix} 0 & 1 \\ 0 & 0 \end{pmatrix}, \quad (3.49)$$

$$\lambda^{[2n]} = 1, \quad \Gamma^{[2n]\uparrow} = \begin{pmatrix} 0 \\ -1 \end{pmatrix}, \quad \Gamma^{[2n]\downarrow} = \begin{pmatrix} 1 \\ 0 \end{pmatrix}. \quad (3.50)$$

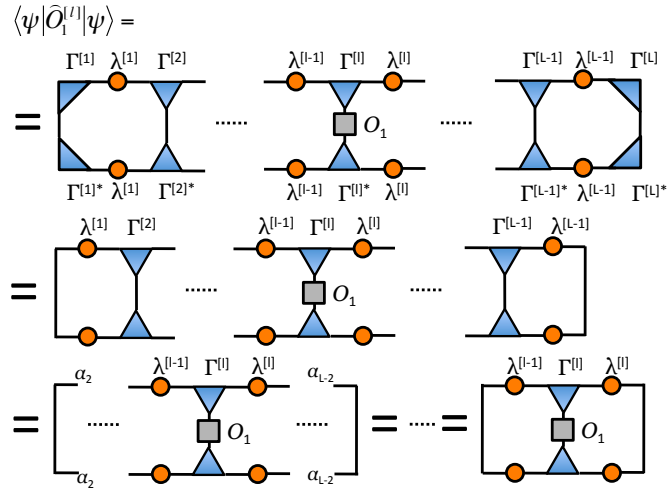


Figure 3.7: Expectation values of one-site operators.

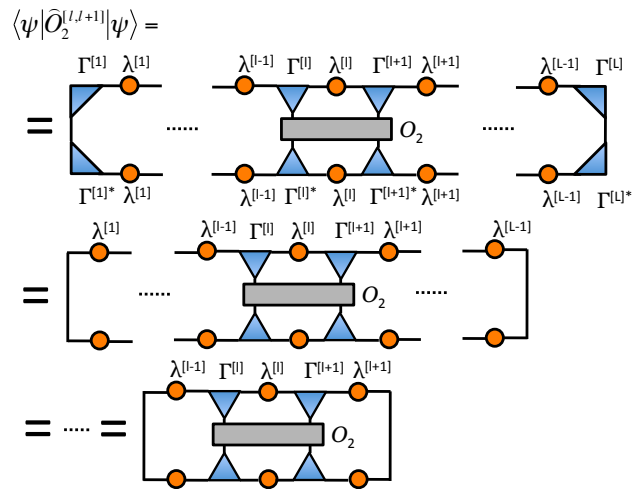


Figure 3.8: Expectation values of two-site operators.

### S=1/2 superposed dimer state

$S = 1/2$  superposed dimer state is the superposition of two dimer states,

$$\begin{aligned} |\text{Superposed Dimer}\rangle \propto & \cdots \otimes \frac{1}{\sqrt{2}} (|\uparrow\rangle_1 |\downarrow\rangle_2 - |\downarrow\rangle_1 |\uparrow\rangle_2) \otimes \frac{1}{\sqrt{2}} (|\uparrow\rangle_3 |\downarrow\rangle_4 - |\downarrow\rangle_3 |\uparrow\rangle_4) \otimes \cdots \\ & + \cdots \otimes \frac{1}{\sqrt{2}} (|\uparrow\rangle_0 |\downarrow\rangle_1 - |\downarrow\rangle_0 |\uparrow\rangle_1) \otimes \frac{1}{\sqrt{2}} (|\uparrow\rangle_2 |\downarrow\rangle_3 - |\downarrow\rangle_2 |\uparrow\rangle_3) \otimes \cdots \end{aligned}$$

This state can be expressed as translational invariant MPS,

$$\lambda^{[n]} = \begin{pmatrix} 1/2 & 0 & 0 \\ 0 & 1/\sqrt{2} & 0 \\ 0 & 0 & 1/2 \end{pmatrix}, \Gamma^{[n]\uparrow} = \begin{pmatrix} 0 & 0 & 0 \\ 1 & 0 & 0 \\ 0 & -1 & 0 \end{pmatrix}, \Gamma^{[n]\downarrow} = \begin{pmatrix} 0 & 1 & 0 \\ 0 & 0 & 1 \\ 0 & 0 & 0 \end{pmatrix}, \quad (3.51)$$

although it is not normalized and canonicalized. This is one of the non-trivial examples of MPS.

## 3.4 Time-Evolving Block Decimation method

In this section, we review the Time-Evolving Block Decimation (TEBD) method. It was proposed by Vidal in 2004 [15] and extended to infinite systems in 2007 by himself [52]. TEBD is an algorithm to calculate imaginary or real time-evolution of a state,

$$|\psi(\tau)\rangle = \frac{e^{-\tau H} |\psi_0\rangle}{\|e^{-\tau H} |\psi_0\rangle\|}, \quad |\psi(t)\rangle = e^{-itH} |\psi_0\rangle, \quad (3.52)$$

in an efficient and clear way using MPS. TEBD is mathematically equivalent to well-known DMRG method, if we formulate DMRG in MPS language. However, practically source and tendency of error in computation are different from each other due to the different schemes of truncation (approximation) in the algorithms. The numerical difference between TEBD and DMRG is reviewed in Ref. [36].

There are two important points in the TEBD algorithm: decomposing time-evolution operator into local mutually-commuting terms and maintaining canonical forms of MPS after the action of time-evolution operator.

### 3.4.1 Suzuki-Trotter decomposition for time-evolution operator

We introduce Suzuki-Trotter decomposition for time-evolution operator. This decomposition makes time-evolution operator into product of local and mutually-commuting terms.

Consider Hamiltonian that can be written as a sum of two-site operators,

$$H = \sum_n H_{n,n+1} = \sum_n H_{2n-1,2n} + \sum_n H_{2n,2n+1} =: H_{\text{even}} + H_{\text{odd}}, \quad (3.53)$$

where  $H_{n,n+1}$  is a two-site operator on site  $n$  and  $n+1$ . First we divide time-evolution operator<sup>9</sup>  $\hat{U}(\tau) = e^{-\tau H}$  into small time steps,  $\delta\tau = \tau/N \ll 1$  ( $N$  is the total number of time steps):

$$\hat{U}(\tau) = e^{-\tau H} = (e^{-\delta\tau H})^N. \quad (3.54)$$

Then  $e^{-\delta\tau H}$  is decomposed into terms which contain only  $H_{\text{even}}$  or  $H_{\text{odd}}$ :

$$\begin{aligned} e^{-\delta\tau H} &= e^{-\delta\tau(H_{\text{even}}+H_{\text{odd}})} \\ &= \begin{cases} e^{-\delta\tau H_{\text{even}}} e^{-\delta\tau H_{\text{odd}}} + O(\delta\tau^2), \\ e^{-\frac{\delta\tau}{2} H_{\text{even}}} e^{-\delta\tau H_{\text{odd}}} e^{-\frac{\delta\tau}{2} H_{\text{even}}} + O(\delta\tau^3), \\ e^{-\frac{\theta\delta\tau}{2} H_{\text{even}}} e^{-\theta\delta\tau H_{\text{odd}}} e^{-\frac{(1-\theta)\delta\tau}{2} H_{\text{even}}} e^{-(1-2\theta)\delta\tau H_{\text{odd}}} \\ \cdot e^{-\frac{(1-\theta)\delta\tau}{2} H_{\text{even}}} e^{-\theta\delta\tau H_{\text{odd}}} e^{-\frac{\theta\delta\tau}{2} H_{\text{even}}} + O(\delta\tau^5), \quad \theta = \frac{1}{2^{-2^{1/3}}} \approx 1.351. \end{cases} \end{aligned}$$

These decompositions in each line are called 1st, 2nd and 4th order Suzuki-Trotter decomposition, respectively.

Each term of  $H_{\text{odd}}$  ( $H_{\text{even}}$ ) is mutually-commuting and the time-evolution operator  $e^{-\delta\tau H_{\text{odd}}}$  ( $e^{-\delta\tau H_{\text{even}}}$ ) can be written as a product of local terms,

$$e^{-\delta\tau H_{\text{odd}}} = \prod_n e^{-\delta\tau H_{2n,2n+1}} =: \prod_n \hat{V}_{2n,2n+1}. \quad (3.55)$$

### 3.4.2 Updating canonical MPS after the action of local operator

As explained in the previous section, the canonical conditions of MPS are crucial to calculate physical quantities efficiently. We need to make the canonical conditions of MPS to hold after the time-evolution. Here we discuss the way to calculate canonical MPS after the action of *local* operators. For local operators, we have to update only several tensors to retain a canonical form of MPS.

#### Action of one-site unitary operator

Consider a one-site unitary operator on site  $l$ ,

$$\hat{U} = \sum_{i_l, j_l} U_{i_l j_l} |i_l\rangle \langle j_l|. \quad (3.56)$$

The problem is how to obtain canonical MPS for  $|\psi'\rangle = \hat{U}|\psi\rangle$  when

$$|\psi\rangle = \sum_{i_1 i_2 \dots i_L} \sum_{\alpha_1 \dots \alpha_{L-1}} \Gamma_{\alpha_1}^{[1]i_1} \lambda_{\alpha_1}^{[i_1]} \Gamma_{\alpha_1 \alpha_2}^{[2]i_2} \lambda_{\alpha_2}^{[2]} \dots \lambda_{\alpha_{L-1}}^{[L-1]} \Gamma_{\alpha_{L-1}}^{[L]i_L} |i_1 i_2 \dots i_L\rangle \quad (3.57)$$

is canonical MPS. The answer is simple because of the locality and unitarity of the operator. We have only to change the tensor  $\Gamma^{[l]}$  into

$$\tilde{\Gamma}_{\alpha_{l-1} \alpha_l}^{[l]i_l} = \sum_{j_l} U_{i_l j_l} \Gamma_{\alpha_{l-1} \alpha_l}^{[l]j_l}, \quad (3.58)$$

and keep the other  $\{\Gamma, \lambda\}$  the same. The unitarity of the matrix  $U$  ensures that the canonical conditions hold for the updated MPS.

<sup>9</sup> When  $\tau$  is real,  $\hat{U}(\tau)$  corresponds to imaginary time-evolution. For real time-evolution, we take  $\tau = it$ .

## Chapter 3. Numerical Methods

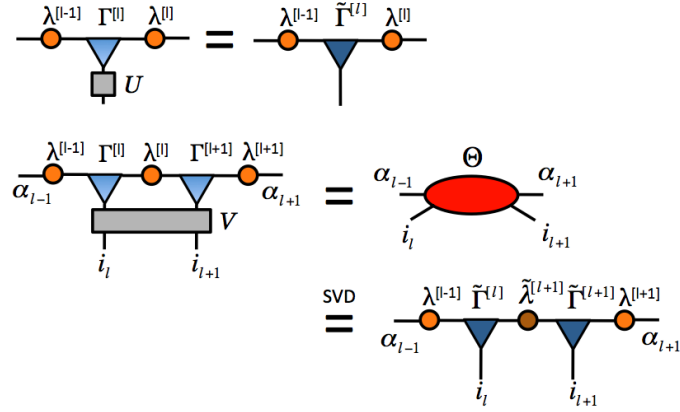


Figure 3.9: Updating MPS after the action of one-side operator  $\hat{U}$  and two-site operator  $\hat{V}$ .

### Action of two-site unitary operator

Consider a two-site unitary operator on site  $l$  and  $l + 1$ ,

$$\hat{V} = \sum_{i_l, i_{l+1}, j_l, j_{l+1}} V_{j_l j_{l+1}}^{i_l i_{l+1}} |i_l i_{l+1}\rangle \langle j_l j_{l+1}|. \quad (3.59)$$

Canonical MPS for  $|\psi'\rangle = \hat{V} |\psi\rangle$  is obtained by modifying the tensors  $\Gamma^{[l]}, \Gamma^{[l+1]}$  and  $\lambda^{[l]}$ . To do this, we define a rank-2 tensor  $\Theta_{(i_l \alpha_{l-1}), (i_{l+1} \alpha_{l+1})}$  and apply SVD to it:

$$\begin{aligned} \Theta_{(i_l \alpha_{l-1}), (i_{l+1} \alpha_{l+1})} &:= \sum_{j_l, j_{l+1}, \alpha_l} \left( \lambda_{\alpha_{l-1}}^{[l-1]} \Gamma_{\alpha_{l-1} \alpha_l}^{[l] j_l} \lambda_{\alpha_l}^{[l]} \Gamma_{\alpha_l \alpha_{l+1}}^{[l+1] j_{l+1}} \lambda_{\alpha_{l+1}}^{[l+1]} \right) V_{j_l j_{l+1}}^{i_l i_{l+1}}, \quad (3.60) \\ \Theta_{(i_l \alpha_{l-1}), (i_{l+1} \alpha_{l+1})} &\stackrel{\text{SVD}}{=} \sum_{\beta=1}^{\tilde{\chi}_l} U_{(i_l \alpha_{l-1}) \beta} \tilde{\lambda}_{\beta}^{[l]} V_{\beta (i_{l+1} \alpha_{l+1})} =: \sum_{\beta=1}^{\tilde{\chi}_l} \lambda_{\alpha_{l-1}}^{[l-1]} \tilde{\Gamma}_{\alpha_{l-1} \beta}^{[l] i_l} \tilde{\lambda}_{\beta}^{[l]} \tilde{\Gamma}_{\beta \alpha_{l+1}}^{[l+1] i_{l+1}} \lambda_{\alpha_{l+1}}^{[l+1]}. \quad (3.61) \end{aligned}$$

Note that the updated tensors can have larger bond dimension  $\tilde{\chi}_l$  than before. If  $\chi_{l-1} = \chi_l = \chi_{l+1} = \chi$ , the size of tensor  $\Theta_{(i_l \alpha_{l-1}), (i_{l+1} \alpha_{l+1})}$  is  $d\chi \times d\chi$ , so  $\tilde{\chi}_l$  could be  $d\chi$  at most. The growth of the bond dimension is physically interpreted as increase of entanglement between sites  $[1 \cdots l]$  and sites  $[l + 1 \cdots L]$  due to the action of  $\hat{V}$ . This is an important point in practical numerical calculations, as we will see below.

These procedures to update MPS are summarized in Fig. 3.9.

### 3.4.3 TEBD algorithm

TEBD algorithm is as follows (we take imaginary time-evolution as an example. Real time-evolution can be done in the same way):

- (a) prepare canonical MPS for  $|\psi_0\rangle$  on which time-evolution operator to act.

- (b) divide the time evolution operator  $\hat{U}(\tau) = e^{-\tau H}$  into small time steps and perform Suzuki-Trotter decomposition. Take 1st order decomposition for example,  $e^{-\delta\tau H} = e^{-\delta\tau(H_{\text{even}}+H_{\text{odd}})} \approx e^{-\delta\tau H_{\text{even}}} e^{-\delta\tau H_{\text{odd}}}$ .
- (c) calculate  $|\psi'\rangle = e^{-\delta\tau H_{\text{odd}}} |\psi_0\rangle$  in MPS language. Now the time-evolution operator is decomposed into a product of local operators  $\hat{V}_{2n,2n+1}$  (Eqn. (3.55)), we should update the tensors  $\Gamma^{[2n]}, \Gamma^{[2n+1]}$  and  $\lambda^{[2n]}$  for every  $n$  according to Eqn. (3.61) (note that the computations can be done in parallel for  $n$ ). However, two problems appear in the updating processes: unitarity of the time-evolution operator and truncation of the state. We discuss these two problems below.
- (d) calculate  $e^{-\delta\tau H_{\text{even}}} |\psi'\rangle$  in the same way and repeat the time-evolution until desired result is obtained. In the case of imaginary time-evolution for ground state search, convergence of energy (expectation value of Hamiltonian) in the time-evolution is one of the indicators to stop the evolution.

### Unitarity of imaginary time-evolution

Imaginary time-evolution operator  $\hat{U}(\tau) = e^{-\tau H}$  and the decomposed operator  $\hat{V}_{2n,2n+1} = e^{-\delta\tau H_{2n,2n+1}}$  are not unitary when  $\tau \neq 0$ . As a result, the updated tensors  $\tilde{\Gamma}^{[2n]}, \tilde{\Gamma}^{[2n+1]}, \tilde{\lambda}^{[2n]}$  in Eqn. (3.61) do not satisfy canonical conditions of MPS. Furthermore, the normalization condition of a state  $\sum_{\alpha_{2n}=1}^{\chi_{2n}} (\lambda_{\alpha_{2n}})^2 = 1$  is violated after the imaginary time-evolution. In the TEBD algorithm for imaginary time-evolution, we have to recover the normalization of a state by modifying Schmidt values

$$\tilde{\lambda}_{\alpha}^{[2n]} \rightarrow \frac{1}{\sqrt{\sum_{\alpha=1}^{\tilde{\chi}_{2n}} (\tilde{\lambda}_{\alpha}^{[2n]})^2}} \tilde{\lambda}_{\alpha}^{[2n]}, \quad (3.62)$$

after SVD. On the other hand, the problem of canonical conditions is ignored<sup>10</sup> in the algorithm because the violation is small enough when  $\delta\tau \ll 1$ .

### Truncation

In practice, we have a limit  $\chi_{\text{max}}$  for the bond dimension of MPS because an amount of memory storage of computers is finite. However, as we discussed, the bond dimension of the updated tensors could be larger than before. If new bond dimension  $\tilde{\chi}_l$  becomes larger than  $\chi_{\text{max}}$ , we have to *truncate* Schmidt vectors which have small values:

$$|\psi'\rangle = \sum_{\alpha_l=1}^{\tilde{\chi}_l} \tilde{\lambda}_{\alpha_l}^{[l]} |\tilde{\tau}_{\alpha_l}^{[1\dots l]}\rangle |\tilde{\tau}_{\alpha_l}^{[l+1\dots L]}\rangle \approx \sum_{\alpha_l=1}^{\chi_{\text{max}}} \tilde{\lambda}_{\alpha_l}^{[l]} |\tilde{\tau}_{\alpha_l}^{[1\dots l]}\rangle |\tilde{\tau}_{\alpha_l}^{[l+1\dots L]}\rangle. \quad (3.63)$$

<sup>10</sup> Detailed discussion on this point is found in Ref. [53].

In addition, we should modify  $\tilde{\lambda}^{[l]}$

$$\tilde{\lambda}_\alpha^{[l]} \rightarrow \frac{1}{\sqrt{\sum_{\alpha=1}^{\chi_{\max}} (\tilde{\lambda}_\alpha^{[l]})^2}} \tilde{\lambda}_\alpha^{[l]} \quad (\alpha = 1, \dots, \chi_{\max}) \quad (3.64)$$

in order to normalize  $|\psi'\rangle$ . *Truncation error*  $\epsilon$  is defined as

$$\epsilon = 1 - \frac{\sum_{\alpha=\chi_{\max}+1}^{d_\chi} (\tilde{\lambda}_\alpha^{[2n]})^2}{\sum_{\alpha=1}^{d_\chi} (\tilde{\lambda}_\alpha^{[2n]})^2}. \quad (3.65)$$

The truncation error gives a good estimate for accuracy of numerical calculations.

### Source of error

There are two sources of error in TEBD: one from Suzuki-Trotter decomposition and the other from truncation. The first one grows linearly in time. It can be reduced by taking smaller time step  $\delta\tau$  or employing higher-order Suzuki-Trotter decomposition. Both treatments increase the total number of SVD to simulate the same duration of time. The error from truncation grows exponentially in time, and become important in longer time scales. It is reduced by using larger  $\chi_{\max}$ , which results in the increase of computational cost of SVD at each time step (computational cost of SVD for  $d_\chi \times d_\chi$  matrix is  $O((d_\chi)^3)$ ). The characteristics of these two errors are thoroughly discussed in Ref. [54].

## 3.5 iTEBD

In this section, infinite Time-Evolving Block Decimation (iTEBD) method is reviewed. This method is an extension of TEBD to infinite systems. The iTEBD can simulate systems in the thermodynamic limit directly, without any extrapolation of system size. In this study, we use iTEBD to simulate the dynamics after the flux quench.

### 3.5.1 infinite MPS

In iTEBD, we assume spatial periodicity of tensors in MPS, and quantum states are expressed by such MPS of infinite length, infinite MPS (iMPS). By assuming periodicity, we have only to treat several tensors to simulate infinite systems. If the support of each term in Hamiltonian is  $m$  sites at most, the periodicity must be set to be larger than  $m$  in order to construct iTEBD method. We note that assuming periodicity to states is potentially dangerous because it restricts possible orders to be commensurate to that periodicity. For example, dimerized order (which has two-site translational symmetry) cannot be expressed by iMPS with odd-number site periodicity. We should be careful about what orders could appear when assuming the periodicity of tensors in MPS.

The canonical conditions of iMPS are defined as the same as MPS. In the same manner as finite MPS, the canonical conditions allow us to compute physical quantities *per site* by using only a few tensors in iMPS.

### 3.5.2 Algorithm

The algorithm of iTEBD is simpler than that of TEBD. For simplicity, consider iMPS with two-site periodicity and Hamiltonian which consists of nearest-neighbor interaction terms. We follow the notation of Vidal [52] below. Tensors of iMPS are written as

$$\Gamma^{[2n]} = \Gamma^A, \lambda^{[2n]} = \lambda^A, \Gamma^{[2n+1]} = \Gamma^B, \lambda^{[2n+1]} = \lambda^B, \quad (3.66)$$

and a state  $|\psi\rangle$  is expressed as

$$|\psi\rangle = \sum_{\{i\}\{\alpha\}} \cdots \Gamma_{\alpha_0\alpha_1}^{Bi_1} \lambda_{\alpha_1}^B \Gamma_{\alpha_1\alpha_2}^{Ai_2} \lambda_{\alpha_2}^A \Gamma_{\alpha_2\alpha_3}^{Bi_3} \lambda_{\alpha_3}^B \cdots |\cdots i_1 i_2 i_3 \cdots\rangle. \quad (3.67)$$

Hamiltonian  $h$  of the system is

$$h = \sum_n h^{[n,n+1]} = \sum_n h^{[2n-1,2n]} + \sum_n h^{[2n,2n+1]}, \quad (3.68)$$

and we perform 1st order Suzuki-Trotter decomposition for the time-evolution operator  $U(\delta\tau) := e^{-\delta\tau h}$ ,

$$U_{\delta\tau}^{[n,n+1]} := \exp(-\delta\tau h^{[n,n+1]}), \quad (3.69)$$

$$U_{\delta\tau}^{AB} := \bigotimes_n U_{\delta\tau}^{[2n,2n+1]}, \quad U_{\delta\tau}^{BA} := \bigotimes_n U_{\delta\tau}^{[2n+1,2n+2]}, \quad (3.70)$$

$$U(\delta\tau) = U_{\delta\tau}^{BA} U_{\delta\tau}^{AB} + O(\delta\tau^2). \quad (3.71)$$

For 2nd order decomposition, we can use  $U(\delta\tau) = U_{\delta\tau/2}^{BA} U_{\delta\tau}^{AB} U_{\delta\tau/2}^{BA} + O(\delta\tau^3)$ .

At each time step, we update tensors  $\Gamma^A, \Gamma^B, \lambda^A$  ( $\Gamma^A, \Gamma^B, \lambda^B$ ) after the action of the decomposed time-evolution operator  $U^{AB}$  ( $U^{BA}$ ). For example, after the action of  $U^{AB}$ , we obtain  $\tilde{\Gamma}^{A,B}$  and  $\tilde{\lambda}^{[A]}$  by

$$\Theta_{(i\alpha),(j\gamma)} := \sum_{i',j',\beta'} \left( \lambda_{\alpha}^B \Gamma_{\alpha\beta'}^{Ai'} \lambda_{\beta'}^A \Gamma_{\beta'\gamma}^{Bj'} \lambda_{\gamma}^B \right) U_{i'j'}^{AB} \quad (3.72)$$

$$\Theta_{(i\alpha),(j\gamma)} \stackrel{\text{SVD}}{=} \sum_{\beta=1}^{\tilde{\chi}^A} X_{(i\alpha)\beta} \tilde{\lambda}_{\beta}^A Y_{\beta(j\gamma)} =: \sum_{\beta=1}^{\tilde{\chi}^A} \lambda_{\alpha}^B \tilde{\Gamma}_{\alpha\beta}^{Ai} \tilde{\lambda}_{\beta}^A \tilde{\Gamma}_{\beta\gamma}^{Bj} \lambda_{\gamma}^B. \quad (3.73)$$

A diagrammatic expression of the update is shown in Fig. 3.10.

Chapter 3. Numerical Methods

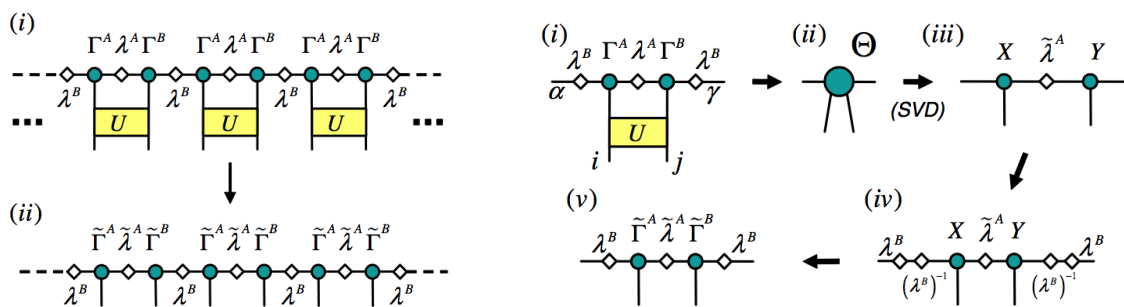


Figure 3.10: Diagrammatic representations of the iTEBD algorithm. Left panel shows the whole picture of update of tensors after the action by  $U^{AB}$ . Right panel shows that the update procedure to obtain new tensors  $\Gamma^A, \Gamma^B, \lambda^A$ . Figures are taken from Ref. [52].

# Chapter 4

## Results and Discussions

In this chapter, we present numerical results of the dynamics of spin current and discuss them.

### 4.1 Numerical data of the dynamics

In numerical calculations, we first prepare the ground state of the XXZ chain with flux

$$H_\theta = - \sum_i \left( \frac{1}{2} e^{i\theta} S_i^+ S_{i+1}^- + \frac{1}{2} e^{-i\theta} S_i^- S_{i+1}^+ + \Delta S_i^z S_{i+1}^z \right) \quad (4.1)$$

by imaginary time-evolution using iTEBD method:

$$|\theta\rangle_{\text{GS}} = \lim_{\tau \rightarrow \infty} \frac{e^{-\tau H_\theta} |\psi_{\text{ini}}\rangle}{\| e^{-\tau H_\theta} |\psi_{\text{ini}}\rangle \|}, \quad (4.2)$$

where  $|\psi_{\text{ini}}\rangle$  is initial state of the imaginary time-evolution.

Then, real time-evolution driven by the XXZ Hamiltonian without flux

$$H_0 = - \sum_i \left( \frac{1}{2} S_i^+ S_{i+1}^- + \frac{1}{2} S_i^- S_{i+1}^+ + \Delta S_i^z S_{i+1}^z \right) \quad (4.3)$$

is performed on the obtained ground state  $|\theta\rangle_{\text{GS}}$ ,

$$|\psi(t)\rangle = e^{-iH_0 t} |\theta\rangle_{\text{GS}}. \quad (4.4)$$

We use iTEBD again for the real time-evolution.

Numerical calculations were done in the following parameters:

$$\begin{aligned} \Delta &= \pm 0.3, \pm 0.5, \pm 0.8, -1.0, -1.2, -1.5, -2.0, (\pm 0.1), \\ \theta &= -\frac{\pi}{2}, -\frac{\pi}{3}, -\frac{\pi}{6}, -\frac{\pi}{10}, -\frac{\pi}{20}, -\frac{\pi}{30}. \end{aligned}$$

$\Delta$  is the strength of interactions and  $|\theta|$  represents the *size* of quench (for larger  $|\theta|$  the initial state becomes more excited one). Since we employ iTEBD, we can treat the system in the thermodynamic limit  $L \rightarrow \infty$  directly without resorting to any extrapolation. There

## Chapter 4. Results and Discussions

is no finite-size effect in our calculations. Instead the bond dimension  $\chi$  of MPS determines accuracy of calculations. As we discussed in the last chapter, in practice the truncation error could appear in the iTEBD algorithm due to the finiteness of  $\chi$ . In order to reduce the truncation error and simulate the dynamics for longer time, we have to take larger  $\chi$ . We carefully check the truncation error and other potential errors in iTEBD calculations, and adopt data in reliable time scale. Technical details are explained in appendix A.

### Numerical results of the dynamics

We show numerical results of the dynamics of the spin current  $J(t)$  in Fig. 4.1 and 4.2. We summarize the dynamics as following. For large  $|\theta|$ ,  $\theta = -\pi/2$  and  $-\pi/3$ , the spin current shows oscillation and decay for all  $\Delta$  (the data for  $\Delta = \pm 0.1$  have too long periods of oscillations and we cannot see them clearly). For smaller  $|\theta|$ ,  $\theta = -\pi/6$  to  $-\pi/30$ , we observe qualitatively different dynamics for  $\Delta > 0$  and  $\Delta < 0$ . For  $\Delta > 0$ , the oscillation in long time scale ( $t \gtrsim 10$ ) is not visible and the decay of the current is small (we will discuss the visible oscillation in short time scale ( $t \lesssim 10$ ) later). The spin current becomes stationary within the accessible time scale of numerical calculations. For  $\Delta < 0$ , the oscillation in long time scale is visible, although for small  $|\theta|$  and  $|\Delta|$  the period is too long for us to confirm the oscillation. The decay of the spin current is larger than that of  $\Delta > 0$  cases. Besides, the relaxation time is larger than in  $\Delta > 0$  cases, and we cannot observe stationary states within the accessible time scale of numerical calculations.

Regarding the long-time limit of the spin current, we observe that it is non-zero in gapless case ( $-1 \leq \Delta < 1$ ) and zero in gapped case ( $\Delta < -1$ ) for any  $\theta$ . However, we mention that for  $\Delta = -0.8$  and  $-1.0$  it is difficult to judge whether the long-time limit is zero or non-zero from the numerical data because of the long time scale of relaxation. We will discuss these points in section 4.2.

Before analyzing the numerical data quantitatively, we comment on the oscillation in short time scale ( $t \lesssim 10$ ) that is visible even in  $\Delta > 0$  for small  $|\theta|$  (Fig. 4.2). This oscillation survives only immediately after the quench and it is observed for almost all parameter regions. Therefore we argue that it does not contain much meaningful information of the system. We do not discuss this oscillation further in this study.

**Fitting for the numerical data.** To quantify characteristics of the dynamics from numerical data, we exploit a simple and empirical fitting function,

$$f(t) = c + (A + B \cos(\omega t + \phi)) e^{-t/\tau}, \quad g(t) = c + A e^{-t/\tau}. \quad (4.5)$$

We use  $f(t)$  for fitting when the oscillation in long time scale is visible. Otherwise we use  $g(t)$  instead. Therefore, by this fitting we analyze the oscillation in long time scale only and the oscillation in short time scale is not treated. The fitting is well for short times, roughly up to the first cycle of oscillation in the case of  $f(t)$ . Examples of fitting are shown in Fig. 4.3.

Among the parameters of this fitting, we focus on  $c$ ,  $\omega$  and  $\tau$  as the long-time limit of the current, the frequency of oscillation and the relaxation time, respectively. Below we discuss these three features of the dynamics in order.

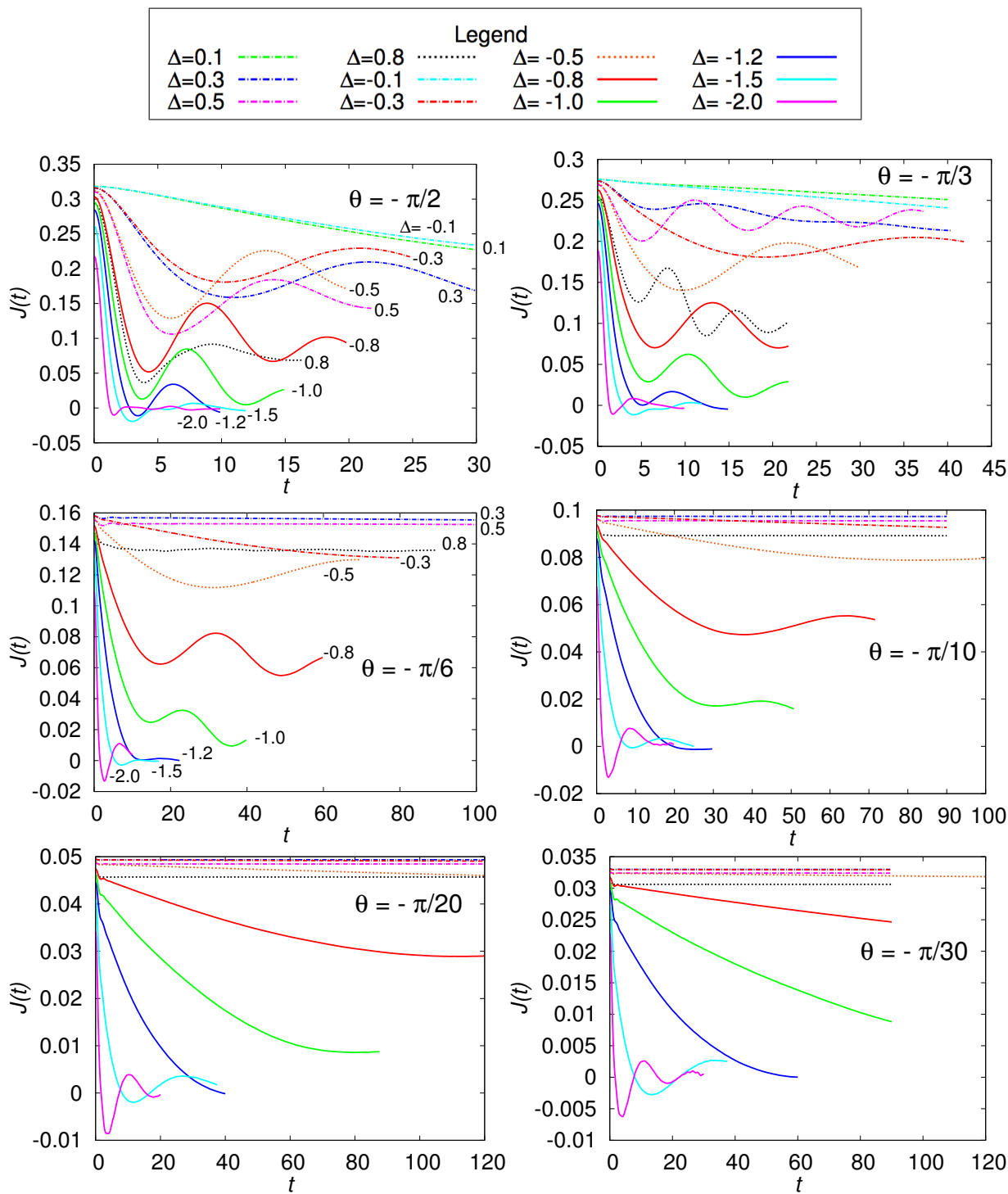
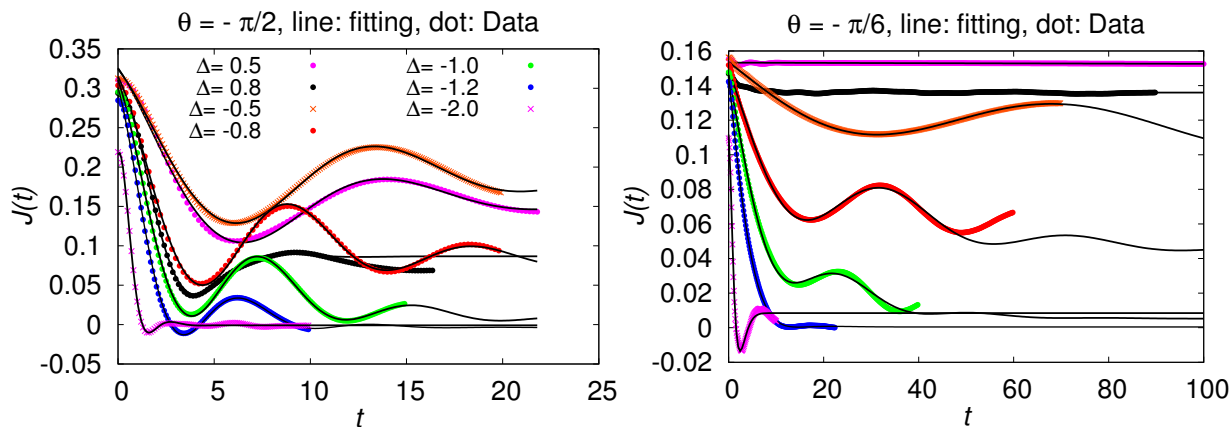
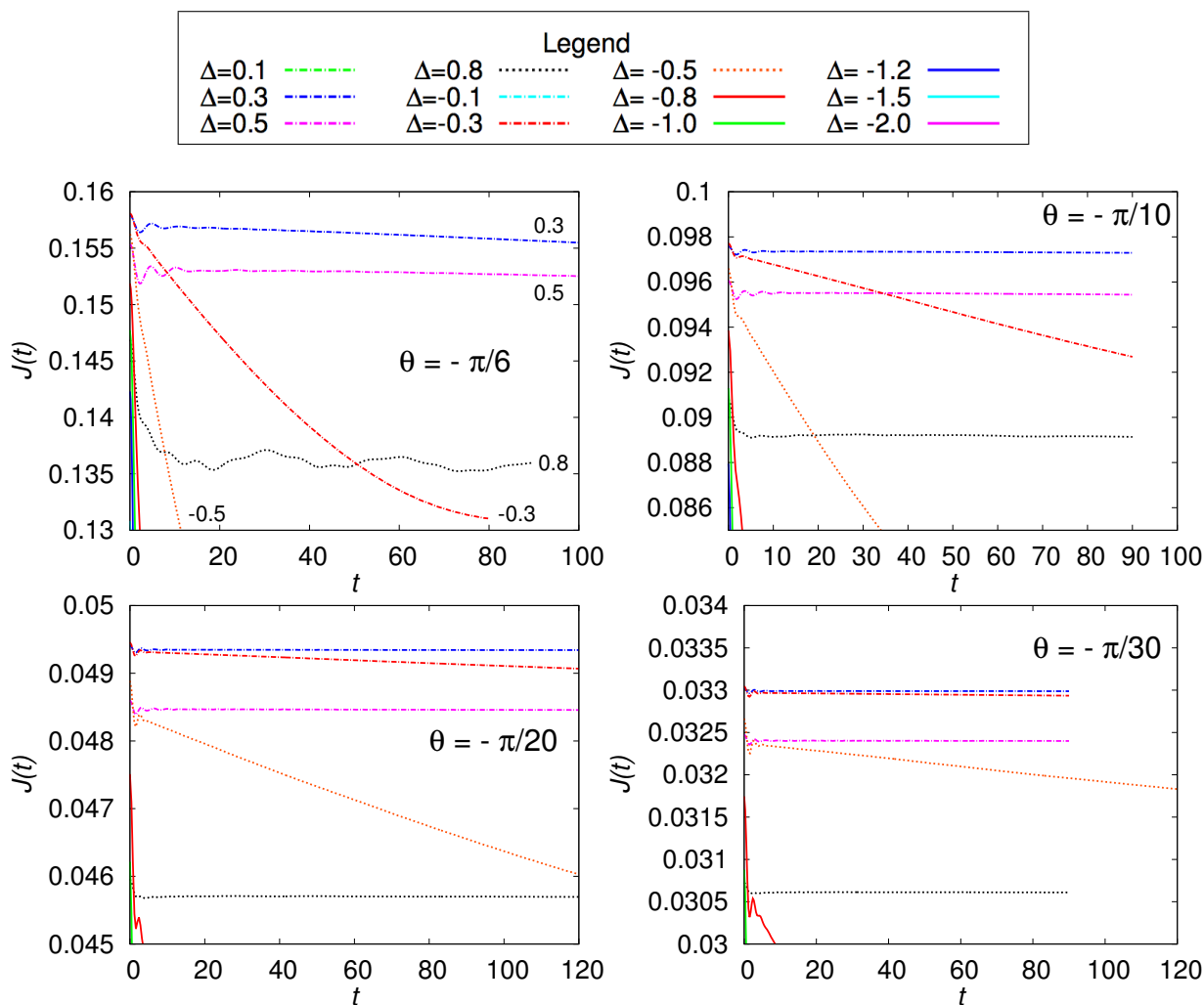


Figure 4.1: Numerical data of the dynamics for  $\theta = \pi/2$  to  $-\pi/30$ .

Chapter 4. Results and Discussions



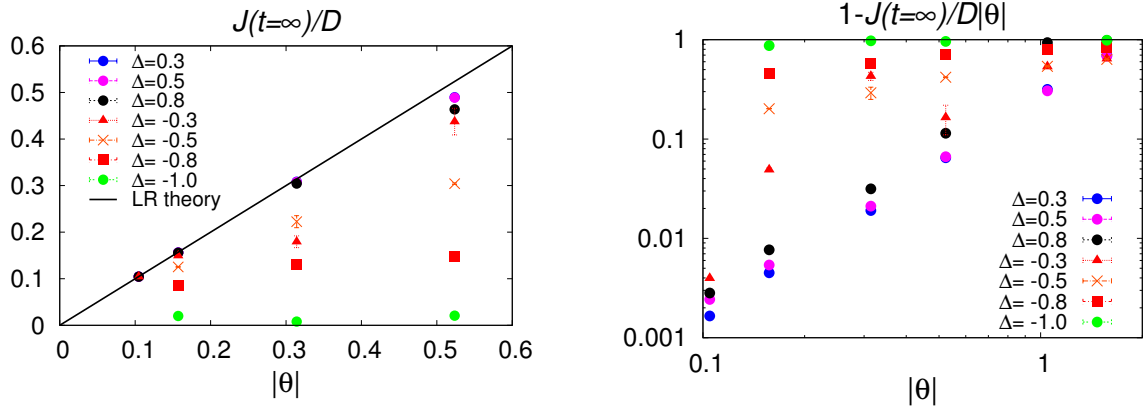


Figure 4.4: Left panel:  $J(t = \infty)/D$ . Right panel:  $1 - J(t = \infty)/(D|\theta|)$ . Note that we cannot obtain reliable data for  $\Delta = -0.5, -0.8, -1$  when  $|\theta| = \pi/30 \approx 0.1$ .

## 4.2 Long-time limit of the current

As we discussed in section 2.2.1, linear response (LR) theory predicts that the long-time limit of the current  $J(t = \infty)$  is given by the Drude weight  $D$ ,

$$J(t = \infty) = D|\theta|. \quad (4.6)$$

Exact value of the Drude weight for the XXZ chain is known as [23]

$$D = \frac{\pi}{4} \frac{\sin \mu}{\mu(\pi - \mu)}, \quad \mu = \arccos(-\Delta). \quad (4.7)$$

$D$  is non-zero only for  $-1 \leq \Delta < 1$  and otherwise zero. Furthermore,  $D$  is even function of  $\Delta$  except<sup>1</sup> at  $\Delta = \pm 1$ . Therefore LR theory predicts that  $J(t = \infty)$  is non-zero only for  $-1 \leq \Delta < 1$  and determined by the absolute value of  $\Delta$  (irrespective of the sign).

As mentioned in the last section, for any  $\theta$  we observe that  $J(t = \infty)$  remains non-zero for gapless case ( $-1 \leq \Delta < 1$ ) and decays to zero for gapped case ( $\Delta < -1$ ). Thus our numerical data are consistent with LR prediction, as far as whether the long-time limit of the current vanishes or not.

However, the value of  $J(t = \infty)$  itself deviates from LR prediction, especially for large  $|\theta|$ . This behavior is natural because LR theory is not reliable when  $|\theta|$  is large. We plot  $J(t = \infty)/D$  in the left panel of Fig. 4.4. If LR theory is exact,  $J(t = \infty)/D$  must be  $|\theta|$ . As expected, when  $|\theta|$  becomes small  $J(t = \infty)/D$  gets to close to  $|\theta|$ . Furthermore, we find that the deviation from LR theory greatly depends on the *sign* of  $\Delta$ . To see this clearly, the normalized deviation from LR theory  $1 - J(t = \infty)/(D|\theta|)$  is plotted in the right panel of Fig. 4.4. For ferromagnetic interactions ( $\Delta > 0$ ), the normalized deviation from LR theory shows power-law in  $|\theta|$ . In contrast, for large anti-ferromagnetic interactions ( $\Delta < 0$ ),  $J(t = \infty)$  still deviates from LR theory even for small  $|\theta|$ , about  $\pi/20 \approx 0.16$ . We expect that if  $|\theta|$  is made to be smaller than the values of our numerical data ( $|\theta| < \pi/20$ ) the deviation will obey power-law in  $|\theta|$  even for  $\Delta < 0$  case.

<sup>1</sup> At  $\Delta = 1$ , the Drude weight is not continuous with respect to  $\Delta$ .  $\lim_{\Delta \nearrow 1} D(\Delta) = 1/4$ ,  $D(\Delta \geq 1) = 0$ .

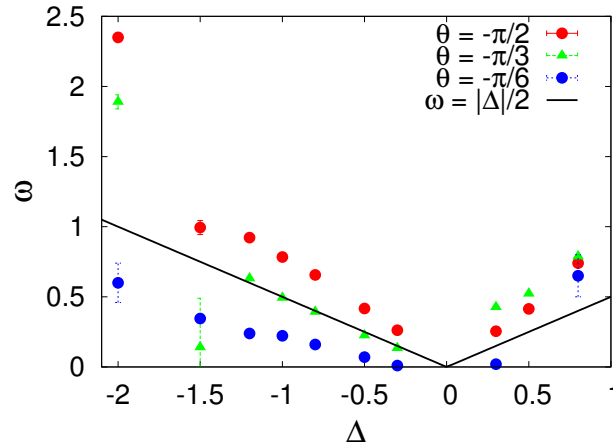


Figure 4.5: Frequency  $\omega$  obtained from fitting of the numerical data.

It is surprising that the deviation from LR theory, or nonlinear response of the system, is larger for  $\Delta < 0$  than for  $\Delta > 0$ .

We may attribute the different behavior of the deviation for  $\Delta > 0$  and  $\Delta < 0$  to *superfluidity* of the system. In one dimension, superfluidity is absent in the strict sense. However, one can observe superfluid-like response in one dimension as dynamical properties of a system [55]. For anti-ferromagnetic interactions ( $\Delta < 0$ ), or repulsive interactions in spinless fermion language, superfluidity of the system is weaker than in the case of ferromagnetic interactions ( $\Delta > 0$ , attractive in spinless fermion). Therefore for  $\Delta < 0$  the large portion of *normal* components dissipates and  $J(t = \infty)$  gets smaller. The smaller value of the long-time limit of the current results in<sup>2</sup> the larger deviation from LR theory.

Finally, we note that this deviation is not an artifact of the fitting. For  $\Delta < 0$  and small  $|\theta|$ , the relaxation time is so large that it is not easy to obtain reliable value of the long-time limit from numerical data. Nevertheless, the decay of current for  $\Delta < 0$  is obviously larger than that of  $\Delta > 0$  when we look at the dynamics (Fig. 4.1). Considering that in LR theory  $J(t = \infty)$  depends on the absolute value of  $\Delta$  (independent on the sign of  $\Delta$ ), we can conclude that the large deviation from LR for  $\Delta < 0$  is not an artifact but an intrinsic behavior of the system.

### 4.3 Frequency of oscillation

The frequency of oscillation is plotted in Fig. 4.5. As already mentioned in section 4.1, we discuss the frequency of oscillation in long time scale only. We found that the frequency  $\omega$  is proportional to  $|\Delta|$ . Furthermore, the proportionality constant (the slope of the plot) is different among  $\theta$ . In gapless phase, there are no time (or energy) scales other than  $\Delta$ , and therefore some dependency of the frequency upon  $\Delta$  is not so surprising. However, the explicit form  $\omega \propto |\Delta|$  is not trivial. Also it should be stressed that even in gapped

<sup>2</sup> Numerically we found that  $J(t = \infty)$  is always smaller than the prediction from LR theory.

phase ( $\Delta < -1$ ) the same relation  $\omega \propto |\Delta|$  holds. In order to explain this relation, we conceive of two scenarios.

### 4.3.1 Equation of motion of spin current

One possible explanation for the relation  $\omega \propto \Delta$  is as below. The second derivative of the equation of motion for the spin current is

$$\begin{aligned} \frac{d^2}{dt^2} J(t) &= \langle [iH_0, [iH_0, \hat{J}]] \rangle (t) \\ &= -\frac{\Delta^2}{4} J(t) + \frac{\Delta^2}{N} \text{Im} \sum_i \langle S_{i-1}^z S_i^+ S_{i+1}^z S_{i+2}^- \rangle (t) \\ &\quad + \frac{\Delta}{N} \text{Im} \sum_i \left( \langle S_i^+ S_{i+2}^- \rangle (t) - \langle S_{i-1}^+ S_i^- S_{i+1}^+ S_{i+2}^- \rangle (t) - \langle S_{i-1}^z S_i^+ S_{i+1}^z S_{i+2}^- \rangle (t) + \langle S_{i-1}^+ S_i^z S_{i+1}^- S_{i+2}^z \rangle (t) \right). \end{aligned} \quad (4.8)$$

If we can neglect the last two terms in the right hand side, this equation becomes simple one describing harmonic oscillations, and its frequency is given by  $\omega = |\Delta|/2$ . Although this is an attracting explanation to the relation  $\omega \propto |\Delta|$ , this cannot explain the different proportionality constants among  $\theta$ ; the frequency of harmonic oscillation is independent of the amplitude (we expect that  $\theta$  is related to the amplitude of oscillation). The equation of motion could help us to understand the behavior of oscillations, although its physical meaning and the validity for neglecting two terms are not clear.

### 4.3.2 Dynamics of momentum distribution $n_q$

As another way to reveal the nature of the dynamics and oscillation, we trace time-evolution of the momentum distribution in spinless fermion picture,

$$n_q = \langle \tilde{c}_q^\dagger \tilde{c}_q \rangle, \quad \tilde{c}_q = \frac{1}{\sqrt{N}} \sum_i e^{-iqr_i} c_i. \quad (4.9)$$

Since the spin current is given by  $\langle J(t) \rangle = N^{-1} \sum_q \sin(q) n_q(t)$ , imbalance of population  $n_q$  between  $q > 0$  and  $q < 0$  means non-zero current. Figure 4.6 and 4.8 show examples of the dynamics of momentum distribution. At first, momentum distribution is the shifted Fermi sea with momentum-shift by  $|\theta|$  (see also Fig. 2.4). After the flux is quenched to zero at  $t = 0$ , the momentum distribution starts evolving. We observed two kinds of oscillation in momentum distribution. One of them coincides with the oscillation of the current in long time scale and could explain the origin of it. Besides, qualitatively different dynamics between in gapless and gapped phase is observed, which gives an interpretation to the behavior of the long-time limit of the current.

#### Two types of oscillation

Two types of oscillation are as follows. One is the collective oscillation of the momentum distribution  $n_q$  in which all momenta  $q$  participate. Amplitude of the oscillation is large for

## Chapter 4. Results and Discussions

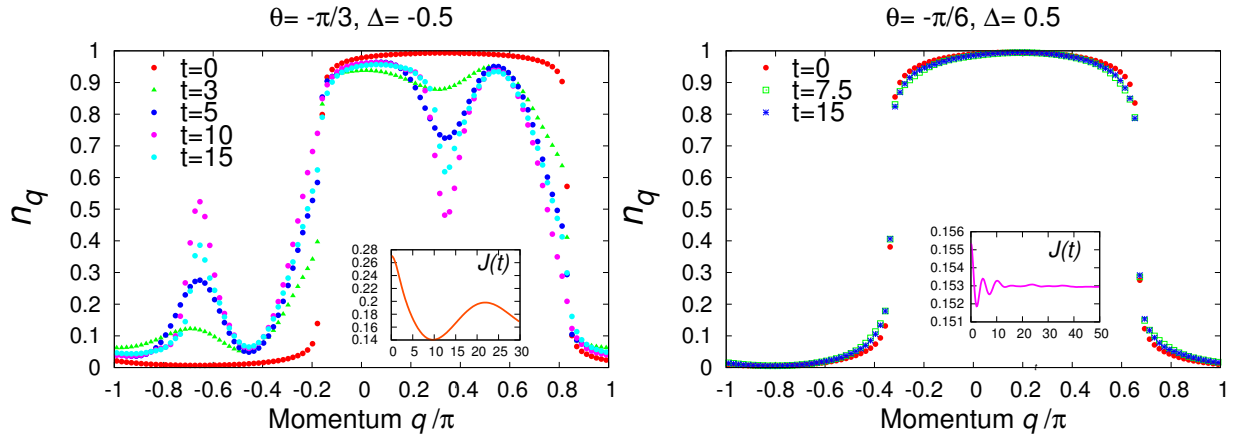


Figure 4.6: Time evolution of momentum distribution. Left panel:  $\theta = -\pi/3$ ,  $\Delta = -0.5$ . Right panel:  $\theta = -\pi/6$ ,  $\Delta = 0.5$ . For the left case, the dip/peak structure and its oscillation is observed though there are no such structures and oscillations in the right case.

$q$  close to the shifted Fermi point,  $k'_F = \pi/2 - |\theta|$ . This type of oscillation is observed for all quench parameters. The other type of oscillation is the oscillation of dip (peak) structure far from the shifted Fermi point. Almost only two momenta  $p_\theta$  and  $p_\theta - \pi$  participate in this oscillation. The visibility of the second type of oscillation almost coincides with the existence of the oscillation in long time scale (compare two panels in Fig. 4.6). In addition, the period of the oscillation in dip (peak) structure matches with the period of the oscillation of the current. Therefore we expect that the dip (peak) structure is related to the oscillation in long time scale.

Taking into account that the dip and peak are separated by momentum  $\pi$ , we can construct a physical picture of the dynamics where only two characteristic modes far from the shifted Fermi point are scattered by the Umklapp process. The oscillation of the current is governed by the oscillation of population between the two modes. This picture is highly non-trivial from the viewpoint of universal TLL, because in TLL the low-energy excitations nearby the Fermi points dictate all of the physics in the system. The validity of TLL picture is ensured by equilibrium renormalization group method and of course there are no guarantees for TLL to be valid in nonequilibrium situations. Besides, we have to treat the shifted Fermi sea in the flux quench, which is not considered by standard TLL theory. Previous studies [19, 20] on the interaction quench in the XXZ chain (see section 2.1) showed that the dynamics after the interaction quench is well described by TLL picture. As far as we know, our study is the first clear illustration in that non-TLL structure strongly affects the dynamics of the system.

Let us discuss the relationship between the dip (peak) structure and the frequency of oscillation. From the picture where only two modes govern the dynamics of the system, we can consider a simplified two-mode Hamiltonian

$$H_{\text{eff}} = \begin{pmatrix} c_{p_\theta}^\dagger & c_{p_\theta - \pi}^\dagger \end{pmatrix} \begin{pmatrix} \varepsilon_{p_\theta} & \beta \\ \beta^* & \varepsilon_{p_\theta - \pi} \end{pmatrix} \begin{pmatrix} c_{p_\theta} \\ c_{p_\theta - \pi} \end{pmatrix}, \quad (4.10)$$

where  $\varepsilon_k := -\cos(k)$  is energy dispersion relation of spinless fermions,  $p_\theta$  is momentum of the particle selectively scattered by the Umklapp process and  $\beta$  is an amplitude of the

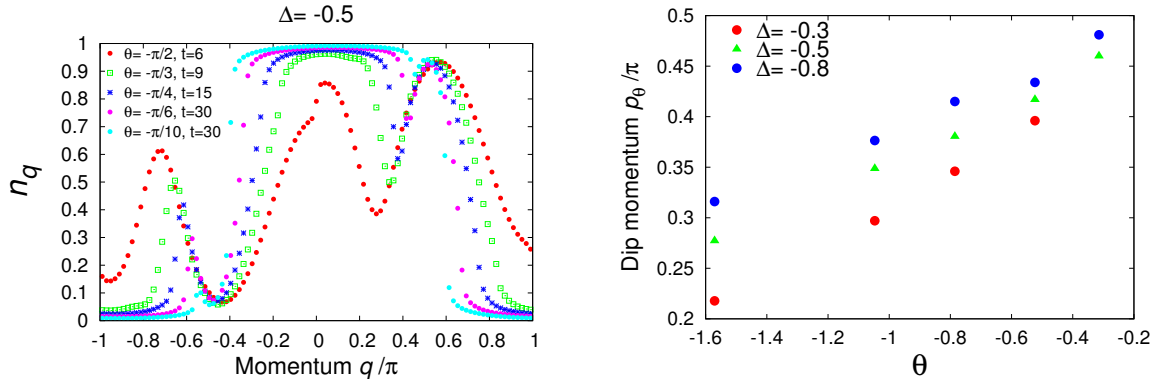


Figure 4.7: Left panel: comparing the momentum distribution with different  $\theta$  at  $\Delta = -0.5$ . Right panel: the momentum of dip,  $p_\theta$ , versus  $\theta$ .

Umklapp scattering expected to be proportional to  $|\Delta|$ . From this simplified two-mode model we can deduce the frequency of the current,

$$\omega \propto \sqrt{\varepsilon_{p_\theta}^2 + |\beta|^2}. \quad (4.11)$$

This would conclude  $\omega \sim |\Delta|$  for small  $\varepsilon_{p_\theta}$ .

Finally, we mention the behavior of  $p_\theta$  as varying  $\Delta$  and  $\theta$ . We calculated the value of  $p_\theta$  from numerical data as the momentum at the bottom of dip structure, and plot  $p_\theta$  versus  $\theta$  in Fig. 4.7. Numerically we found

$$p_\theta = \frac{\pi}{2} - a|\theta|, \quad a \approx 0.40 \sim 0.53 \text{ (depending on } \Delta). \quad (4.12)$$

We have not yet understood the origin of this characteristic momentum  $p_\theta$ .

### Qualitatively different dynamics between in gapless and gapped phase

There is qualitative difference in the dynamics of momentum distribution between in gapless and gapped phase, irrespective of  $\theta$ . In gapless phase, the shifted Fermi sea structure in initial state is *robust* against time-evolution and it survives even after the system becomes stationary (Fig. 4.6). The momentum distribution of the stationary states looks like the shifted Fermi sea again with broader shoulder than the initial states. Shifted, imbalanced momentum distribution results in the persistent current. Therefore, the remaining shifted Fermi sea structure agrees with the non-zero long-time limit of the current in gapless phase. On the other hand, in gapped phase, the shifted Fermi sea structure in initial state is *not robust* against time-evolution and it disappears in relatively short time scale (Fig. 4.8). In that case the whole momentum distribution moves towards the center ( $q = 0$ ) quickly and the imbalance of  $n_q$  between  $q > 0$  and  $q < 0$  is lost, which brings about  $J(t = \infty) = 0$ .

This contrasted difference in the dynamics of momentum distribution between in gapless and gapped phase might be related to additional conserved quantities recently found only in gapless phase [56]. *Additional* means that they are not obtained by the usual algebraic Bethe ansatz. Those additional conserved quantities are responsible for ballistic transport, or non-zero Drude weight, at finite temperature in gapless phase [56]. In a

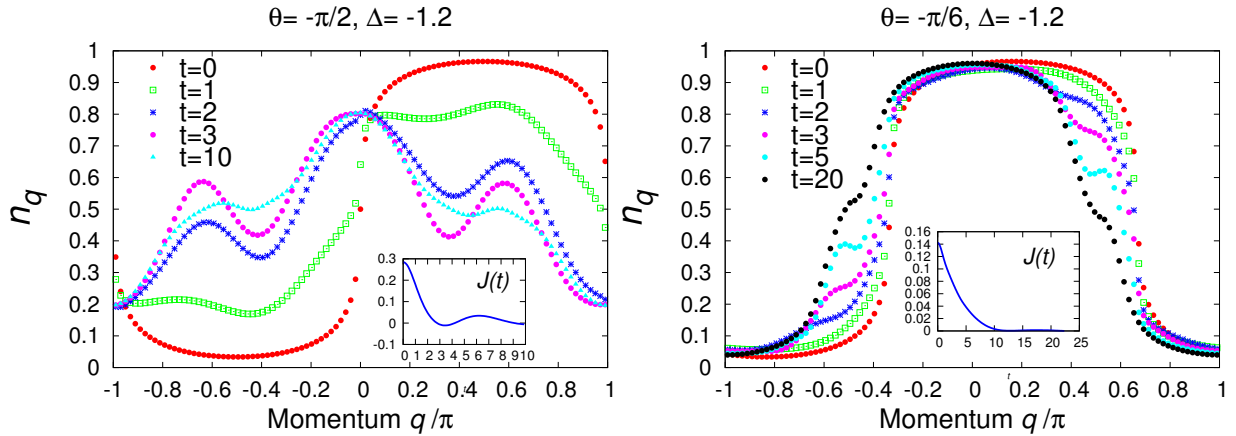


Figure 4.8: Time evolution of momentum distribution for gapped phase. Left panel:  $\theta = -\pi/2, \Delta = -1.2$ . Right panel:  $\theta = -\pi/6, \Delta = -1.2$ . In both cases, the whole momentum distributions move towards the center ( $q = 0$ ) and the current decays to zero.

similar manner, the additional conserved quantities that exist only in gapless phase would prevent the whole movement of momentum distribution, although it is not clear how the conserved quantities affect the dynamics.

## 4.4 Relaxation time

The relaxation time  $\tau$  is plotted in Fig. 4.9. When the time scale of the decay is much larger than the accessible time scale of our calculations, we cannot obtain reliable  $\tau$  from fitting. We omit the data in such cases.

In general, larger  $|\Delta|$  and larger  $|\theta|$  result in smaller  $\tau$  (faster decay). This is natural because the time derivative of the current  $dJ(t)/dt$  is proportional to  $\Delta$  (Eqn. (2.18)). When  $\Delta = 0$  (free fermion point), the spin current is conserved and  $\tau$  must be  $\infty$ . In agreement with this fact,  $\tau$  seems to diverge as  $|\Delta| \rightarrow 0$ . From the plots, we cannot conclude that  $\tau$  obeys exponential-law or power-law in  $\Delta$ . The relationship between  $\tau$  and  $\Delta$  might be complicated than the simple relationship between the frequency  $\omega$  and  $\Delta$ ,  $\omega \propto |\Delta|$ . We have not obtained a good explanation for the data of  $\tau$  yet. In the following, we introduce an analytical result of the relaxation time in the bosonic flux quench, as a possibly related result to our numerical data.

In bosonic case, the decay rate of the current (inverse of the relaxation time) after the flux quench is well computed by the instanton method [57]. In that study, one-dimensional Bose-Hubbard model at large filling  $\nu$  is mapped to  $O(2)$  quantum rotor model and the decay of current is treated as a quantum tunneling between states with different winding numbers. The decay rate of the current is estimated by the action of instanton corresponding to such tunneling. Their conclusion is  $\Gamma \propto p^{2K-2}$ , where  $\Gamma$  is the decay rate of the current,  $p$  is momentum given to initial state and  $K$  is the Luttinger parameter of effective TLL corresponding to the Bose-Hubbard model.

Motivated by this study, we plot  $\tau$  versus the Luttinger parameter  $K$  of the XXZ Hamiltonian ( $K = \pi/(2\arccos(\Delta))$ , Eqn. (2.7)) in Fig. 4.10. The points of this plot are not in line, which means that we cannot conclude simple relation between  $\tau$  and  $K$  as in

## Chapter 4. Results and Discussions

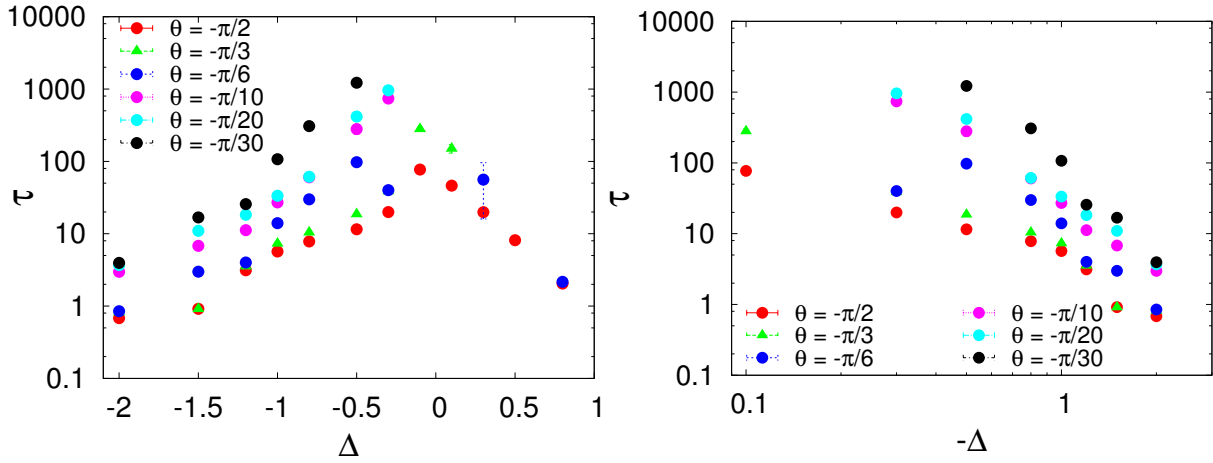


Figure 4.9: Relaxation time  $\tau$ . Left panel shows semi-log plot and right panel shows log-log plot.

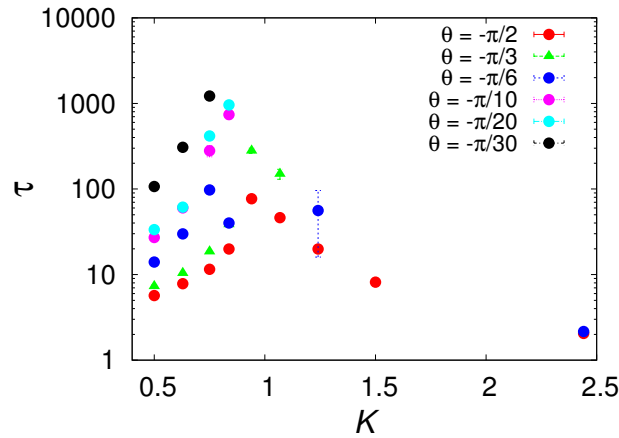


Figure 4.10: Relaxation time  $\tau$  versus the Luttinger parameter  $K$  of the XXZ chain.  $1/2 < K < 1$ ,  $K = 1$  and  $1 < K$  corresponds to repulsive, free and attractive regime, respectively.

the Bose-Hubbard model.

# Chapter 5

## Conclusion, Future Work

In this thesis, we study the flux quench problem in the  $S = 1/2$  XXZ chain by numerical calculations. We focus on two aspects: the long-time limit of the spin current and its dynamics during the time-evolution.

We find that both are dependent strongly on the anisotropy (interaction) parameter  $\Delta$  of the XXZ chain and the amount of flux initially inserted. The long-time limit of the current matches with the predictions of linear response (LR) theory for sufficiently small initial flux. However, its nonlinearity (deviation from LR theory) is largely affected by the sign of interactions. Anti-ferromagnetic interactions, or repulsive interactions for spinless fermions, suppress superfluidity in the system and result in smaller (and also further to LR theory's) values of the current. Regarding the dynamics, the current decays in time after the quench in all parameter regions and its time scale depends on the strength of interactions and the initial flux. Furthermore, in the parameter region where the initial flux is large or the interactions are anti-ferromagnetic (repulsive), the current oscillates in long time scale. We numerically find that the frequency of the oscillation is proportional to  $|\Delta|$ . Remarkably, the dynamics of momentum distribution of spinless fermions indicates that this oscillation of current is caused by excitations deep inside the Fermi sea. This mechanism of oscillations cannot be explained by the effective Luttinger model corresponding to the XXZ chain, which is in contrast with the previous studies on different types of quench in the same XXZ chain.

As future work, we must reveal the nature of specific momentum  $p_\theta$  that appears in momentum distributions. It will help us to understand the oscillation of the current completely. Besides, the origin of nonlinearity of  $J(t = \infty)$  is under investigation. It would need deeper knowledge of superfluid-like response in one-dimensional systems. The clear relationship between the relaxation time  $\tau$  and  $\Delta$  also remains to be solved.

# Appendix A

## Technical details on numerical calculations

### A.1 Details on numerical calculations, error estimate

For numerical simulations of the dynamics, we prepare the ground state of the XXZ Hamiltonian with flux

$$H_\theta = - \sum_i \left( \frac{1}{2} e^{i\theta} S_i^+ S_{i+1}^- + \frac{1}{2} e^{-i\theta} S_i^- S_{i+1}^+ + \Delta S_i^z S_{i+1}^z \right), \quad (\text{A.1})$$

by imaginary time-evolution of iTEBD. Second-order Suzuki-Trotter decomposition is used and typically we take  $\chi = 500$ -1000. Imaginary time step  $\delta\tau$  is reduced from  $\delta\tau = 0.1$  to 0.01 and 0.001 after imaginary time-evolution at coarser  $\delta\tau$  converges. At each  $\delta\tau$ , the convergence is checked by the difference of energy and entanglement entropy of a half chain between two successive time steps. We set a criterion of convergence to 1e-8 for energy and 1e-6 for entanglement entropy. After the imaginary time-evolution at  $\delta\tau = 0.001$  converges, we compare the energy of the obtained states with the exact ground state energy of the XXZ chain [11]<sup>1</sup>,

$$E_{\text{gs}} = -\frac{\Delta}{4} - \frac{\sin \mu}{\mu} \int_0^\infty dx \left( 1 - \frac{\tanh(x)}{\tanh(\pi x/\mu)} \right) \quad (-1 \leq \Delta \leq 1) \quad (\text{A.2})$$

$$E_{\text{gs}} = -\frac{\Delta}{4} - \sinh \rho \left( \frac{1}{2} + \sum_{n=1}^\infty \frac{2}{e^{2n\rho} + 1} \right) \quad (\Delta < -1) \quad (\text{A.3})$$

where  $\mu = \arccos(-\Delta)$  and  $\rho = \text{arccosh}(-\Delta)$ . The energy of the obtained states matches with the exact value for 5 or 6 digit. Therefore, even if the system is in gapless phase ( $-1 \leq \Delta \leq 1$ ) where entanglement entropy of a half chain diverges in the thermodynamic limit (this means  $\chi \rightarrow \infty$ ), we confirm that the converged states of iTEBD with finite bond dimension simulate the true ground states well (related discussion is found in Ref. [20]).

---

<sup>1</sup> Chapter 4 in his textbook, Eqn. (4.28) and (4.44). Note that the interval of integral is misprinted in Eqn (4.44) of his book.

## Appendix A. Technical details on numerical calculations

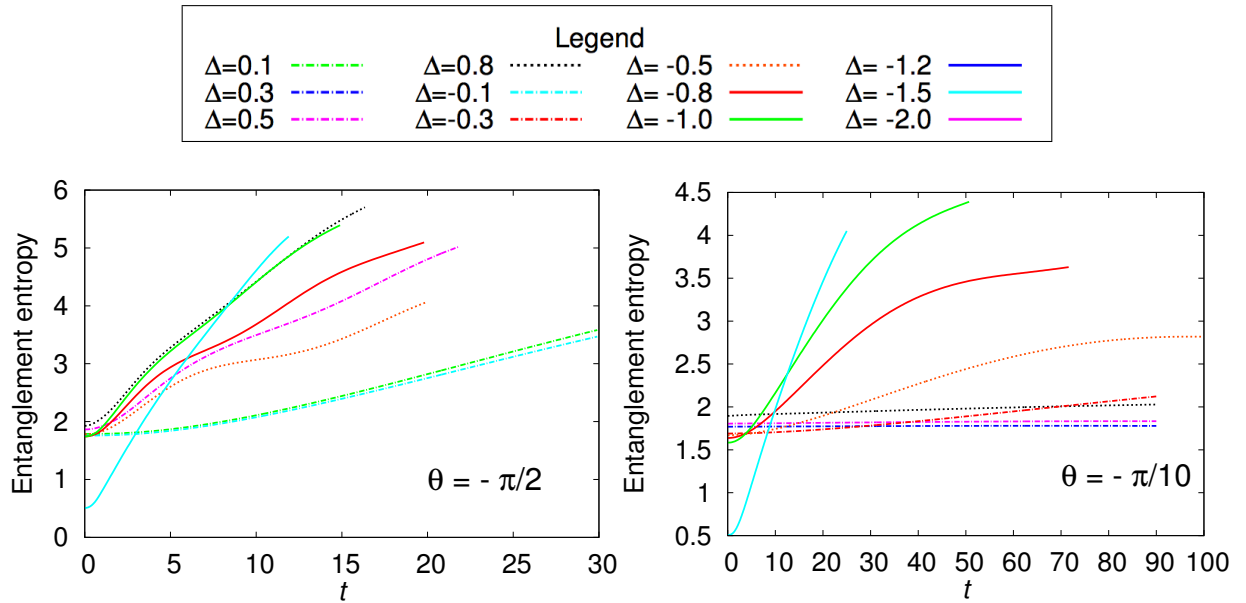


Figure A.1: Entanglement entropy of a half chain after the quench. Left panel shows  $\theta = \pi/2$ , right  $\theta = \pi/10$ . Smaller  $|\Delta|$  results in slower growth of entanglement entropy. Note that we do not show some data for the clarity of the figure.

Next, using iTEBD again, we perform real time-evolution by the XXZ Hamiltonian without flux

$$H_0 = - \sum_i \left( \frac{1}{2} S_i^+ S_{i+1}^- + \frac{1}{2} S_i^- S_{i+1}^+ + \Delta S_i^z S_{i+1}^z \right), \quad (\text{A.4})$$

for the obtained ground states. We take time step  $dt = 0.01$  or  $0.02$ . As the system evolves, the entanglement entropy of a half chain grows almost linearly in time<sup>2</sup> (Fig. A.1). This growth of entanglement entropy increases the truncation error in the iTEBD algorithm and it severely limits the accessible time scale of our calculations.

In order to check the validity of numerical data of the real time-evolution, three criteria are used:

- (a) accumulated truncation error during the dynamics is smaller than  $1e-4$
- (b) energy conservation (unitarity of real time-evolution) is fulfilled within  $1e-4$
- (c) total magnetization  $L^{-1} \sum_i \langle S_i^z \rangle$  is zero in machine precision. We take this criterion because initial states have no magnetization and the time-evolution by  $H_0$  preserves the magnetization.

In addition to these criteria, for some  $\Delta$  and  $\theta$  we changed the time step  $dt$  and the bond dimension  $\chi$ , and confirmed the exactly same numerical data. An example of  $\chi$  dependency of the dynamics is shown in Fig. A.2.

<sup>2</sup> In finite one-dimensional critical systems, entanglement entropy of a half chain grows linearly in time after a *global* quench [58]. By global we mean that the change of parameter happens homogeneously in space.

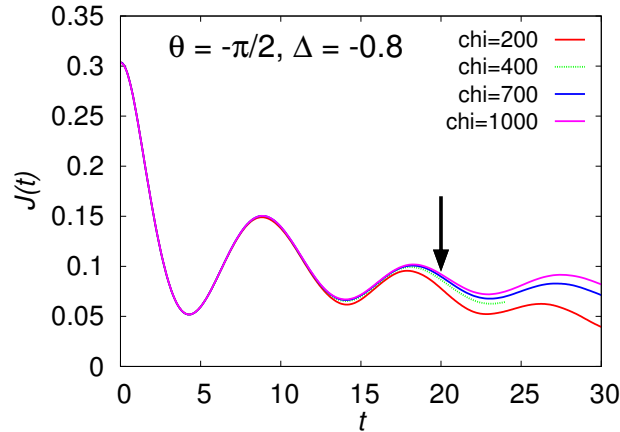


Figure A.2: An example of  $\chi$  dependency of the dynamics. We adopt the data of  $\chi = 1000$  up to  $t = 20$  (indicated by arrow).

Among these criteria, usually the one from truncation error sets the most strict limit on the accessible time scale of calculations. In practice, especially for large  $|\theta|$  and  $\Delta = -0.5$  to  $-1.0$ , we sometimes loosened this criterion to around  $1e-3$ . Even for such cases we confirmed the reliability of data by checking their  $\chi$  dependency or the criteria (b)(c).

## A.2 iTEBD algorithm exploiting a symmetry

Considering symmetries of a system in numerical algorithms greatly reduces computational costs. As an example, let us consider exact diagonalization for a  $L$  site spin-1/2 chain. The dimension of the Hilbert space is  $2^L$ . If Hamiltonian which we want to diagonalize preserves total magnetization, or has a global  $U(1)$  (abelian) symmetry, it can be block-diagonalized according to the value of magnetization (quantum number of that symmetry). The largest size of the block-Hamiltonian (the dimension of the decomposed Hilbert space) is about  ${}_L C_{L/2}$ , which is much smaller than that of the whole Hilbert space (when  $L = 20$ ,  $2^{20} = 1048576$  and  ${}_{20}C_{10} = 184756$ ). Thus computational cost of diagonalization is reduced by several magnitudes. This example clearly illustrates the advantages of exploiting symmetries in numerical algorithms.

In tensor networks, utilizing symmetries of quantum states and Hamiltonian is also possible [59]. For numerical calculations of this study we exploit a symmetry of the XXZ Hamiltonian, conservation of total magnetization, to reduce computational cost<sup>3</sup>. In this section we describe how to incorporate that symmetry of the XXZ Hamiltonian into the iTEBD algorithm [60]. First we prove that quantum states that have definite magnetization can be expressed as MPS explicitly encoding the value of magnetization. Next we describe (i)TEBD algorithm which respects the conservation of magnetization in Hamiltonian.

<sup>3</sup> The time needed to perform simulations was reduced by 40% in our case.

## Appendix A. Technical details on numerical calculations

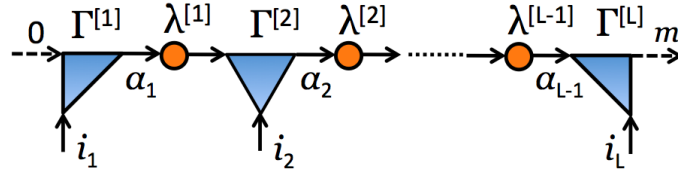


Figure A.3: MPS which encodes magnetization. All bonds have quantum numbers and the arrows indicate the conservation of magnetization at every site.

## MPS associated with magnetization

Consider the same system as we discussed in section 3.3. The Hilbert space consists of  $L$  times tensor product of local Hilbert space,  $\mathcal{H} = \mathbb{C}^d \otimes \mathbb{C}^d \otimes \dots \otimes \mathbb{C}^d = (\mathbb{C}^d)^{\otimes L}$ . For simplicity, here we consider spin-1/2 chain case ( $d = 2$ ) only. The (total) magnetization of the system is defined as

$$\hat{m} = \sum_i \hat{S}_i^z. \quad (\text{A.5})$$

When given state  $|\psi\rangle$  has definite magnetization, or being eigenstate of  $\hat{m}$ , we can construct MPS for  $|\psi\rangle$  which encodes the magnetization (quantum number). In order to do this, we must take local basis  $\{|i\rangle\}$  as eigenstates of local magnetization:  $\{|i\rangle\} = \{|\uparrow\rangle, |\downarrow\rangle\}$ . We associate the local basis with quantum numbers,

$$M(|\uparrow\rangle) = 1/2, \quad M(|\downarrow\rangle) = -1/2, \quad (\text{A.6})$$

which is equal to the magnetization of each basis vector. Specifically, when the eigenvalue of  $|\psi\rangle$  is  $m$ , we can construct MPS

$$|\psi\rangle = \sum_{i_1 i_2 \dots i_L} \sum_{\alpha_1 \dots \alpha_{L-1}=1}^{\chi_i} \Gamma_{\alpha_1}^{[1]i_1} \lambda_{\alpha_1}^{[1]} \Gamma_{\alpha_1 \alpha_2}^{[2]i_2} \lambda_{\alpha_2}^{[2]} \dots \Gamma_{\alpha_{L-2} \alpha_{L-1}}^{[L-1]i_{L-1}} \lambda_{\alpha_{L-1}}^{[L-1]} \Gamma_{\alpha_{L-1}}^{[L]i_L} |i_1 i_2 \dots i_L\rangle, \quad (\text{A.7})$$

where all indices  $\alpha_k$  are associated with some quantum numbers  $M(\alpha_k)$  and the tensors  $\Gamma_{\alpha_{k-1} \alpha_k}^{[k]i_k}$  can have non-zero value only when

$$\begin{cases} M(|i_1\rangle) = M(\alpha_1) \\ M(\alpha_{k-1}) + M(|i_k\rangle) = M(\alpha_k) \quad (1 < k < L) \\ M(\alpha_{L-1}) + M(|i_L\rangle) = m \end{cases}. \quad (\text{A.8})$$

Furthermore, all Schmidt vectors  $|\tau_{\alpha_k}^{[1 \dots k]}\rangle = \sum_{\{i\}\{\alpha\}} \Gamma_{\alpha_1}^{[1]i_1} \lambda_{\alpha_1}^{[1]} \dots \Gamma_{\alpha_{k-1} \alpha_k}^{[k]i_k} |i_1 \dots i_k\rangle$  become eigenstates of magnetization, and physical meaning of  $M(\alpha_k)$  is the eigenvalue of magnetization for  $|\tau_{\alpha_k}^{[1 \dots k]}\rangle$ . Thus the condition (A.8) can be interpreted as the conservation of magnetization at site  $k$ .

Diagrammatically, the condition (A.8) is represented by drawing all bonds as arrows (Fig. A.3). The fictitious arrow labeled as 0 comes in from left and the fictitious arrow labeled as  $m$  comes out to right.

## Appendix A. Technical details on numerical calculations

**Proof**

When  $|\psi\rangle = \sum_{i_1 \dots i_L} c_{i_1 \dots i_L} |i_1 \dots i_L\rangle$  have definite magnetization  $m$ , its wave function  $c_{i_1 i_2 \dots i_L}$  can be non-zero only if

$$M(|i_1\rangle) + M(|i_2\rangle) + \dots + M(|i_L\rangle) = m. \quad (\text{A.9})$$

Therefore,  $2 \times 2^{L-1}$  matrix  $C^{[1]} = (c_{i_1, (i_2 \dots i_L)})$  can be block-diagonalized according to each value  $m_1 := M(|i_1\rangle)$  by permuting the basis  $(i_2 \dots i_L)$  properly. In other words, by choosing proper  $2^{L-1} \times 2^{L-1}$  permutation matrix<sup>4</sup>  $Q^{[1]}$

$$C^{[1]}Q^{[1]} = \begin{pmatrix} A_1 & 0 & 0 \\ 0 & A_2 & 0 \end{pmatrix} \begin{matrix} \leftarrow m_1 = 1/2 \\ \leftarrow m_1 = -1/2 \end{matrix}, \quad (\text{A.10})$$

where  $A_1$  and  $A_2$  are  $1 \times {}_{L-1}C_{m+L/2-1}$  and  $1 \times {}_{L-1}C_{m+L/2}$  matrices. SVD for  $C^{[1]}$  is obtained from SVDs for  $A_1$  and  $A_2$ ,

$$A_1 \stackrel{\text{SVD}}{=} U_1 S_1 V_1, \quad A_2 \stackrel{\text{SVD}}{=} U_2 S_2 V_2, \\ C^{[1]} \stackrel{\text{SVD}}{=} \begin{pmatrix} U_1 & 0 \\ 0 & U_2 \end{pmatrix} \cdot \begin{pmatrix} S_1 & 0 \\ 0 & S_2 \end{pmatrix} \cdot \begin{pmatrix} V_1 & 0 & 0 \\ 0 & V_2 & 0 \end{pmatrix} (Q^{[1]})^{-1}. \quad (\text{A.11})$$

Note that unitarity of  $Q^{[1]}$  assures that this decomposition for  $C^{[1]}$  is actually SVD. In the same way as explained in section 3.3, we define

$$\Gamma_{\alpha_1}^{[1]i_1} = \begin{pmatrix} U_1 & 0 \\ 0 & U_2 \end{pmatrix}_{i_1, \alpha_1}, \quad \lambda_{\alpha_1}^{[1]} = \begin{pmatrix} S_1 & 0 \\ 0 & S_2 \end{pmatrix}_{\alpha_1, \alpha_1}, \quad V_{\alpha_1, i_2 \dots i_L}^{[1]} = \begin{pmatrix} V_1 & 0 & 0 \\ 0 & V_2 & 0 \end{pmatrix} (Q^{[1]})^{-1} \Big|_{\alpha_1, i_2 \dots i_L} \\ c_{i_1, (i_2 \dots i_L)} = \sum_{\alpha_1=1}^{\chi_1} \Gamma_{\alpha_1}^{[1]i_1} \lambda_{\alpha_1}^{[1]} V_{\alpha_1, i_2 \dots i_L}^{[1]}. \quad (\text{A.12})$$

From construction, Schmidt vector  $|\tau_{\alpha_1}^{[1]}\rangle = \sum_{i_1} \Gamma_{\alpha_1}^{[1]i_1} |i_1\rangle$  becomes an eigenvector of magnetization. We can associate index  $\alpha_1$  with quantum number

$$M(\alpha_1) := M(|i_1\rangle) (= m - M(|i_2\rangle) + \dots + M(|i_L\rangle)), \quad (\text{A.13})$$

which is equal to the magnetization of Schmidt vector  $|\tau_{\alpha_1}^{[1]}\rangle$ .

As a next step, we perform SVD on  $\bar{V}_{\alpha_1 i_2, i_3 \dots i_L}^{[1]} := \lambda_{\alpha_1}^{[1]} V_{\alpha_1 (i_2 \dots i_L)}^{[1]}$ . From the definition of  $V^{[1]}$ , we know that  $\bar{V}_{\alpha_1 i_2, i_3 \dots i_L}^{[1]}$  can be non-zero only when

$$M(\alpha_1) + M(|i_2\rangle) + \dots + M(|i_L\rangle) = m. \quad (\text{A.14})$$

Again  $\bar{V}^{[1]}$  is block-diagonalized according to  $m_2 := M(|\alpha_1\rangle) + M(|i_2\rangle)$  by permuting indices  $(\alpha_1 i_2)$  and  $(i_3 \dots i_L)$ ,

$$P^{[2]}\bar{V}^{[1]}Q^{[2]} = \begin{pmatrix} B_1 & 0 & 0 & 0 \\ 0 & B_2 & 0 & 0 \\ 0 & 0 & B_3 & 0 \end{pmatrix} \begin{matrix} \leftarrow m_2 = 1 \\ \leftarrow m_2 = 0 \\ \leftarrow m_2 = -1 \end{matrix}, \quad (\text{A.15})$$

<sup>4</sup> when elements of matrix  $A = (a_{ij})$  satisfies  $a_{ij} = \mathcal{P}_{ij}$ ,  $\mathcal{P} \in \mathfrak{S}_N$  (symmetric group of degree  $n$ ),  $A$  is called permutation matrix. Permutation matrix is unitary,  $A^\dagger A = 1$ .

## Appendix A. Technical details on numerical calculations

where  $P^{[2]}$  and  $Q^{[2]}$  are  $2\chi_1 \times 2\chi_1$  and  $2^{L-2} \times 2^{L-2}$  permutation matrices. SVDs for each matrix  $B_i \stackrel{\text{SVD}}{=} U_i S_i V_i$  yield SVD for  $\bar{V}^{[1]}$ ,

$$\bar{V}^{[1]} \stackrel{\text{SVD}}{=} (P^{[2]})^{-1} \begin{pmatrix} U_1 & 0 & 0 \\ 0 & U_2 & 0 \\ 0 & 0 & U_3 \end{pmatrix} \cdot \begin{pmatrix} S_1 & 0 & 0 \\ 0 & S_2 & 0 \\ 0 & 0 & S_3 \end{pmatrix} \cdot \begin{pmatrix} V_1 & 0 & 0 & 0 \\ 0 & V_2 & 0 & 0 \\ 0 & 0 & V_3 & 0 \end{pmatrix} (Q^{[2]})^{-1}.$$

Then  $\Gamma^{[2]}$  and  $\lambda^{[2]}$  are defined by

$$\begin{aligned} \Gamma_{\alpha_1 \alpha_2}^{[2] i_2} &:= (\lambda_{\alpha_1}^{[1]})^{-1} \cdot (P^{[2]})^{-1} \begin{pmatrix} U_1 & 0 & 0 \\ 0 & U_2 & 0 \\ 0 & 0 & U_3 \end{pmatrix} \Big|_{\alpha_1 i_2, \alpha_2}, & \lambda_{\alpha_2}^{[2]} &= \begin{pmatrix} S_1 & 0 & 0 \\ 0 & S_2 & 0 \\ 0 & 0 & S_3 \end{pmatrix} \Big|_{\alpha_2, \alpha_2}, \\ V_{\alpha_2, i_3 \dots i_L}^{[2]} &:= \begin{pmatrix} V_1 & 0 & 0 & 0 \\ 0 & V_2 & 0 & 0 \\ 0 & 0 & V_3 & 0 \end{pmatrix} (Q^{[2]})^{-1} \Big|_{\alpha_2, i_3 \dots i_L}, \\ \bar{V}_{\alpha_1 i_2, i_3 \dots i_L}^{[1]} &= \sum_{\alpha_2=1}^{\chi_2} \lambda_{\alpha_1}^{[1]} \Gamma_{\alpha_1 \alpha_2}^{[2] i_2} \lambda_{\alpha_2}^{[2]} V_{\alpha_2, i_3 \dots i_L}^{[2]}. \end{aligned} \quad (\text{A.16})$$

Schmidt vector  $|\tau_{\alpha_2}^{[12]}\rangle = \sum_{i_2 \alpha_1} \lambda_{\alpha_1}^{[1]} \Gamma_{\alpha_1 \alpha_2}^{[2] i_2} |\tau_{\alpha_1}^{[1]}\rangle |i_2\rangle$  becomes an eigenstate of magnetization, and new index  $\alpha_2$  can be associated with quantum number (magnetization of  $|\tau_{\alpha_2}^{[12]}\rangle$ )

$$M(\alpha_2) := M(\alpha_1) + M(|i_2\rangle). \quad (\text{A.17})$$

Obviously, the condition (A.8) for  $\Gamma^{[2]}$  is satisfied.

Repeating this procedure (block-diagonalizing  $\bar{V}^{[k]}$  and performing SVD for each block), we can construct MPS for  $|\psi\rangle$  exploiting quantum numbers and satisfying the condition (A.8). ■

## TEBD, iTEBD algorithm with conservation of magnetization

When Hamiltonian conserves quantum numbers exploited by MPS, the block structure of  $\{\Gamma^{[k]}\}_k$  in MPS (Eqn. (A.8)) is preserved during time-evolution. In that case, TEBD and iTEBD algorithm respecting the quantum numbers can be constructed. As we will see later, by exploiting symmetry computational cost of the algorithm is reduced by one or two magnitude.

Consider Hamiltonian on spin-1/2 chain which can be decomposed as the sum of two-site operators  $\hat{H} = \sum_l \hat{H}_{l, l+1}$  and each term preserves total magnetization:  $[\hat{m}, \hat{H}_{l, l+1}] = 0$ . In that case, time-evolution operators used in the (i)TEBD algorithm, such as  $\hat{V} = e^{-\delta\tau \hat{H}_{l, l+1}}$ , also preserve magnetization:  $[\hat{m}, \hat{V}] = 0$ . Hence matrix representation of  $\hat{V} = \sum_{ij} V_{j_i j_{i+1}}^{i_i i_{i+1}} |i_i i_{i+1}\rangle \langle j_i j_{i+1}|$  has non-zero components only when

$$M(|i_i\rangle) + M(|i_{i+1}\rangle) = M(|j_i\rangle) + M(|j_{i+1}\rangle). \quad (\text{A.18})$$

## Appendix A. Technical details on numerical calculations

As a consequence, if initial MPS satisfies the condition (A.8), the matrix  $\Theta$  considered in (i)TEBD algorithm

$$\Theta_{(i_l\alpha_{l-1}), (i_{l+1}\alpha_{l+1})} = \sum_{j_l, j_{l+1}, \alpha_l} \left( \lambda_{\alpha_{l-1}}^{[l-1]} \Gamma_{\alpha_{l-1}\alpha_l}^{[l]j_l} \lambda_{\alpha_l}^{[l]} \Gamma_{\alpha_l\alpha_{l+1}}^{[l+1]j_{l+1}} \lambda_{\alpha_{l+1}}^{[l+1]} \right) V_{j_l j_{l+1}}^{i_l i_{l+1}} \quad (\text{A.19})$$

has non-zero elements only when

$$M(|i_l\rangle) + M(\alpha_{l-1}) = M(|i_{l+1}\rangle) + M(\alpha_{l+1}). \quad (\text{A.20})$$

Then  $\Theta$  has block-diagonal structure according to  $m_l := M(|i_l\rangle) + M(\alpha_{l-1})$ ,

$$P\Theta Q = \begin{pmatrix} \Theta_1 & 0 & \cdots \\ 0 & \Theta_2 & \cdots \\ \vdots & \vdots & \ddots \end{pmatrix}, \quad (\text{A.21})$$

where  $P$  and  $Q$  are some permutation matrices of size  $2\chi_{l-1} \times 2\chi_{l-1}$  and  $2\chi_{l+1} \times 2\chi_{l+1}$ . SVDs for each block  $\Theta_i = U_i S_i V_i$  yield SVD for  $\Theta$ ,

$$\Theta \stackrel{\text{SVD}}{=} P^{-1} \begin{pmatrix} U_1 & 0 & \cdots \\ 0 & U_2 & \cdots \\ \vdots & \vdots & \ddots \end{pmatrix} \cdot \begin{pmatrix} S_1 & 0 & \cdots \\ 0 & S_2 & \cdots \\ \vdots & \vdots & \ddots \end{pmatrix} \cdot \begin{pmatrix} V_1 & 0 & \cdots \\ 0 & V_2 & \cdots \\ \vdots & \vdots & \ddots \end{pmatrix} Q^{-1}. \quad (\text{A.22})$$

New tensors  $\tilde{\Gamma}^{[l]}, \tilde{\Gamma}^{[l+1]}, \tilde{\lambda}^{[l]}$  are obtained by

$$\begin{aligned} \tilde{\Gamma}_{\alpha_{l-1}\alpha_l}^{[l]i_l} &= \left( \lambda_{\alpha_{l-1}}^{[l-1]} \right)^{-1} \left( P^{-1} \begin{pmatrix} U_1 & 0 & \cdots \\ 0 & U_2 & \cdots \\ \vdots & \vdots & \ddots \end{pmatrix} \right)_{i_l\alpha_{l-1}, \alpha_l}, \\ \tilde{\Gamma}_{\alpha_l\alpha_{l+1}}^{[l+1]i_{l+1}} &= \left( \lambda_{\alpha_{l+1}}^{[l+1]} \right)^{-1} \left( \begin{pmatrix} V_1 & 0 & \cdots \\ 0 & V_2 & \cdots \\ \vdots & \vdots & \ddots \end{pmatrix} Q^{-1} \right)_{\alpha_l, i_{l+1}\alpha_{l+1}}, \quad \tilde{\lambda}_{\alpha_l}^{[l]} = \begin{pmatrix} S_1 & 0 & \cdots \\ 0 & S_2 & \cdots \\ \vdots & \vdots & \ddots \end{pmatrix}_{\alpha_l, \alpha_l} \\ \Theta_{(i_l\alpha_{l-1}), (i_{l+1}\alpha_{l+1})} &= \sum_{\alpha_l=1}^{\tilde{\chi}_l} \lambda_{\alpha_{l-1}}^{[l-1]} \tilde{\Gamma}_{\alpha_{l-1}\alpha_l}^{[l]i_l} \tilde{\lambda}_{\alpha_l}^{[l]} \tilde{\Gamma}_{\alpha_l\alpha_{l+1}}^{[l+1]i_{l+1}} \lambda_{\alpha_{l+1}}^{[l+1]}. \end{aligned} \quad (\text{A.23})$$

Quantum numbers associated with new indices  $\alpha_l (= 1, \dots, \tilde{\chi}_l)$  are

$$M(\alpha_l) := M(|i_l\rangle) + M(\alpha_{l-1}) (= M(|i_{l+1}\rangle) + M(\alpha_{l+1})), \quad (\text{A.24})$$

which are equal to the magnetization of Schmidt vector  $|\tau_{\alpha_l}^{[1\dots l]}\rangle = \sum_{i_l\alpha_{l-1}} \lambda_{\alpha_{l-1}}^{[l-1]} \tilde{\Gamma}_{\alpha_{l-1}\alpha_l}^{[l]i_l} |\tau_{\alpha_{l-1}}^{[1\dots l-1]}\rangle |i_l\rangle$ .

By definition, the updated tensors  $\tilde{\Gamma}, \tilde{\lambda}$  satisfy the condition (A.8).

### Practical procedure of the algorithm and computational cost

In order to implement the (i)TEBD algorithm exploiting a symmetry into actual computer programs, we have to prepare lists of quantum numbers  $\{M(\alpha_k)\}_k$  as well as MPS  $\{\Gamma^{[k]}, \lambda^{[k]}\}_k$ . The update of tensors  $\Gamma^{[l]}, \Gamma^{[l+1]}$  is performed as below (we write bond dimension as  $\chi$ ):

## Appendix A. Technical details on numerical calculations

- (1) computing  $\Theta_i$  by using the list  $\{M(\alpha_k)\}_k$  and the condition (A.20). We do not have to calculate  $\Theta$ .
- (2) doing SVD for each  $\Theta_i$ . Because the size of matrix  $\Theta_i$  is smaller than that of  $\Theta$ , the cost of SVD is greatly reduced (we will see an example below).
- (3) sorting all Schmidt values obtained from the SVDs for  $\Theta_i$  ( $i = 1, 2, \dots$ ). In practice we merge lists of the singular value from each  $\Theta_i$  and sort it. If the number of the Schmidt values is larger than  $\chi$  in total, we have to truncate Schmidt vectors with smaller singular values (irrespective of the number  $i$ ).
- (4) storing the Schmidt vectors and Schmidt values into tensors  $\tilde{\Gamma}$  and  $\tilde{\lambda}$  properly, by using the list  $\{M(\alpha_k)\}_k$ .

Let us discuss how much computational cost of SVD is reduced by exploiting the symmetry (the conservation of magnetization). SVD for  $n \times n$  matrix takes  $O(n^3)$  time. Therefore without exploiting the symmetry, cost of SVD is  $O((2\chi)^3)$ . On the other hand, when we consider the symmetry, we have only to perform SVD for the smaller matrix,  $\Theta_i$ . Typically we have experienced that the largest size of matrix  $\Theta_i$  ( $i = 1, 2, \dots$ ) is nearly a quarter of the size of  $\Theta$ , and therefore we gain  $4^3 = 64$  times speed-up by exploiting the symmetry<sup>5</sup>. For example, in the case of the ground state for  $\Delta = -0.5$ ,  $\chi = 1000$ , the number of indices  $\alpha_k$  ( $k \in$  odd sites) that have quantum number  $M(\alpha_k) = [3, 2, 1, 0, -1, -2, -3, -4, -5]$  is  $[8, 52, 147, 241, 261, 186, 83, 20, 2]$ , respectively<sup>6</sup>. The largest size of  $\Theta_i$  in this case is  $241 + 261 = 502$ , much smaller than the size of  $\Theta$ , 2000.

**Comment on quantum numbers in iMPS and iTEBD**

In iMPS and iTEBD, the physical meaning of quantum numbers for indices  $\alpha_k$  can be subtle because magnetization of Schmidt vector can become infinite. However, this subtlety is avoided if we consider the quantum numbers as the *difference* of magnetization of Schmidt vectors between initial state and current state [60].

<sup>5</sup> We have to do many SVDs for each time step, so actual speed-up of the algorithm is less than 64 times.

<sup>6</sup> for  $k \in$  even sites, the number of indices  $\alpha_k$  that have  $M(\alpha_k) = [7, 5, 3, 1, -1, -3, -5, -7, -9]$  is  $[2, 25, 94, 198, 267, 231, 131, 45, 7]$ , respectively.

# Bibliography

- [1] M. Lewenstein, A. Sanpera and V. Ahufinger. *Ultracold Atoms in Optical Lattices: Simulating quantum many-body systems*. Oxford University Press (2012).
- [2] A. Polkovnikov, K. Sengupta, A. Silva and M. Vengalattore. “Colloquium : Nonequilibrium dynamics of closed interacting quantum systems”. *Rev. Mod. Phys.* **83**, 863–883 (2011).
- [3] J. Dziarmaga. “Dynamics of a quantum phase transition and relaxation to a steady state”. *Advances in Physics* **59**, 1063–1189 (2010).
- [4] M. Rigol, V. Dunjko and M. Olshanii. “Thermalization and its mechanism for generic isolated quantum systems”. *Nature* **452**, 854–858 (2008).
- [5] M. Rigol, V. Dunjko, V. Yurovsky and M. Olshanii. “Relaxation in a Completely Integrable Many-Body Quantum System: An *Ab Initio* Study of the Dynamics of the Highly Excited States of 1D Lattice Hard-Core Bosons”. *Phys. Rev. Lett.* **98**, 050405 (2007).
- [6] M. Mierzejewski, P. Prelovšek and T. Prosen. “Breakdown of the Generalized Gibbs Ensemble for Current-Generating Quenches”. *Phys. Rev. Lett.* **113**, 020602 (2014).
- [7] M. A. Cazalilla. “Effect of Suddenly Turning on Interactions in the Luttinger Model”. *Phys. Rev. Lett.* **97**, 156403 (2006).
- [8] N. Nesi, A. Iucci and M. A. Cazalilla. “Quantum Quench and Prethermalization Dynamics in a Two-Dimensional Fermi Gas with Long-Range Interactions”. *Phys. Rev. Lett.* **113**, 210402 (2014).
- [9] T. Giamarchi. *Quantum physics in one dimension*. Number 121 in The international series of monographs on physics. Clarendon Press (2004).
- [10] A. A. Abrikosov, L. P. Gorkov and I. E. Dzyaloshinski. *Methods of quantum field theory in statistical physics*. Courier Dover Publications (1975).
- [11] M. Takahashi. *Thermodynamics of One-Dimensional Solvable Models*. Cambridge University Press (1999). Cambridge Books Online.
- [12] P. Di Francesco, P. Mathieu and D. Sénéchal. *Conformal field theory*. Graduate texts in contemporary physics. Springer (1997).

Bibliography

---

- [13] A. W. Sandvik. “Computational Studies of Quantum Spin Systems”. In *AIP Conf. Proc*, volume 1297, 135 (2010).
- [14] S. White. “Density matrix formulation for quantum renormalization groups”. *Phys. Rev. Lett.* **69**, 2863–2866 (1992).
- [15] G. Vidal. “Efficient Simulation of One-Dimensional Quantum Many-Body Systems”. *Phys. Rev. Lett.* **93**, 040502 (2004).
- [16] E. Lieb, T. Schultz and D. Mattis. “Two soluble models of an antiferromagnetic chain”. *Annals of Physics* **16**, 407 – 466 (1961).
- [17] P. Barmettler, M. Punk, V. Gritsev, E. Demler and E. Altman. “Relaxation of Antiferromagnetic Order in Spin-1/2 Chains Following a Quantum Quench”. *Phys. Rev. Lett.* **102**, 130603 (2009).
- [18] M. Fagotti, M. Collura, F. H. L. Essler and P. Calabrese. “Relaxation after quantum quenches in the spin- $\frac{1}{2}$  Heisenberg XXZ chain”. *Phys. Rev. B* **89**, 125101 (2014).
- [19] C. Karrasch, J. Rentrop, D. Schuricht and V. Meden. “Luttinger-liquid universality in the time evolution after an interaction quench”. *Phys. Rev. Lett.* **109**, 126406 (2012).
- [20] F. Pollmann, M. Haque and B. Dóra. “Linear quantum quench in the Heisenberg XXZ chain: Time-dependent Luttinger-model description of a lattice system”. *Phys. Rev. B* **87**, 041109 (2013).
- [21] J.-S. Caux and F. H. L. Essler. “Time Evolution of Local Observables After Quenching to an Integrable Model”. *Phys. Rev. Lett.* **110**, 257203 (2013).
- [22] W. Liu and N. Andrei. “Quench Dynamics of the Anisotropic Heisenberg Model”. *Phys. Rev. Lett.* **112**, 257204 (2014).
- [23] B. Shastry and B. Sutherland. “Twisted boundary conditions and effective mass in Heisenberg-Ising and Hubbard rings”. *Phys. Rev. Lett.* **65**, 243–246 (1990).
- [24] B. Sutherland and B. Shastry. “Adiabatic transport properties of an exactly soluble one-dimensional quantum many-body problem”. *Phys. Rev. Lett.* **65**, 1833–1837 (1990).
- [25] V. KOREPIN and A. WU. “ADIABATIC TRANSPORT PROPERTIES AND BERRY’S PHASE IN HEISENBERG-ISING RING”. *International Journal of Modern Physics B* **05**, 497–507 (1991).
- [26] C. J. Hamer, G. R. W. Quispel and M. T. Batchelor. “Conformal anomaly and surface energy for Potts and Ashkin-Teller quantum chains”. *Journal of Physics A: Mathematical and General* **20**, 5677 (1987).
- [27] J. Mun, P. Medley, G. K. Campbell, L. G. Marcassa, D. E. Pritchard and W. Ketterle. “Phase Diagram for a Bose-Einstein Condensate Moving in an Optical Lattice”. *Phys. Rev. Lett.* **99**, 150604 (2007).

- 
- [28] S. Peotta, C.-C. Chien and M. Di Ventra. “Phase-induced transport in atomic gases: From superfluid to Mott insulator”. *Phys. Rev. A* **90**, 053615 (2014).
- [29] S. Hild, T. Fukuhara, P. Schauß, J. Zeiher, M. Knap, E. Demler, I. Bloch and C. Gross. “Far-from-Equilibrium Spin Transport in Heisenberg Quantum Magnets”. *Phys. Rev. Lett.* **113**, 147205 (2014).
- [30] J. Schachenmayer, G. Pupillo and A. J. Daley. “Time-dependent currents of one-dimensional bosons in an optical lattice”. *New Journal of Physics* **12**, 025014 (2010).
- [31] R. Orús. “A practical introduction to tensor networks: Matrix product states and projected entangled pair states”. *Annals of Physics* **349**, 117 – 158 (2014).
- [32] M. Troyer and U.-J. Wiese. “Computational Complexity and Fundamental Limitations to Fermionic Quantum Monte Carlo Simulations”. *Phys. Rev. Lett.* **94**, 170201 (2005).
- [33] P. Corboz, R. Orús, B. Bauer and G. Vidal. “Simulation of strongly correlated fermions in two spatial dimensions with fermionic projected entangled-pair states”. *Phys. Rev. B* **81**, 165104 (2010).
- [34] F. Verstraete and J. I. Cirac. “Renormalization algorithms for Quantum-Many Body Systems in two and higher dimensions”. *arXiv:cond-mat/0407066* (2004).
- [35] G. Vidal. “Class of Quantum Many-Body States That Can Be Efficiently Simulated”. *Phys. Rev. Lett.* **101**, 110501 (2008).
- [36] U. Schollwöck. “The density-matrix renormalization group in the age of matrix product states”. *Annals of Physics* **326**, 96 – 192 (2011).
- [37] X. G. Wen. “TOPOLOGICAL ORDERS IN RIGID STATES”. *International Journal of Modern Physics B* **04**, 239–271 (1990).
- [38] X. Chen, Z.-C. Gu and X.-G. Wen. “Local unitary transformation, long-range quantum entanglement, wave function renormalization, and topological order”. *Phys. Rev. B* **82**, 155138 (2010).
- [39] X. Chen, Z.-C. Gu, Z.-X. Liu and X.-G. Wen. “Symmetry protected topological orders and the group cohomology of their symmetry group”. *Phys. Rev. B* **87**, 155114 (2013).
- [40] F. Pollmann, A. Turner, E. Berg and M. Oshikawa. “Entanglement spectrum of a topological phase in one dimension”. *Phys. Rev. B* **81**, 064439 (2010).
- [41] F. Pollmann, E. Berg, A. Turner and M. Oshikawa. “Symmetry protection of topological phases in one-dimensional quantum spin systems”. *Phys. Rev. B* **85**, 075125 (2012).
- [42] J. Eisert, M. Cramer and M. Plenio. “Colloquium : Area laws for the entanglement entropy”. *Rev. Mod. Phys.* **82**, 277–306 (2010).

Bibliography

---

- [43] M. Hastings and T. Koma. “Spectral Gap and Exponential Decay of Correlations”. *Communications in Mathematical Physics* **265**, 781–804 (2006).
- [44] M. B. Hastings. “An area law for one-dimensional quantum systems”. *Journal of Statistical Mechanics: Theory and Experiment* **2007**, P08024 (2007).
- [45] M. Wolf, F. Verstraete, M. Hastings and J. Cirac. “Area Laws in Quantum Systems: Mutual Information and Correlations”. *Phys. Rev. Lett.* **100**, 070502 (2008).
- [46] P. Calabrese and J. Cardy. “Entanglement entropy and quantum field theory”. *Journal of Statistical Mechanics: Theory and Experiment* **2004**, P06002 (2004).
- [47] S. Sen. “Average Entropy of a Quantum Subsystem”. *Phys. Rev. Lett.* **77**, 1–3 (1996).
- [48] D. Poulin, A. Qarry, R. Somma and F. Verstraete. “Quantum Simulation of Time-Dependent Hamiltonians and the Convenient Illusion of Hilbert Space”. *Phys. Rev. Lett.* **106**, 170501 (2011).
- [49] M. Hastings. “Solving gapped Hamiltonians locally”. *Phys. Rev. B* **73**, 085115 (2006).
- [50] G. Golub and C. Van Loan. *Matrix Computations*. Johns Hopkins studies in the mathematical sciences. Johns Hopkins University Press (1996).
- [51] D. Perez-Garcia, F. Verstraete, M. M. Wolf and J. I. Cirac. “Matrix Product State Representations”. *Quantum Info. Comput.* **7**, 401–430 (2007).
- [52] G. Vidal. “Classical Simulation of Infinite-Size Quantum Lattice Systems in One Spatial Dimension”. *Phys. Rev. Lett.* **98**, 070201 (2007).
- [53] R. Orús and G. Vidal. “Infinite time-evolving block decimation algorithm beyond unitary evolution”. *Phys. Rev. B* **78**, 155117 (2008).
- [54] D. Gobert, C. Kollath, U. Schollwöck and G. Schütz. “Real-time dynamics in spin- $\frac{1}{2}$  chains with adaptive time-dependent density matrix renormalization group”. *Phys. Rev. E* **71**, 036102 (2005).
- [55] T. Eggel, M. Cazalilla and M. Oshikawa. “Dynamical Theory of Superfluidity in One Dimension”. *Phys. Rev. Lett.* **107**, 275302 (2011).
- [56] T. Prosen and E. Ilievski. “Families of Quasilocal Conservation Laws and Quantum Spin Transport”. *Phys. Rev. Lett.* **111**, 057203 (2013).
- [57] I. Danshita and A. Polkovnikov. “Quantum phase slips in one-dimensional superfluids in a periodic potential”. *Phys. Rev. A* **85**, 023638 (2012).
- [58] P. Calabrese and J. Cardy. “Evolution of entanglement entropy in one-dimensional systems”. *Journal of Statistical Mechanics: Theory and Experiment* **2005**, P04010 (2005).

- [59] S. Singh, R. N. C. Pfeifer and G. Vidal. “Tensor network decompositions in the presence of a global symmetry”. *Phys. Rev. A* **82**, 050301 (2010).
- [60] M. B. Hastings. “Light-cone matrix product”. *Journal of Mathematical Physics* **50**, 095207 (2009).

# Acknowledgement

I would like to thank my supervisor Masaki Oshikawa for his comments, remarks and suggestions throughout my master's course. Furthermore, I express my gratitude to Grégoire Misguich for introducing me the problem studied in this thesis. Without his kind comments, helpful discussions and encouragement, I could not complete my master's thesis.

Discussions with Ippei Danshita, Shintaro Takayoshi and Shunsuke Furukawa were helpful for me to carry out the study. I would like to acknowledge them.

I would like to thank our group members: Yasuhiro Tada, Wenxing Nie, Miklos Lajko, James Quach, Yuta Kumano, Yohei Fuji, Emika Takata, Soichiro Mohri, Yoshiki Fukusumi, Hiroyuki Fujita and secretary Atsuko Tsuji. My life in Kashiwa with them was really enjoyable and academically fruitful.

Finally, I'm happy to thank my parents for their patients and constant supports in my whole life.

The numerical calculations of this study were done mainly in Super Computer Center of ISSP. I acknowledge Advanced Leading Graduate Course for Photon Science (ALPS) for financial support and my sub-supervisor in ALPS, Professor Makoto Kuwata-Gonokami.